Determinants of Increased Energy Cost in Prosthetic Gait

by

Michael E. J. Peasgood

A thesis
presented to the University of Waterloo
in fulfillment of the
thesis requirement for the degree of
Master of Applied Science
in
Systems Design Engineering

Waterloo, Ontario, Canada 2004

I hereby declare that I am the sole author of this thesis. This is a true copy of the thesis, including any required final revisions, as accepted by my examiners.
I understand that my thesis may be made electronically available to the public.

Michael E. J. Peasgood

Abstract

The physiological energy requirements of prosthetic gait in lower-limb amputees have been observed to be significantly greater than those for able-bodied subjects. However, existing models of energy flow in walking have not been very successful in explaining the reasons for this additional energy cost. Existing mechanical models fail to capture all of the components of energy cost involved in human walking.

In this thesis, a new model is developed that estimates the physiological cost of walking for an able-bodied individual; the same cost of walking is then computed using a variation of the model that represents a bi-lateral below-knee amputee. The results indicate a higher physiological cost for the amputee model, suggesting that the model more accurately represents the relative metabolic costs of able-bodied and amputee walking gait.

The model is based on a two-dimensional multi-body mechanical model that computes the joint torques required for a specified pattern of joint kinematics. In contrast to other models, the mechanical model includes a balance controller component that dynamically maintains the stability of the model during the walking simulation. This allows for analysis of many consecutive steps, and includes in the metabolic cost estimation the energy required to maintain balance.

A muscle stress based calculation is used to determine the optimal muscle force distribution required to achieve the joint torques computed by the mechanical model. This calculation is also used as a measure of the metabolic energy cost of the walking simulation.

Finally, an optimization algorithm is applied to the joint kinematic patterns to find the optimal walking motion for the model. This approach allows the simulation to find the most energy efficient gait for the model, mimicking the natural human tendency to walk with the most efficient stride length and speed.

Acknowledgements

"Let us always greet each other with a smile, for the smile is the beginning of love." - Mother Theresa

When I first stepped into Eric's office, the quotation of Mother Theresa above caught my eye. It was precariously written with dry-erase ink in the upper corner of his white board. Over the next couple of years, John, Eric and I often met in Eric's office, and that whiteboard was often the focus of discussion as diagrams of new ideas and graphs of results were sketched and just as quickly erased.

All of the planning and clever designing of one week's meeting inevitably went the way of all whiteboard sketches before our next meeting, as it was replaced with the new and improved solution of the day. Mother Theresa's quote, however, always managed to escape the eraser brush, and after 3 years it still remains there as a reminder of what really matters in this world. Solving challenging problems in engineering and academics may appear as great accomplishments as we improve the standards of living for the world or achieve personal goals; but such passing accomplishments are insignificant if we lose sight of the true importance in life, our relationships with one another.

I thank John and Eric for their guidance throughout this project, and for the freedom they gave me to solve problems in my own time. This project could not have been completed without Eric's insights into human motion and John's gift for explaining the mysteries of mechanical system analysis.

I thank my parents for instilling in me the value of education and the belief that anything worth doing is worth doing right; and I am forever grateful for the loving patience of my wife Kelly, who never ceases to support me in everything I do.

This work was supported by the Natural Sciences and Engineering Research Council of Canada.

Contents

List of Tables

List of Figures

Chapter 1

Introduction

1.1 History of Gait Analysis

The study of human locomotion has a long and distinguished history. Kinesiology, the science of the movement of the body, has its roots in ancient Greece, where Aristotle (384-322 B.C.) began the field of study with his treatises *Parts of Animals*, *Movement of Animals*, and *Progression of Animals*. His writings contain the first description of the actions of muscles in producing movement, and geometrical descriptions of the process of walking by conversion of rotary joint motion into forward progression [6].

1800 years later, Leonardo da Vinci (1452-1519) described the mechanics of various human movements, including standing up, walking, and running [52]. However, early studies of the mechanics of walking were restricted to qualitative discussions of the motions and forces involved.

By the early 1900s the development of motion capture systems using cinematography allowed for more detailed and quantitative research. Fischer [29] derived the equations of motion for a mechanical model of human walking in 1906, and in the 1930s Elftman used motion captured on film to complete by hand a full inverse-dynamics analysis of the torques required at each lower limb joint during the gait cycle [28]. The methods pioneered by Fischer and Elftman have been refined and adapted to study different facets of human walking over the past decades, as will be discussed in Chapter 2.

1.2 Motivation

Recent studies in human locomotion have aimed to discover the advantages of particular walking motions by examining the patterns of motion in the body, and the resulting forces within the muscles and joints that produce that motion. Once the forces and motions have been measured, they can be used to determine the flow of energy between muscles and limbs during gait. From an analysis of the motion, force, and energy flow patterns, we can begin to understand the reasons for certain features of gait, such as our preference to walk at a particular speed and with a particular stride length.

In addition to the general advancement of scientific knowledge, there are numerous practical applications that continue to motivate this research. The results can be applied to improve methods of sports training, rehabilitation programs, ergonomics, and the design of bipedal robots, to name but a few.

Another application that could be greatly aided by a better understanding of the flow of energy between muscles and limbs in walking is the design of prosthetic legs for amputees. Numerous experimental studies have demonstrated that amputees expend substantially more metabolic energy in walking a given distance as compared to a healthy individual [18], [65], [66]. However, existing models of energy flow in walking have not been very successful in explaining the reasons for this additional energy consumption, such as the analysis by Gitter et al. using center-of-mass dynamics to predict energy cost [34].

The challenge of determining the factors affecting metabolic energy consumption in amputee gait is apparent from studies that compare the effect of simple design changes, such as varying the mass of the prosthetic limb. Popular beliefs suggest that lighter prosthetics are better, since less energy is required to carry the extra mass; this has led to the use of more exotic and expensive materials to design the lightest possible limbs. By minimizing the mass, however, the dynamics of the swinging motion are also changed, and become less symmetric with the remaining limb. The reduction in mass, change in dynamics, and loss of symmetry may have the opposite of the desired effect, and increase the energy required for the amputee to walk [21].

The value of an accurate model of walking gait with prosthetic legs is clear. By varying the parameters of the model, the effect of design changes to prosthetic limbs on the energy cost of walking could be determined. Using such a model, the designers of prosthetic

limbs could find optimal designs that reduce the energy required for amputees to walk, and provide them with maximum mobility and independence.

1.3 Goals and Contributions

As explained in more detail in Chapter 2, the energy cost of walking is the rate at which metabolic energy is consumed by the muscles while walking. This cost can be estimated experimentally by having a subject walk at a given pace and measuring the rate of oxygen consumption.

Externally, the energy cost of walking may be estimated by considering the motion of the body as a mechanical system, and determining the amount of energy required to move the body through an observed walking motion. Ideally, this would give the same result as the experimentally determined energy consumption. By comparing the motion of a mechanical model of normal gait to that of prosthetic gait, we should therefore be able to observe a corresponding difference in energy consumption.

Unfortunately, the results of these two methods rarely agree, for a variety of confounding reasons. Purely mechanical models of the human body usually fail to take into account a number of factors: the efficiency of conversion of metabolic energy into mechanical motion; the metabolic energy cost of a muscle holding a static position under stress but performing no mechanical work; and the need for co-contraction, the result of two muscles acting in opposition to each other to increase joint stiffness.

The first goal of this thesis is to develop a model of human walking that is based on a multi-body mechanical simulation, while taking into account the factors mentioned above in estimating the metabolic energy cost of a particular gait pattern.

The second goal is to incorporate the hypothesis that the human body attempts to minimize energy consumption and muscle fatigue when walking. This tendency to minimize energy cost has been shown in numerous studies [1] [18] [72]. The principle can be applied to two sub-problems: finding the distribution of muscle forces within the leg required to generate the joint torques for walking using the least amount of energy; and finding a gait pattern for the model that is representative of natural energy-optimal human walking.

Using this model of energy consumption and the minimal-energy gait pattern simu-

lations, an optimal gait pattern for both a normal and prosthetic walking model will be determined. This will establish a method for evaluating and comparing gait efficiency in useful terms, and provide insight into the additional energy cost of prosthetic gait.

1.4 Thesis Outline

The theory, implementation, and results of the model development are presented in the following chapters.

Chapter 2 gives a review of background material and prior research into walking gait analysis and metabolic energy consumption.

Chapter 3 presents an overview of the system, and describes the interfaces between the optimization loop, the mechanical model, and the metabolic energy model components of the system.

Chapter 4 reviews the methods of mechanical system analysis, followed by details of the mechanical simulation design for the normal and prosthetic walking models.

Chapter 5 describes the model used for determining muscle forces required by the simulation, and the calculations used to estimate the metabolic energy cost of motion.

Chapter 6 discusses the problem of maintaining balance in a forward-dynamics bipedal walking simulation, and presents the stabilizing control system that is used in the model.

Chapter 7 presents and compares the results of the optimization solutions for the normal and the prosthetic models.

Chapter 8 discusses conclusions that can be drawn from this work and areas where the model may be enhanced through future development.

Chapter 2

Background Literature Review

2.1 Walking Gait Analysis

Most experimental analyses of human walking gait, such as those of Bianchi and Borghese [11] [9], begin with the measurement of the kinematics (motion) of the body and limb segments. Numerous measurement methods have been used, ranging from simple photographic capture to more sophisticated three-dimensional sensing of markers placed at known positions on the body [69]. From the position data, captured over a sequence of frames spanning one or more periods of the gait cycle, other kinematic data can be approximated, such as the joint angles and velocities as functions of time.

The second component of gait analysis is the measurement of the kinetics (forces and moments) applied on and within the body [69]. External forces applied during walking are relatively easy to determine using force-plates on the ground. Vertical and horizontal ground reaction forces applied at the feet and their point of application can be measured directly, and are useful in identifying the net forces and moments applied to the body. A more challenging problem is computing the forces and moments that are present at the joints within the body. These are of particular interest to this research because they provide insight into the efficiency of energy flow between limb segments, as discussed later in this chapter.

A third component of gait analysis is energy consumption, which gives a measure of the energy required to walk a given distance [70]. Energy can be measured in terms

of metabolic consumption (the amount of energy used by the muscles), or in mechanical energy terms computed from the kinematic and kinetic measurements discussed above. The measurement methods and correlations between these two approaches to energy analysis are the primary subjects of the remainder of this chapter.

2.1.1 Normal Human Gait

In two articles on human locomotion, Edmond Ayyappa gives an introduction to measurement and analysis techniques. The first article reviews the phases of the gait cycle and parameters and terminology used in gait measurement [7]. A second article reviews kinematic and kinetic measurement techniques [8]. These articles provide a useful baseline for normal human locomotion, to which prosthetic gait variations can be compared.

2.1.1.1 Phases of Gait

To identify and refer to different motion patterns that occur during a walking stride, the gait cycle is commonly broken down into a set of phases, defined by events and time intervals in the stride. For the purposes of normal and amputee gait analysis, a common definition of phases based on certain identifiable events is sufficient, as used by MacFarlane [43]. The events within the gait cycle are defined in Table 2.1.

Heel-strike	Instant of initial foot contact with the ground
Midstance	Instant of crossing of midshanks (corresponds to contralateral midswing event)
Toe-off	Instant of loss of foot contact with the ground
Midswing	Instant of crossing of midshanks (corresponds to contralateral midstance event)

Table 2.1: Gait Events

The phases of gait identify periods of time within the gait cycle, and are defined in Table 2.2 as the time between identifiable events.

Early stance phase	Time from heel-strike to midstance
Late stance phase	Time from midstance to toe-off
Early swing phase	Time from toe-off to midswing
Late swing phase	Time from midswing to heel-strike

Table 2.2: Gait Phases

2.1.2 Variations in Prosthetic Gait

When part of a lower limb is lost and replaced with a prosthesis, changes to the normal gait patterns are expected due to the loss of muscular control of the lower joints. Changes to the rate of energy consumption during walking have also been observed, as discussed in the following sections.

2.1.2.1 Kinematics and Kinetics

To maintain stability without active ankle or knee joint control, amputees must make a number of changes to their gait kinematics, as observed by Czerniecki [20]. During stance, there is typically no knee flexion in the first 30% to 40% of the stance phase, to avoid buckling of the knee. This requires additional hip extension to maintain the knee extension at heel-strike. Approaching the swing phase, the amputee must compensate for the lack of gastrocnemius and soleus muscle power at the ankle by increasing hip flexor power, despite the reduced mass of the prosthetic limb relative to a normal leg. Based on his analysis, Czerniecki noted that:

> Part of the impetus for the development of new prosthetic components and socket designs has been to reduce the metabolic costs of ambulation. In spite of the biomechanical evidence that supports the energy absorption and restoration of energy-storing feet, they have not been shown to significantly reduce the metabolic costs of walking in the majority of studies.

2.1.2.2 Metabolic Energy Cost

Hoffman et al. [38] examined aerobic demands in bilateral above-knee amputees compared to matched able-bodied subjects. The comparison showed a preferred walking speed 21% slower and aerobic demands 49% higher for the amputees. At specified speeds, aerobic demands were 55% to 83% higher for the amputee subjects. The explanatory model indicates the higher metabolic costs are due to greater demands for maintenance of balance and posture, and for performing the walking movement.

These observations summarize the need for further development of walking analysis, particularly in the area of amputee gait. While the energy consumption of amputees is substantially higher than for normal subjects, current analysis methods that are used for prosthetic design (such as the centre-of-mass dynamics approach used by Gitter et al. [34]) are not correctly predicting the actual changes in metabolic energy cost for the users. The reasons for the failure of some of these methods when applied to amputee gait will be discussed in the following sections.

2.2 Metabolic Energy in Gait

The rate of energy consumption during normal walking has been the subject of numerous studies by many researchers, such as Booyens in the 1950s [10], and more recently Waters [63], [66]. A measure of the amount of energy consumed per minute or per unit distance travelled can be used to determine differences in metabolic efficiency, for example between normal subjects and trained athletes as shown by Waters [61]. Waters has also investigated the additional metabolic cost due to various pathologies and disabilities, such as arthrodesis [64], the use of crutches [62], paraplegia [63], and amputation [65].

2.2.1 Oxygen Consumption

To determine the amount of energy consumed by the body over time, an indirect calorimetric method is used, based on the measurement of energy produced in a calorimeter by combustion of carbohydrate, fat, and protein with oxygen [61]. By the conservation of energy, the complete metabolization of the same food in a metabolic system will produce

an equal amount of energy (approximately 4.82 kcal in one litre of O_2 [61]) that is used to generate mechanical motion, or is eventually released as heat.

Mechanical energy is produced from biochemical energy by the conversion of adenosine triphosphate (ATP) into adenosine diphosphate (ADP), which frees one phosphate atom and releases energy that shortens the contractile elements in muscle:

$$ATP \rightarrow ADP + P + Energy \tag{2.1}$$

During aerobic exercise, such as walking, ATP is generated by aerobic oxidation, which consumes O_2 and releases CO_2. Using the assumption that the oxygen transfer that takes place at the cellular level is equally represented by oxygen consumption and carbon dioxide expulsion during breathing, the rate of ATP and energy production in the body can be determined by measuring the volumetric rate of O_2 consumption, or $\dot{V}O_2$.

2.2.2 Energy Calculations

To determine the amount of energy consumed based on oxygen analysis, a scaling factor dependent on the food source is required. This is termed the respiratory quotient (RQ); for a typical diet of 60% metabolized fats and 40% metabolized carbohydrates, the RQ is 0.82, resulting in 4.8 calories of energy per ml O_2 consumed [61]. Using the conversion of 4.18 Joules per calorie, the metabolic energy rate is given by

$$\dot{E} = 20.1 \cdot \dot{V}O_2 \tag{2.2}$$

where $\dot{E}$ is in units of Watts and the oxygen uptake rate $\dot{V}O_2$ is in units of ml/s.

Subject Group	Mass (kg)	Speed $\left(\frac{m}{s}\right)$	Oxygen rate $\left(\frac{ml}{s}\right)$	Energy rate $\left(\frac{J}{s}\right)$	Normalized Energy $\left(\frac{J}{kg \cdot m}\right)$
Able-bodied	62.8	0.9	10.3	207.7	3.7
Amputees	64.1	0.8	15	301.5	5.9

Table 2.3: Metabolic Energy Consumption Calculation based on [38]

Table 2.3 compares the metabolic energy consumption between an average able-bodied subject and an amputee. The masses and oxygen consumption rates are taken from the average values of the five bilateral above-knee amputee subjects and the matched able-bodied control subjects used in Hoffman's analysis [38]. The energy rate in Table 2.3 is computed using Equation (2.2), and the normalized energy consumption is computed by dividing by mass and walking speed.

2.3 Mechanical Energy in Gait

One of the fundamental problems in the study of biomechanics has been in the calculation of forces and torques generated internally in the muscles and joints during human motion. The value of such information is significant in the case of locomotion. For example, knowledge of the forces generated in muscles and tendons can be used to determine which muscles provide energy for propulsion during particular phases of gait. This may give insight into the reasons for gait variations resulting from pathologies affecting certain muscles.

Determining the internal forces during gait is also one means of measuring the efficiency of locomotion. If the force generated by a muscle is known along with the excursion of the muscle (it's length change over time), the mechanical work performed by the muscle can be simply calculated using the product of force and distance:

$$W = \vec{F} \cdot \vec{d} \tag{2.3}$$

or, integrating velocity over the period of a motion:

$$W = \int \vec{F}(t) \cdot \vec{v}(t) dt. \tag{2.4}$$

Once calculated and summed across all active muscles, the mechanical work can be compared to the metabolic energy consumed to determine the efficiency of the conversion from metabolic to mechanical energy. Conversely, in the case of locomotion, the work performed can be divided by the distance travelled to compute a cost of locomotion, or a measure of the efficiency of a particular gait pattern in terms of mechanical energy.

In practice, directly measuring the forces *in vivo* would require invasive and impractical methods, such as the attachment of strain gauges to each of the muscles under investigation.

Instead, numerous methods have been used, with varying degrees of success, to estimate the actual mechanical work performed by the muscles, based on externally observable measurements. The most common methods are reviewed and compared here, along with a summary of the results of various studies using the various calculations.

2.3.1 Energy Calculation Methods

Numerous different methods have been used to estimate the energy consumed in the motion of biological systems by representing the system with a mechanical model and computing the mechanical energy consumed by the model. This section reviews the most frequently used methods, in order of increasing model complexity.

2.3.1.1 Centre of Mass

One of the simplest methods of estimating the amount of work performed by the muscles during walking is to simply observe the motion of the centre of mass of the body. This method measures only the external work performed; that is, no measure is made of the work performed to move the limbs relative to the torso.

Cavagna et al. [16] measured the translational kinetic and potential energy of the body using the centre of mass motion over a range of walking speeds; the rotational kinetic motion was assumed to be negligible. This gave a simple expression of the total energy of the body:

$$E_{tot} = E_p + E_{kf} + E_{kv} \tag{2.5}$$

where E_p is the potential energy and E_{kf} and E_{kv} are the kinetic energies in the forward and vertical directions respectively. Cavagna notes that during walking gait, the sum of potential and kinetic energies oscillates with lower amplitude than either of the individual components. Hence, there is presumably an efficient transfer of energy between potential and kinetic forms during gait. However, this simple model gives no insight into the work involved in moving the limb segments relative to the centre of mass.

2.3.1.2 Segmental Energy Analysis

This method is based on measurements of the kinetic and potential energies of each of the limb segments, using known mass distribution properties of the segments and kinematic data gathered for a particular motion. It is an attempt to estimate the energy provided by the muscles to move the limbs during a prescribed motion; that is, an estimate of internal work required by the motion. ("Internal work" is used to describe the work done to move the limbs relative to the body centre of mass, while "external work" refers to work performed on the environment and work that moves the body centre of mass [69].)

Winter [70] gives a description of the use of instantaneous segment energies in gait analysis and gives details of the calculation based on kinematic data captured on film. The total energy of a limb segment (E_i), if treated as a rigid body, can be simply calculated as the sum of its translational and rotational kinetic energy ($KE_i + RE_i$) and its gravitational potential (PE_i) energy:

$$E_i = KE_i + RE_i + PE_i. \tag{2.6}$$

Substituting the common expressions for kinetic energy of a rigid body in two dimensions gives the instantaneous energy in terms of the measured kinematic velocities:

$$E_i = \frac{1}{2} m_i v_i^2 + \frac{1}{2} I_i \omega_i^2 + m_i g h \tag{2.7}$$

where m_i is the mass of the segment, I_i is its moment of inertia about the centre of mass, h is the height above some fixed datum, and v and ω are the linear and angular speeds respectively.

The variation in the total energy of a segment over a small period of time represents the amount of energy flow into or out of that segment. Thus, by summation of the changes in energy over time (an approximate integral of the energy rate), an estimate of the work done on a limb segment can be calculated. For a series of n samples in time, the summation gives a net amount of energy flow into the segment as:

$$WNet_i = \sum_{k=1}^{n} \Delta KE_{i,k} + \Delta RE_{i,k} + \Delta PE_{i,k}. \tag{2.8}$$

This gives a simple expression for the net work done on a limb segment. However, problems quickly arise when applied to a cyclic motion, such as human gait. In cyclic

motion, the energy of each limb segment is the same at the beginning and end of each cycle; the positive and negative energy flows are equal and cancel to give a net work of zero. In terms of mechanical analysis, the result is correct; by the definition of mechanical work, no net work has been done. In a biological system however, metabolic energy is usually required to perform both positive and negative work.

Experimental studies of muscle dynamics have shown that the amount of metabolic effort required for positive work (accelerating a body) is greater than that for negative work (decelerating a body). A classic example has two subjects on stationary bicycles that are driving the same flywheel [69]. The first subject must pedal to accelerate the wheel (performing positive work) while the second subject pedals to decelerate the wheel (performing negative work). As would be expected, the first subject will require more energy and tire much more quickly than the second subject, since the negative work involves partially passive absorption of energy by the muscles, rather than the constant active generation of energy by the muscles of the first subject.

Although this has demonstrated that negative work requires less metabolic energy, it is common in many studies for the positive and negative energy flows to be weighted equally by taking the absolute value of the energy changes in each limb segment. This gives an expression used by Norman et al. [47] for the work performed on each segment:

$$WTot_i = \sum_{k=1}^{n} |\Delta KE_{i,k}| + |\Delta RE_{i,k}| + |\Delta PE_{i,k}|. \tag{2.9}$$

This effectively accounts for all mechanical energy gained and lost in the segment. Again, however, a flaw can be seen by a simple example. If the lower leg of a seated person is considered as a simple pendulum, swinging freely from the knee, there is no metabolic work required by the muscles, except to overcome the minimal friction in the knee. However, there is a continual transfer of energy between forms, from potential when the leg stops at the top of the swing to kinetic when it moves through the bottom of the arc. Norman's expression will account for all of these energy transfers as work performed on the limb segment, when in fact no work is done. This will lead to over-estimations of the actual work done by the muscles when passive energy transfer takes place within a segment.

To allow the transfer of energy between translational, rotational, and kinetic forms,

all forms of mechanical energy in the segment may be summed before taking the absolute value:

$$WTot_i = \sum_{k=1}^{n} \left|\Delta(KE_{i,k} + RE_{i,k} + PE_{i,k})\right|. \tag{2.10}$$

This allows for passive transfer between energy forms within a segment, since conversion between kinetic and potential energy will negate each other.

However, passive energy transfer may also take place between limb segments. In a freely swinging double pendulum model of the leg, for example, energy is continually transferred between the upper and lower limb segments. Again, the energy transfer will be accounted for twice, once as it leaves one segment, and again as it enters the other, when in fact no mechanical or metabolic energy is involved. Winter [68] therefore suggested measuring the changes in the mechanical energy of the entire body of n segments over m samples using:

$$WBody = \sum_{i=1}^{m} \left|\Delta \sum_{k=1}^{n} (KE_{i,k} + RE_{i,k} + PE_{i,k})\right| \tag{2.11}$$

which effectively allows for passive transfer of any mechanical energy between any limb segments in the body. However, it will underestimate the work performed by the muscles in the case where some segments are actively accelerated and others are actively decelerated.

Shorten [56] discusses these various models and notes that an energy flow model of the human body, defining all possible means of energy transfer between limb segments, would be required to use segment energies to accurately estimate the actual mechanical work performed.

The results of segmental analysis methods also give no indication of the source of the energy in each segment. By examination of the energy curves of two limb segments, one increasing in energy and the other decreasing, one may speculate that there is a passive transfer of energy between the two. However, it is equally possible that active muscle contraction is providing the energy increase to one segment, and an independent contraction is absorbing the energy of the other.

Despite its application in relatively recent research such as Bianchi's examination of kinematic coordination in gait [9], the segmental energy method of estimating internal work has serious flaws. Williams [67] summarized the results of numerous studies using segmental energy analysis for measuring the power output requirements of running, and found results

ranging between 172 and 1650 Watts. Williams also found the power calculations highly sensitive to filtering of the kinematic data; varying the cutoff frequency of the digital filter between 4 and 10 Hz caused a variation in power estimation of over 50%.

The segmental analysis requires many assumptions to be made about energy transfer within and between segments. To accurately estimate the work performed by the muscles, and obtain any insight into the flow of energy through the biomechanical system, another method of analysis is required. A method based on a rigorous accounting of the forces and torques acting at each joint reveals the actual flow of mechanical energy between limb segments; this method is termed *Joint Powers*.

2.3.1.3 Joint Powers

The method of joint powers uses a technique from mechanical systems analysis called inverse dynamics to estimate more accurately the sources of power and the flow of energy through the joints in the biomechanical model. This method requires a more complex computation than the segmental energy method, but provides insight into the joints where energy is being supplied or absorbed, and accounts for passive energy transfer between limb segments.

To determine the forces and moments at the joints for a specified kinematic motion, the limb segments are modeled as a set of rigid bodies connected by ideal joints.

The equations of motion for the rigid bodies in 2-D are the familiar

$$\vec{F} = m \cdot \vec{a} \tag{2.12}$$

and

$$\vec{M} = I \cdot \vec{\alpha} \tag{2.13}$$

where $\vec{F}$ and $\vec{M}$ are the forces and moments applied to the body, m and I are the mass and moment of inertia, and $\vec{a}$ and $\vec{\alpha}$ are the linear and angular accelerations of the body.

The equations of motion for all of the bodies in the system are combined with the constraint equations of the joints that relate the relative position of the joint centres of connected segments. Given the linear and angular accelerations of each segment, and the externally applied (ground reaction) forces, this set of equations can be solved for the unknown forces and torques in each joint at each instant in time.

Once the forces and torques have been calculated, the instantaneous power into segment i is given by [54]:

$$P_i = \vec{F_d} \cdot \vec{v_d} + \vec{F_p} \cdot \vec{v_p} + \vec{M_d} \cdot \dot{\vec{\theta}_d} + \vec{M_p} \cdot \dot{\vec{\theta}_p} \tag{2.14}$$

where subscripts p and d represent proximal (closer to the torso) and distal (farther from the torso) joints respectively. The total work performed by the body can be found by summing across all of the segments, and integrating over the period of the motion. For all joint force terms between two segments ($\vec{F} \cdot \vec{v}$), the force applied to one segment will be equal and opposite to the force applied to the other segment; the velocities at the pin joint must be equal as required by the joint constraint equations. These terms therefore cancel out when calculating the power of the entire body [9]. For gait analysis, the remaining force terms are between the foot and the ground, where the velocity is zero, removing that term from the power expression.

After cancellation, the expression for total mechanical power of the n-segment body reduces to:

$$P(t) = \sum_{i=1}^{n} \vec{M_i} \cdot \dot{\vec{\theta}_i} \tag{2.15}$$

where $\dot{\vec{\theta}_i}$ is the net joint velocity ($\dot{\vec{\theta}_d} - \dot{\vec{\theta}_p}$) and $\vec{M_i}$ is the net joint torque.

As in the segmental energy analysis, over a cyclic motion with minimal external work such as walking, the positive and negative powers are approximately equal and cancel out when integrated over time. In a similar approach to the segmental energy cancellation problem, an assumption is made that the positive and negative mechanical powers require equal muscle power, resulting in an expression for estimated muscle work [14]:

$$W = \int \left| \sum_{i=1}^{n} \vec{M_i} \cdot \dot{\vec{\theta}_i} \right| dt \tag{2.16}$$

This method was used in early research into walking gait by Elftman [28], where the kinematic data was gathered by cinematic film of a subject walking behind a rectangular grid, and ground reaction forces were measured from a force plate. Accelerations were determined by double graphical differentiation of the plots of the limb positions, and the forces and torques in the joints were determined by solving the equations of motion for each segment, beginning at the foot where the ground reaction forces were known. Elftman

generated plots of the energy flow into each segment to describe the energy flow between limb segments and the torso through the gait cycle.

From his analysis, Elftman notes a key feature of energy analysis in biomechanical models: "Muscles not only provide forces that guide the limbs into trajectories impossible for compound pendulums, but they also regulate the energy distribution of the body." It is the metabolic cost of this energy distribution that is most challenging to quantify; the energy flow is observable as a change in segmental energy, but may take place with isometric muscle contraction. Hence, no mechanical work is performed as calculated with the joint powers method ($\dot{\theta}_i = 0$), and a metabolic cost of the muscle contraction remains unaccounted.

Though not perfect, this method has some significant advantages over the segmental energy approach. First, it includes both internal and external work [69]; as external loads increase, so do the reaction forces applied to the model. This results in increased joint moments calculated from the rigid body equations, and increased power output to perform the additional external work. The joint powers method also gives insight into the sources of energy and the mechanisms of energy transfer within the system that are unobservable with the joint segments technique.

However, the joint powers method cannot account for the metabolic energy required to maintain a constant torque at a joint that performs no work. For this, a model that estimates the metabolic cost of force generation, rather than mechanical work, is required.

2.3.2 Relation to metabolic cost

To be of value in predicting physiological effort, the results of a mechanical energy analysis should have some correlation to the metabolic energy requirements of performing the same motion. Numerous studies have investigated this correlation by measuring the metabolic energy consumption of a cyclic motion while capturing the kinematic and kinetic data required to calculate the mechanical energy cost. The two resulting cost measures are then compared, usually over a range of speeds of motion.

2.3.2.1 Correlation of metabolic and mechanical energy costs

A correlation between metabolic and mechanical energy cost was established by Burdett et al. [13] by measuring the metabolic energy consumption of quiet standing and walking at 5 different speeds. Metabolic energy cost was determined using the oxygen consumption rate ($\dot{V}O_2$), and was normalized by body mass. The mechanical energy for each walk was calculated using 3 methods: total energy of the center of the mass, determined by integration of ground reaction forces; segmental energy, using the sum of kinetic and potential energy changes for each segment; and joint moments, integrating over time the product of angular acceleration and moment at each joint over the walking gait cycle. The correlation is measured using r, the correlation coefficient. (A value of $r = 1$ indicates a perfect linear correlation, and a value of $r = 0$ indicates no linear correlation.)

Burdett's results show that the metabolic energy consumption rate was closely correlated with velocity squared ($r = 0.93$), in agreement with other researchers [74]. The mechanical energy rates from all methods of calculation also increased with velocity, and reasonably correlated with both velocity and velocity squared ($r = 0.81 - 0.91$). Comparing the metabolic rate to mechanical energy rate at each velocity, the strongest correlation was found using the centre of mass energy calculation ($r = 0.89$) followed by the joint moment calculation ($r = 0.85$) followed by the segmental work method ($r = 0.79$). While the center of mass calculation neglects the movement of the limbs in the calculation, it requires only force plate data to be measured, and is less subject to errors in measurement and calculation. This was proposed as a possible reason for improved correlation with metabolic energy rate over the segment energy and joint moment calculation methods.

2.3.2.2 Failure of Segment Kinematics and Joint Moments Methods

Martin et al. [44] investigated the relationships between aerobic energy demand and estimates of mechanical power and energy transfer. The purpose of this study was to determine if individual differences in metabolic energy ($\dot{V}O_2$) are correlated with differences in mechanical power output and efficiency gained through inter-segmental energy transfers. Again, mechanical energy requirements were calculated using three methods: the center of mass method; the segment kinematics; and joint torques. Calculations were also made with varying allowable energy transfers, from no energy transfer (defined by Equation (2.8)) to

allowing energy transfer between kinetic and potential energy (Equation (2.10)) or allowing energy transfer between limb segments (Equation (2.11)). The energy transfer could then be determined by taking the difference between the energy required when no transfers were assumed, and when full energy transfer was assumed.

The results gave relatively poor correlations between metabolic and mechanical energy requirements, with very low correlations ($r = 0.14 - 0.17$ for walking) with the segmental energy method and even negative correlations when measuring joint powers. Their conclusions suggest that mechanical energy estimates are insufficient to draw conclusions regarding corresponding individual metabolic energy requirements.

2.3.2.3 Use of Mechanical Models to Estimate Variation in Energy Cost

In more recent work, Donelan et al. [26] used a mechanical model to predict the metabolic cost of walking with varying step width. A three-dimensional model of passive-dynamic walking [40] was used, from which a mechanical cost of transport is measured based on the energy lost in the transition from one stance leg to the next. This model has been used to accurately predict the preferred speed-step relationships observed in human gait [41]. Based on the increased effort required to redirect the body centre of mass when walking with a wide stance, Donelan predicted an increase in metabolic cost correlated with the square of the step width. Experimental data including kinematic, kinetic, and metabolic rates based on $\dot{V}O_2$ consumption was gathered. The mechanical cost of step-to-step transitions was determined using the negative external mechanical work performed by the leading leg during double support. In addition, the external work was determined as calculated using Cavagna's combined-limb method from force-plate data [15].

As predicted by the model, the mechanical cost of transport based on negative work done during step-to-step transitions increased with the square of step width, as did the metabolic cost, suggesting that the step transition energy is a good estimate of metabolic cost of transport. In contrast, the external work as calculated by Cavagna provided a very poor correlation, remaining approximately constant throughout the range of step widths. The flaw in Cavagna's approach is that it measures the net force of both limbs on the force plate during double support; at the time of heel-strike, there is both negative work performed by the leading foot and positive work by the trailing foot, which maintains the

net energy of the body [27]. In Cavagna's calculations, the two powers are summed and cancel out, underestimating the actual work performed. The success of Donelan's model in predicting metabolic cost increases as a function of a specific gait parameter indicates the practicality of the mechanical analysis, as well as the importance of the selection of an appropriate measure of mechanical energy cost.

2.3.2.4 Summary

The studies cited in this section appear to give conflicting conclusions regarding the value of mechanical model analysis in estimating metabolic energy cost. Examining the results, however, gives some useful insight into the type of comparisons where a mechanical model is appropriate.

Martin's work compared the metabolic energy consumption of different subjects to the computed mechanical power output of the individual. The poor correlations in the results suggest that the mechanical models do not accurately capture all of the components of metabolic energy cost; some subjects may walk much more efficiently than others without a mechanically observable explanation. This may be due to a more efficient energy conversion or storage within the muscles. For example, muscles have an elastic component which can store mechanical energy for short periods of time when stretched. By selecting an appropriate gait pattern, the body may use this elastic property of the muscle to store energy as the soleus is stretched during the late stance phase and release it at toe-off providing efficient propulsion. This efficiency would not be observable in a purely mechanical model.

The work by Burdett and Donelan, however, demonstrated that the change in metabolic energy cost for an individual is closely correlated with the changes in energy for a mechanical model where some parameter of gait, such as step length or speed, is varied. This suggests that the use of mechanical model analysis should be constrained to understanding the effect of varying parameters for one individual, and should not be used to compare the efficiency of gait patterns across multiple subjects.

2.4 Energy Optimization

2.4.1 Optimization in Nature

Numerous studies have demonstrated the energy-optimal properties of animal and human gait. Like other animals, humans have a "preferred walking speed" at which they walk if not otherwise constrained [1]. Based on oxygen consumption measurements, it has been repeatedly observed that the metabolic cost of locomotion (in energy consumption per unit distance traveled) is at a minimum at the preferred walking speeds, and increases at both faster and slower walking speeds [18], [72].

Hoffman et al. [38], in studies comparing energy requirements of amputee gait, also found that the speed chosen by both unilateral and bilateral amputees tended to minimize the metabolic cost per distance travelled. For unilateral amputees, this corresponds to a walking speed slow enough to maintain a metabolic rate equal to that of an able-bodied subject. For bilateral amputees, the speed is reduced further, but the metabolic rate is still higher than that for able-bodied gait, suggesting that reducing the metabolic rate further would require moving so slowly that the cost per distance travelled would increase.

Zarrugh et al. [75] investigated the effect on energy consumption of varying step speed and step length independently. For freely selected step speed and length, the results of several studies including a total of 86 subjects were compiled to arrive at an average equation for the energy expenditure per minute per kilogram:

$$E_w = 32 + 0.0050v^2 \tag{2.17}$$

where E_w is the energy rate in $(cal/min)/kg$, and v is the walking speed in metres per minute. Dividing by v and setting the derivative to zero, Zarrugh finds a minimum energy cost per metre of $E_m = 0.8cal/m/kg$ at a speed of $80m/min$.

Experiments with constrained walking, where the subject is required to walk at a specified speed, found that as either step speed or length is increased independently, metabolic energy cost increases quadratically. The minimal energy requirement across the range of normal walking speeds corresponds to step speed and length increasing proportionally, as is found in freely selected gait.

Donelan et al. [26] found a similar optimal pattern in the freely selected step width in

human walking. In experiments where the subjects were forced to walk with either a wider or narrower step width, the metabolic cost of transport increased with the square of the variation from the freely selected width. This suggests that metabolic energy cost may be a strong determinant in the kinematic patterns selected in normal walking.

While investigating the kinematics patterns in gait, Borghese et al. [11] sought a kinematic parameter that was consistent across various speeds of gait and individual subjects. Step rate and length vary proportionally with speed, as discussed above, and joint angle trajectories vary depending on the individual and walking speed. One measure of gait that was relatively consistent was the relative elevation angles of the limb segments. (The elevation angle of a segment is a measure of the rotation of the limb segment in the sagittal plane.) When the elevation angle measurements for a complete cycle of gait are plotted in the three dimensional position space of the foot, shank, and thigh, the gait trajectories form loops on a plane, as shown in Figure 2.1. The figure was generated using the methods described by Borghese [11] and the experimental measures of Winter [69]; the points correspond to samples at instants during the walking gait, and the line is the plane of best fit for all the points.

The plane containing the elevation angle trajectory loop was termed the "plane of covariation." Borghese proposed that this "law of intersegmental co-ordination" was a means of maintaining dynamic equilibrium that was a fundamental feature of walking gait at any speed.

Bianchi et al. [9] followed up on this work, and noted that the orientation of the plane varied slightly with speed. As walking speed increased, the trajectory of limb elevation angles rotated about an axis lying in the plane. This rotation reflects a change in relative elevation angles of the limb segments during the gait cycle. Bianchi speculated that this change was correlated to an energy minimization as speed increased. Using the segmental energy analysis method, the mechanical power required for walking at varying speeds was measured and plotted against the rotation of the plane of covariation. The results demonstrated again that the changes in gait kinematics are driven by a goal of minimizing metabolic energy cost.

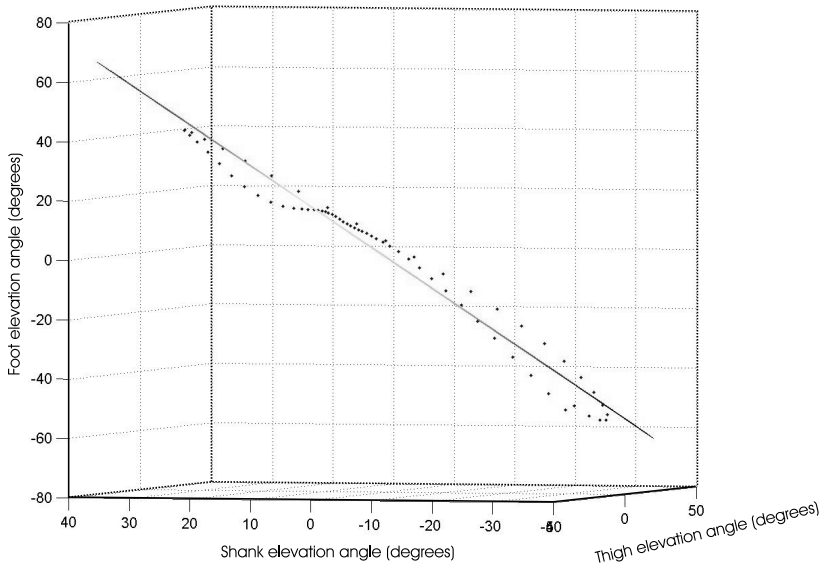

Figure 2.1: Plane of covariation

2.4.2 Optimization in Models

Based on the observations of energy cost minimization in biological systems, it is reasonable to incorporate similar optimization goals into biomechanical models. Minetti and Saibene [45] for example, used a simple mathematical model of a planar bipedal walker to estimate energy cost of locomotion at varying stride frequencies. Optimization of the energy cost was successfully used to predict the preferred stride frequency as a function of walking speed, verified against experimental data from human subjects walking on a treadmill. Minetti's model was simple enough to derive an analytical solution for the optimal stride frequency. In general, however, numerical techniques are required to minimize the energy cost function in more complex models.

Optimization is also applicable to the problem of determining force distribution among muscles. Because multiple muscles may be able to contribute to a required moment about a joint, there is no single solution to which muscle, or set of muscles, should be activated; this is sometimes referred to as a redundant actuation problem. To find the muscle acti-

vations that achieve the desired joint moments with a minimal metabolic energy cost, an optimization approach is required to solve the force distribution problem in the model.

2.4.3 Static and Dynamic Optimization Solutions

Two different approaches have be used to find an optimal set of muscle force patterns that will generate an efficient walking gait, as reviewed by Yamaguchi [73].

The first method is a *static* optimization of muscle forces this is used in conjunction with an inverse dynamics mechanical model analysis. The inverse dynamics analysis begins with the specified measured (or desired) kinematic motion of the body, and computes the joint torques required to generate that motion. From this solution, the optimal muscle forces that can generate the required joint torques are computed at each instant in time. The optimization is termed *static* because the dynamics of the muscle and skeletal model are not considered in the optimization; the optimal solution at each instant is independent of time, and no muscle state information is required.

Silva and Ambrosio [58] review the theory and details of the static optimization method for solving the redundant actuation problem, and discuss the effect of varying the objective function used in the optimization process [57]. The method has become popular among researchers interested in more general body motion than just walking gait, and has been developed into the relatively generic human motion analysis package *AnyBody* described by Damsgaard, Christensen and Rasmussen [22].

The alternative method for finding an optimal solution is termed a *direct-dynamic simulation*. Rather than working backward from known kinematics to the required muscle forces, a forward-dynamics musculoskeletal simulation is driven by a selected muscle force pattern. The resulting kinematic patterns are then compared to the desired kinematics to determine the suitability of the current muscle force patterns. This method is much more computationally expensive than the static optimization approach: the solution of the forward-dynamics system equations is more complex than for the inverse-dynamics problem; and the optimization algorithm must operate on a continuous function of the muscle activation patterns over the entire simulation time instead of solving each instant in isolation.

Some early simulations using direct-dynamic simulations were developed in the 1980s

by Pandy and Berme [48] and Davy and Audu [23]. Yamaguchi notes in his review [73] that, because of computational constraints, these simulations were very limited to very few degrees of freedom. More recently, a more complex direct-dynamic simulation was developed by Anderson and Pandy [2] based on a three-dimensional model with 23 degrees of freedom and 24 muscles. Simulation of one complete cycle of gait required over 10,000 hours of CPU processing time using 8 parallel processors on IBM SP-2 and Cray T3E supercomputers.

To evaluate the benefit of the additional computational resources required for direct-dynamic simulations, Anderson and Pandy compared the results of a static optimization analysis of gait with a forward dynamics simulation of the same problem [4]. They conclude that:

> The striking similarity between the dynamic and static optimization solutions provides strong evidence that static optimization is entirely adequate for predicting joint contact forces during gait, provided that the net joint torques exerted by the muscles are known with confidence. Similarity between the two solutions implies that (1) activation dynamics may be neglected in the static optimization problem for gait and (2) there is a functional equivalence between minimizing metabolic energy over the entire gait cycle (a time-dependent performance criterion) and minimizing the sum of muscle forces squared at any instant (a time-independent performance criterion).

Based on Anderson and Pandy's results, a model based on inverse dynamics and static optimization was proposed for the development of this thesis.

2.4.4 Fatigue as an Objective Function

For any optimization problem, an objective function is required to compute a measure of the quality of a particular solution. In the case of gait analysis, the desired objective to minimize is the metabolic energy cost. As discussed in Section 2.3, however, deriving an estimate of actual metabolic cost from the results of a mechanical model is not a simple problem. Even when the forces and moments at each joint are determined from the model,

there may be metabolic energy costs due to isometric muscle contraction that do not appear in the mechanical energy cost analysis.

A solution based on *fatigue rate* was proposed by Crowninshield [19] as an objective function for solving the force distribution problem. The term fatigue was used as a measure of the rate at which a muscle tired while maintaining a specified force. Since the joint torques and moment arms of each muscle are known from the model, the instantaneous fatigue can be computed for a given muscle force distribution. The physiological justification and derivation of the method is discussed in detail in Chapter 5.

This fatigue measure proved effective for solving the redundant force problem, and when integrated over the period of the gait cycle also provides a useful objective function measure for the optimization of the walking simulation kinematics.

2.5 Walking Model Control Systems

Bipedal walking generally requires an active control system to maintain a continuous and stable walking gait. Of notable exception are the passive-dynamic walking models created by Tad McGeer and Art Kuo [40]. The models, after a great deal of careful tuning, were capable of maintaining a regular gait while walking down a smooth incline.

In the general case, however, a system is required to control the vertical orientation of the torso and the forward velocity of the model. Jerry Pratt has made some significant observations and developments in the area of control systems for bipedal robots in both his Masters [49] and PhD [50] research.

Using both computer simulations and physical robots, Pratt has developed successful strategies for maintaining stable and efficient gait. He observes that, when viewed as generic mechanical dynamic systems, bipedal walking mechanisms present an extremely difficult control problem. The system includes non-linear dynamics that change discretely at step transitions; the system is a multi-input multi-output (MIMO) model; and the biped is statically unstable. For these reasons, traditional controller design techniques are not well suited for the problem [50].

In contrast, if treated as a specific rather than general mechanism, certain features of the system dynamics can be used to advantage, and the problem can be solved by

decomposing it into subproblems that can be tackled at an intuitive level. His algorithms are based on a number of fundamental principles: control laws should be simple (linear and low-order); the problem should be decoupled into subproblems, such as maintaining pitch and maintaining velocity; and the controller should be intuitively based on the physics of the system, with parameters that are physically meaningful [50].

Pratt [49] notes that because bipedal robots are nonlinear, nominally unstable, time variant systems,

> ...it is difficult, if not impossible, to perform an acceptable mathematical analysis of why the control algorithms employed on these robots are successful in making them run.

Though lacking a mathematical proof of the control theory, the general methods proposed by Pratt were successfully applied to the control problems encountered in the development of this thesis.

2.6 Summary

Many methods have been developed in an attempt to accurately estimate the metabolic cost of walking using mechanical models of biological systems. While spanning a wide range of complexity, none of the traditional methods reviewed effectively accounts for all of the metabolic costs of motion, or for the tendency of biological systems to find a minimal-energy solution for a required motion.

By combining the techniques of inverse dynamics analysis, muscle fatigue, and numerical optimization, a more realistic model may be created that gives insight into the differences in energy consumption between normal and prosthetic gait.

Chapter 3

Optimization Model Overview

> Nature creates nothing without a purpose, but always the best possible in each kind of living creature by reference to its essential constitution. Accordingly if one way is better than another that is the way of Nature.
>
> - Aristotle, *On the Gait of Animals*, 350 B.C.
> translated by A. S. L. Farquharson

3.1 Motivation for Optimization

People can walk in many different ways, all of which accomplish the task of getting from one place to another. The different forms of walking are simple to distinguish; ambling, shuffling and marching all bring to mind very different motions, yet all produce forward progression. What is it then, that determines the natural gait patterns people select when walking freely?

This question was considered by Aristotle over 2300 years ago; his treatise *On the Gait of Animals* [6] reflects his observation that Nature tends to select the best possible solution available. The motion we observe is therefore Nature's optimal solution for the locomotion of a particular animal. This hypothesis has been tested many times by modern science, and found to hold true for human walking when the "optimal solution" means the most

energy-efficient motion [1], [18]. People naturally walk in whatever way gets them to their destination using the least amount of energy.

Numerous studies have observed the minimization of energy cost in human gait. Like other animals, humans have a "preferred walking speed" at which they walk if not otherwise constrained, as shown by Alexander [1]. Using oxygen consumption measurements, it has been repeatedly observed that the metabolic cost of locomotion (measured as energy consumption per unit distance traveled) is at a minimum at the preferred walking speeds, and increases at both faster and slower walking speeds [18], [72].

More recently, research by Donelan [26] has shown that subjects also have preferred values of other parameters of gait, such as step-width. Similar to deviations from the preferred walking speed, walking with a wider or narrower step than the naturally selected width results in greater energy consumption.

It seems reasonable then that a simulation of walking that is used to analyze the efficiency of gait should incorporate a similar cost optimization, in order to model the natural selection of energy-efficient walking motion.

3.1.1 Optimization in Simulation

This section gives an overview of the optimization method applied to the walking simulation, using the terms commonly used to define an optimization problem. Each of these elements of optimization are discussed in more detail in the remainder of the chapter.

3.1.1.1 Optimization Variables

The optimization variables are the parameters of the model that can be changed during the optimization process. For the walking simulation, the optimization variables are discrete values that are used to compute the hip, knee, and ankle kinematic joint trajectories. The optimization process is therefore modifying the kinematic patterns of the lower limb joints for each execution of the walking simulation.

3.1.1.2 Objective Function

To evaluate the quality of a particular set of values of the optimization variables, an objective function is required. The objective function gives a numerical result, the *objective value*, which represents the relative quality of the current set of optimization variable values. In this walking simulation, the objective function computes an estimate of the metabolic cost of walking a given distance, based on a calculation of muscle fatigue [19], discussed in detail in Chapter 5.

3.1.1.3 Search Algorithm

The goal of the search algorithm is to modify the optimization variables in such a way as to find the values that minimize or maximize the objective function. Depending on the nature of the problem this may be accomplished in several different ways. Often an iterative approach is used, where each step of the algorithm depends on the objective value of the previous step, which has led to the term *optimization loop*. Numerous texts give an introductory review of some common search algorithms that may be applied to this type of problem [25]. In this case, a pattern search algorithm [42] varies the joint kinematics and attempts to find the trajectories that minimize the total muscle fatigue over a given distance.

3.1.1.4 Expected Results

As with any model, this model of energy optimization is only an approximate representation of the behaviour observed in the real world, and is limited by our ability to represent the actual processes. The objective function, for example, does not attempt to compute the actual metabolic energy cost of the simulated motion, and does not include other factors that may contribute to human gait patterns (such as minimization of internal joint forces for example). Instead, the fatigue calculation gives a measure that is well correlated with metabolic cost [19], and therefore serves to guide the search algorithm in an appropriate direction.

Supposing that this model reasonably represents the tendency of humans to walk in a way that minimizes energy cost, the result of the optimization process should be a set of

joint kinematics that reasonably match those measured in experimental studies of walking gait.

3.1.2 Effect of Optimization on Parameter Measurement Errors

In addition to finding kinematic patterns that are based on energy-minimization goals similar to natural human gait, a potential benefit of an optimization loop around the simulation is that the effects of errors in model parameters may be reduced. When building a mechanical simulation of walking based on experimentally measured data, some errors will always be present. For example, measurement of the moments of inertia and mass centres of limb segments are not exact, because the limb segment cannot be removed from the body and measured precisely.

By incorporating a cost minimization in the model, the result of the simulation is not the cost of an approximate representation of a person forced to walk following the trajectory of a slightly different person. Instead, the result reflects the optimal cost of walking for the model, which need not be identical to the parameters of the original subject. As shown in this section, when simulating oscillatory systems such as simple pendulums and walking motion, the optimization of the motion can lead to a substantial difference in energy cost for a very small change in the motion of the system.

To estimate the effect of inaccuracies in model measurements, consider a simple model of a frictionless pendulum, driven by a motor torque τ at the pin joint and swinging through a small angle, as shown in Figure 3.1. This example is particularly relevant to the simulation of walking, since the leg can swing with a pendulum-like motion during the swing phase of the gait cycle, and the joint torques are created by muscles.

For this example, the variable of interest is the frequency ω at which the pendulum is driven by the motor; the goal is to find the value of ω that requires the minimum amount of energy from the motor. A reasonable estimate for the optimal value of ω is the natural frequency of the pendulum if it were swinging freely. The impact of a small error in the estimate and the effectiveness of optimization in reducing this impact are investigated in the remainder of this subsection.

If the torque of the motor is set to zero, the pendulum swings freely at its natural frequency, requiring no energy input. For rotations of small magnitude A, using the linear

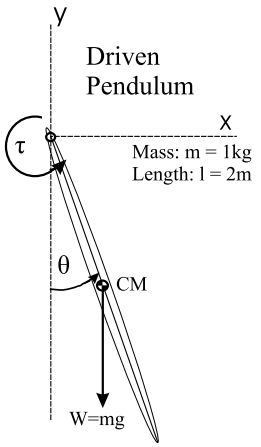

Figure 3.1: Driven Pendulum Model

approximation $\theta \approx \sin(\theta)$, the motion of the pendulum is given by:

$$\theta(t) = A\cos(\omega_0 t) \tag{3.1}$$

when the pendulum is released from rest at $\theta(0) = A$. The natural frequency of the pendulum, ω_0, is computed from the mass m, the acceleration of gravity g, distance d from the center of mass to the pivot point, and moment of inertia I:

$$\omega_0 = \sqrt{\frac{mgd}{I}} \tag{3.2}$$

For this example, using $g = 9.81 m/s^2$ and assuming the pendulum is a uniform thin rod with mass $m = 1.0kg$ and length $l = 2m$, the computed natural frequency is $\omega_0 = 2.711 rad/s$.

If the motor drives the pendulum through a specified trajectory given by

$$\theta = A\cos(\omega t) \tag{3.3}$$

where A is a small angle as used in Equation (3.1) and ω is close to the natural frequency ω_0, the energy required by the motor should be close to zero, since the dynamics of the pendulum produce almost the same kinematics with no applied torque. However, some

energy will be required because the trajectory equation and natural frequency were derived using a linear approximation of the non-linear system, and are therefore not exact.

To estimate the error introduced in the energy calculation of the model due to the approximation used to calculate ω_0, a simulation of the driven pendulum was generated in Working Model 2D [53]. A kinematic driver was used to control the joint angle according to Equation (3.3), with an amplitude of $A = 5°$ for a duration of 6 seconds. Working Model includes a simple optimization script that varies one parameter within a specified range to minimize a single measure. The optimization was configured to vary the frequency ω (the optimization variable) and to minimize the total energy consumed by the torque driver at the joint (the objective function) over a fixed period of time. The objective function was calculated by integrating the product of the torque and joint velocity over time, to compute the total mechanical work performed by the torque driver:

$$W = \int_0^6 \tau\dot{\theta}dt \tag{3.4}$$

The optimization loop was started with an initial value of $\omega = 2.711 rad/s$, equal to the computed natural frequency. It then found the optimal driving frequency for minimal energy consumption ω_{opt}, and the corresponding amount of energy required to drive the motor.

The results of the simulations are summarized in Table 3.1. The first column shows the simulation results of driving the motor at the computed natural frequency $\omega = \omega_0$. In the second column are the results of the simulation driven at the optimal frequency $\omega = \omega_{opt}$. The third column shows the error in the computed natural frequency and the additional energy cost of driving the motor at the computed frequency.

	Computed (ω_0)	Optimized (ω_{opt})	Error in Computed
$\omega(\frac{rad}{s})$	2.711	2.915	$\mathbf{-0.204(-7\%)}$
$W(J)$	0.961	0.019	$\mathbf{0.942(4957\%)}$

Table 3.1: Sensitivity of energy analysis to parameter error

From the third column, note that the computed natural frequency is 7% less than the optimal frequency; however, the energy required to drive the simulation at this frequency

is almost 50 times the amount required at the optimal frequency. The magnitude of this error is a function of the amplitude of the pendulum motion; the larger the amplitude, the greater the error in the linear approximation of the natural frequency. While in this example the parameter error was due to a linear approximation of a non-linear system, an error in measurement of the physical system parameters (mass or moment of inertia for example) would have a similar effect since it would result in a different natural frequency for the model than for the actual system.

Since walking motion involves similar cyclic and pendulum-like motion of the legs, it is likely that unavoidable small errors in the model parameters and un-modelled dynamics of the system may result in significant errors in the energy consumption estimates for the simulated model. The use of an optimization algorithm in the simulation eliminates these errors by finding the optimal kinematics for the modeled system, effectively correcting for errors in measurement of the original system.

3.1.3 Comparison of Results with Model Variations

Another benefit of this optimization approach is that more useful comparisons can now be made between simulations with different models. For example, when simulating a model with a prosthetic leg, the change in efficiency of the most optimal gait can be observed as the mass distribution of the prosthesis is changed. The desired or expected motion of the models being compared is not required to run the simulation; instead the optimal motion is generated by the simulation itself.

3.2 Optimization Loop Components

The components of the optimization loop and the flow of computed variables between components are shown in Figure 3.2. In the variable names, the subscript $Init$ represents the initial guess for the search algorithm, it represents the variables at each iteration of the loop, and Opt represents the final values found by the system. The components in the block diagram are described in the remainder of this chapter.

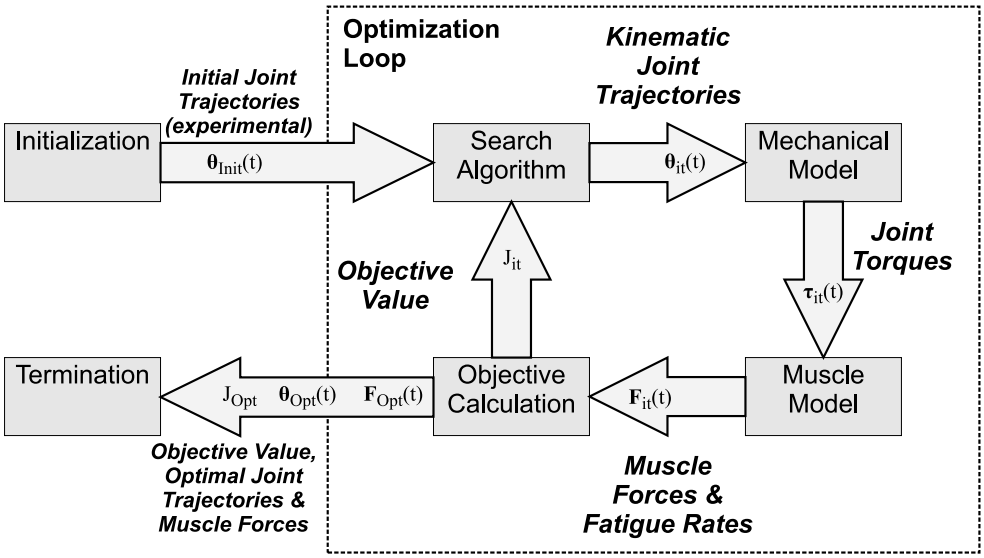

Figure 3.2: Fatigue-Minimization Optimization Loop

3.2.1 Joint Trajectory Variables

The optimization variables being controlled are the kinematic trajectories of the ankle, knee, and hip joints as functions of time for one period of steady-state walking motion. One period consists of a complete cycle from heel contact to the following heel contact of the same foot. To represent the trajectories (which are continuous functions) in terms of a set of discrete optimization variables, a Fourier series representation is used. This representation is ideal for this problem since the trajectories are periodic with one period per stride.

A five-term series was used for each joint function $\theta_j(t)$, as defined in Equation (3.5):

$$\theta_j(t) = C_0 + \sum_{k=1}^{5} \left[A_k \sin\left(\frac{2\pi kt}{period}\right) + B_k \cos\left(\frac{2\pi kt}{period}\right) \right] \tag{3.5}$$

where C_0 is the DC (constant offset) coefficient, A_k and B_k are the coefficients of the sin and cos terms at the k^{th} multiple of the fundamental frequency ($f = 1/periodHz$), and *period* is the length of one complete gait cycle in seconds.

To find initial values for the coefficients, a curve-fitting method was used to match the Fourier series function to empirical data measured from human subjects [69]. The curve-fitting method fits functions to data points by solving an optimization problem where the optimization variables are the function parameters and the objective function is the sum of the mean squared error between each data point and the corresponding value of the curve function. In this case, the method was used to solve for the values of the coefficients of the Fourier series function that most closely fit the experimentally measured data. For details of the implementation and the computed coefficient values, refer to Appendix A. The measured data and the Fourier series curves for the joints of one limb are shown in Figure 3.3.

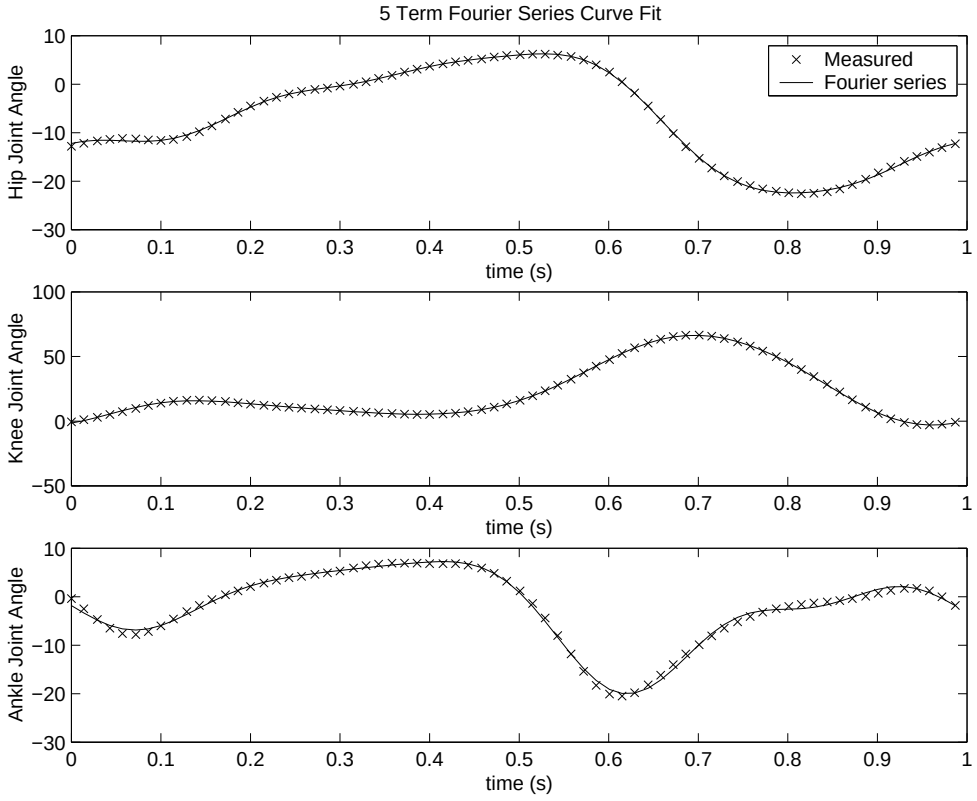

Figure 3.3: Fourier Series Representation Curve Fitting

To generate the kinematic trajectories for the opposite leg, the functions are simply shifted in phase by 180 degrees:

$$\theta_j(t) = C_0 + \sum_{k=1}^{5} \left[A_k \sin\left(\frac{2\pi kt}{period} + k\pi\right) + B_k \cos\left(\frac{2\pi kt}{period} + k\pi\right) \right] \tag{3.6}$$

Given this representation, the optimization algorithm can completely specify the joint kinematic trajectories, containing components up to a frequency of 5 times the gait cycle frequency, by varying the Fourier series coefficients.

3.2.2 Search Algorithm

The purpose of the optimization search algorithm is to vary the optimization variables to find the set of values that minimizes the objective function. The optimization algorithm uses the change in objective value to determine the relative quality of the current kinematic trajectories of the joints, and to guide the search for an improved trajectory.

There are a wide variety of search algorithms available to solve non-linear optimization problems [25]. Many are gradient based methods that require an expression for the derivative of the objective function in terms of the optimization variables. For the walking gait optimization, numerical simulations are required to compute the joint torques, muscle forces, and muscle fatigue to evaluate the objective function, as described in Section 3.2.5. There is therefore no analytical expression relating the value of the objective function to the optimization variables, making gradient based methods less practical.

Instead, a pattern search algorithm is used, which is one form of the direct search optimization techniques commonly applied to such numerical non-linear problems. The pattern search method is relatively straightforward in concept and implementation, and is described in detail by Lewis and Torczon [42]. Conceptually, a search is performed by varying each of the optimization variables by steps of a given value, which is called the grid size. The initial value of the grid size is relatively large, allowing large steps to be taken around the search space.

By following a pattern that decreases the value of the objective function, the optimal point is found in the search space for the current grid size. Starting at this new base point, the grid size is then reduced by a factor of 2, and the pattern search is repeated, to find

a more accurate minimum within a smaller search space. This algorithm is repeated until the grid size is reduced to the desired resolution of accuracy of the optimization variables.

An initial grid size for the pattern search is specified that determines the variation applied to each variable at each iteration. A value of 0.25 radians was selected to allow for variations in the trajectories of approximately 15 degrees with each optimization step. This was found to be the largest practical variation in the kinematics while maintaining a reasonable gait pattern. As the search progresses and new optimal points are found, the grid size is reduced to refine the search.

The algorithm is terminated after the grid size is reduced to a pre-defined value. A value of 0.0025 radians was selected, based on observation of the convergence of objective function as the variation in the trajectory variables was reduced to that value. At termination, the optimal objective value, joint trajectories, and muscle forces are saved as the final result of the optimization loop.

3.2.3 Mechanical Model

The joint trajectories selected by the search algorithm are used to drive a mechanical model simulation, implemented using the MSC.ADAMS dynamics simulation package. This mechanical model attempts to drive the joints through the specified trajectories, and computes the torques required to drive the model through the specified trajectories at each joint. The output of this model is the set of joint torques over time that correspond to the kinematics of the current iteration. The design and implementation details of the model are presented in detail in Chapter 4.

3.2.4 Muscle Force Distribution Model

The purpose of the muscle model is to determine the muscle forces required to generate the torques computed by the mechanical model, by considering the contribution of each muscle group in the lower limb. Nine major muscle groups involved in locomotion are included in the muscle model. For each muscle group that crosses a particular joint, the torque generated around that joint is the product of the contractile force in the muscle and the moment arm between the muscle and the joint centre.

The expression relating the three joint torques (ankle, knee, and hip) to the nine muscle forces at an instant in time is therefore:

$$\boldsymbol{\tau} = \mathbf{MF} \tag{3.7}$$

where $\boldsymbol{\tau}$ is a 3×1 vector of torques, $\mathbf{F}$ is a 9×1 vector of muscle forces, and $\mathbf{M}$ is 3×9 matrix of moment arms, where each element (i, j) is the shortest distance between joint i and muscle j. The moment arms are approximated as constant in this work, since the rotations of the joints during normal walking are relatively small.

The determination of the muscle force patterns required to produce the calculated joint torques is a non-trivial problem, since for any instant in time, Equation (3.7) has an infinite number of solutions for $\mathbf{F}$, given $\boldsymbol{\tau}$ and $\mathbf{M}$. Physically, most of these solutions correspond to various levels of co-contraction, which is the activation of opposing muscles across one joint. Solutions containing negative values in $\mathbf{F}$ are invalid, since muscles can only produce contractile (positive) force.

To find a unique and valid solution, another optimization process is applied, which determines the set of muscle forces that can produce the required joint torques while minimizing the total muscle fatigue, computed as a function of the stress in each muscle. This component is based on the muscle force distribution method proposed by Crowninshield [19], and is described in detail in Chapter 5.

3.2.5 Objective Function Calculation

The objective for the walking model is to minimize total muscle fatigue while covering the greatest distance possible. The objective value Φ is computed by integrating the muscle fatigue rates computed by the muscle model component, summing across all of the muscles, and dividing by the distance traveled by the centre of mass of the model (d_{CM}):

$$Fatigue = \sum_{m=1}^{n_{muscles}} \int FatigueRate_m dt \tag{3.8}$$

$$\Phi = \frac{Fatigue}{d_{CM}} \tag{3.9}$$

Chapter 5 includes details of the computation of the fatigue rate for each muscle.

Chapter 4

Mechanical Model

4.1 Model Design

To determine the joint torques required to generate the motions observed in human walking, a mechanical model of the body is required. The underlying principles of mechanical model analysis of human gait are well established, and have been used since the work of Fischer in 1906 [29] and Elftman in the 1930s [28].

A two-dimensional (2D) multibody mechanical model of the body is typically constructed by representing each limb segment as a rigid body, and each joint as a constraint upon the relative motion of the rigid bodies, as shown in Figure 4.1. Each leg is modelled as 3 rigid bodies representing the foot, shank, and thigh, connected by revolute (pin) joints representing the ankle, and knee. The upper body consisting of the head, arms, and trunk (HAT) is modelled as a single rigid body, connected to the legs by two revolute joints representing the hips.

Other than the gravitational force on each limb segment, the only externally applied forces are the ground reaction forces (GRF) applied to the feet. For each foot, the reaction force consists of a vertical component that supports the weight of the body, and a horizontal component representing friction with the ground. Depending on how the model is used, these forces may be known from measured force-place data (for an inverse-dynamics analysis), or may be generated during the simulation (for a forward-dynamics simulation).

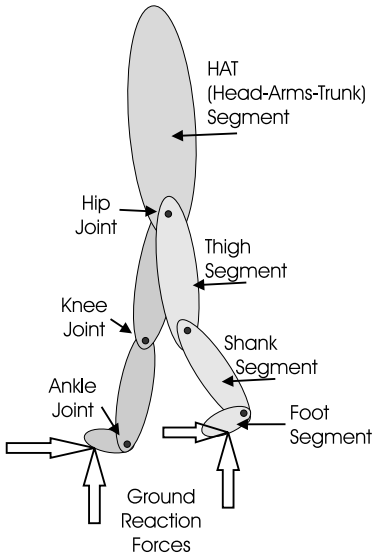

Figure 4.1: Typical multi-body mechanical walking model

4.1.1 Model Complexity Considerations

Many improvements can be made to this simple model to better reflect the true mechanics of the human body. The upper body could include shoulder and elbow joints allowing for swinging arm motion. The torso could be modelled as a flexible body reflecting the flexibility of the spine. The hip and ankle joints would be more accurately modelled as spherical joints, allowing rotation about all three axes instead of one, and the joint centres could be determined as a function of the joint angle to accurately reflect the rolling motion of biological joints.

However, determining an appropriate degree of fidelity in the model involves a tradeoff between computational complexity and the improvements in results given by a more accurate model. A finely detailed model that includes all of the subtleties of human motion may produce more accurate results; but if the model includes too much detail, the problem becomes intractable due to the increased complexity in solving the equations of motion, and the model is of no value at all.

4.1.2 Selection of a 2D vs 3D Model

For the development of this model, a 2D analysis was selected over a 3D model. This selection was based on a number of factors. Primarily, the vast majority of limb motion during steady level walking is in the sagittal plane, and a common modelling approach is to assume that motion in the transverse and frontal planes is negligible. This is particularly relevant for comparison of results to other studies of both models and human subjects, since often only sagittal plane results are available, such as those by Anderson and Pandy [3] and Winter [69].

Extending the joint model to support 3D motion is relatively trivial. Additional revolute joints can be added at the ankle and the hip to support rotation around three axes. However, many other aspects of the simulation become more complex. Solving the muscle force distribution problem (discussed in Chapter 5) becomes substantially more difficult since each muscle may generate a torque about an arbitrary 3D axis at each joint. Stabilization of the model also becomes more challenging since the sway (about the sagittal axis) and yaw (about the vertical axis) of the torso must be controlled, in addition to the pitch stabilization required for a 2D model. This stabilization problem is discussed in more detail in Chapter 6. Since the interest of this study is the substantial energy transfer between limb segments, which occurs primarily in the sagittal plane, the additional complexity of a 3D model was not justified.

4.1.3 Foot Contact Model

Modelling the reaction force of the ground is one of the most challenging aspects of the model developed in this thesis. In most analyses of walking where data is taken from a human subject, the reaction forces are measured by having the subject walk across a force plate on the ground, such as those by Burdett [13] and Gitter [34]. The measured reaction forces are then used as external forces applied to the mechanical model.

In the simulations developed in this thesis, however, the reaction force data must be generated by the model as each variation in gait is analysed. This requires a model of foot contact at the floor that includes a vertical reaction force supporting the weight of the model and a horizontal force representing friction between the foot and the ground.

To allow for a realistic analysis of the full gait cycle, a foot-floor contact model was created within the ADAMS simulation package. Refer to Appendix A for more details regarding the simulation implementation details. Contact forces are defined as a force between two ADAMS geometry elements, which may be certain combinations of one-dimensional (points), two dimensional (planes and surfaces) or three-dimensional geometries. Simulations were created with two different contact models: one based on three-dimensional models, where the floor was a rectangular box and the foot was represented as an ellipsoid; and a second simpler model where the floor was a flat plane and the contact with each foot was defined for two points, one at the foot and one at the heel.

The three-dimensional contact model was expected to give better results, since the ellipsoidal foot shape would allow the foot to roll more naturally over the floor from heel contact to toe-off. However, computing the contact conditions of overlap between the two three-dimensional objects is very computationally expensive, and resulted in extremely slow simulations, requiring 10 minutes for a simulation of two steps on a 1.8GHz Pentium 4 PC.

The point-to-plane contact model is a computationally simpler model, requiring only a calculation of the distance between each point and the plane of the floor to determine the contact conditions. The resulting simulation ran approximately 20 times faster, requiring only 30 seconds for a simulation of two steps. The reaction forces from the simpler model were also found to match the reaction forces measured from experimental force place data reasonably accurately. The contact model for one heel contact point is shown in Figure 4.2, and defined in Equation (4.1).

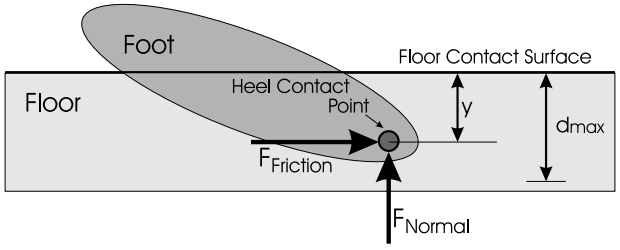

Figure 4.2: Point-to-plane contact model

When a contact condition is detected, the model computes the normal (vertical) contact

force on the foot F_{Normal} using a non-linear spring and damper expression:

$$F_{Normal} = k(y^e) + Step(y, 0, 0, d_{max}, c_{max})\dot{y} \tag{4.1}$$

where y is the penetration between the contact point and floor contact surface, and $\dot{y}$ is the penetration rate. In the first term, the contact parameters k and e determine the spring coefficient and spring exponent. In the second term, a damping force is added that is proportional to the penetration rate $\dot{y}$. The damping coefficient is a function that varies linearly between 0 and c_{max} (maximum damping coefficient) as y varies between 0 and d_{max} (overlap required for maximum damping). The damping coefficient is 0 for $y < 0$, and c_{max} for $y > d_{max}$. This step function smoothly ramps up the damping force as contact penetration increases. This avoids the instantaneous normal force that would otherwise be created at initial contact by a simple damping term such as $(c_{max}\dot{y})$.

The horizontal force ($F_{Friction}$) at the contact point is modelled using a coulomb friction force given by the expression:

$$F_{Friction} = \mu N sgn(\dot{x}) \tag{4.2}$$

where $\dot{x}$ is the relative horizontal velocity of the contact point to the floor, and μ is the coefficient of friction; the $sgn(\dot{x})$ term ensures that $F_{Friction}$ acts in a direction opposing the relative motion. A more complex friction model including transitions between static and dynamic friction coefficients was considered. In this application, however, it was found by experimentation to be sufficient to use a constant coefficient, since slipping and dynamic friction effects were negligible.

Nominal values of the contact force parameters were taken from ADAMS documentation for contact between nylon and steel to approximate the contact surface between the sole of a shoe and a hard floor. To further approximate the behaviour of realistic contact forces during normal human walking, the contact model parameters were tuned to generate ground reaction forces similar to those measured by Winter [69] using a force plate (refer to Figure 4.3). Table 4.1 summarizes the contact model parameters used in the model.

The ground reaction forces were computed for 15 consecutive steps of the walking model, and the average and standard deviation are plotted in Figure 4.3.

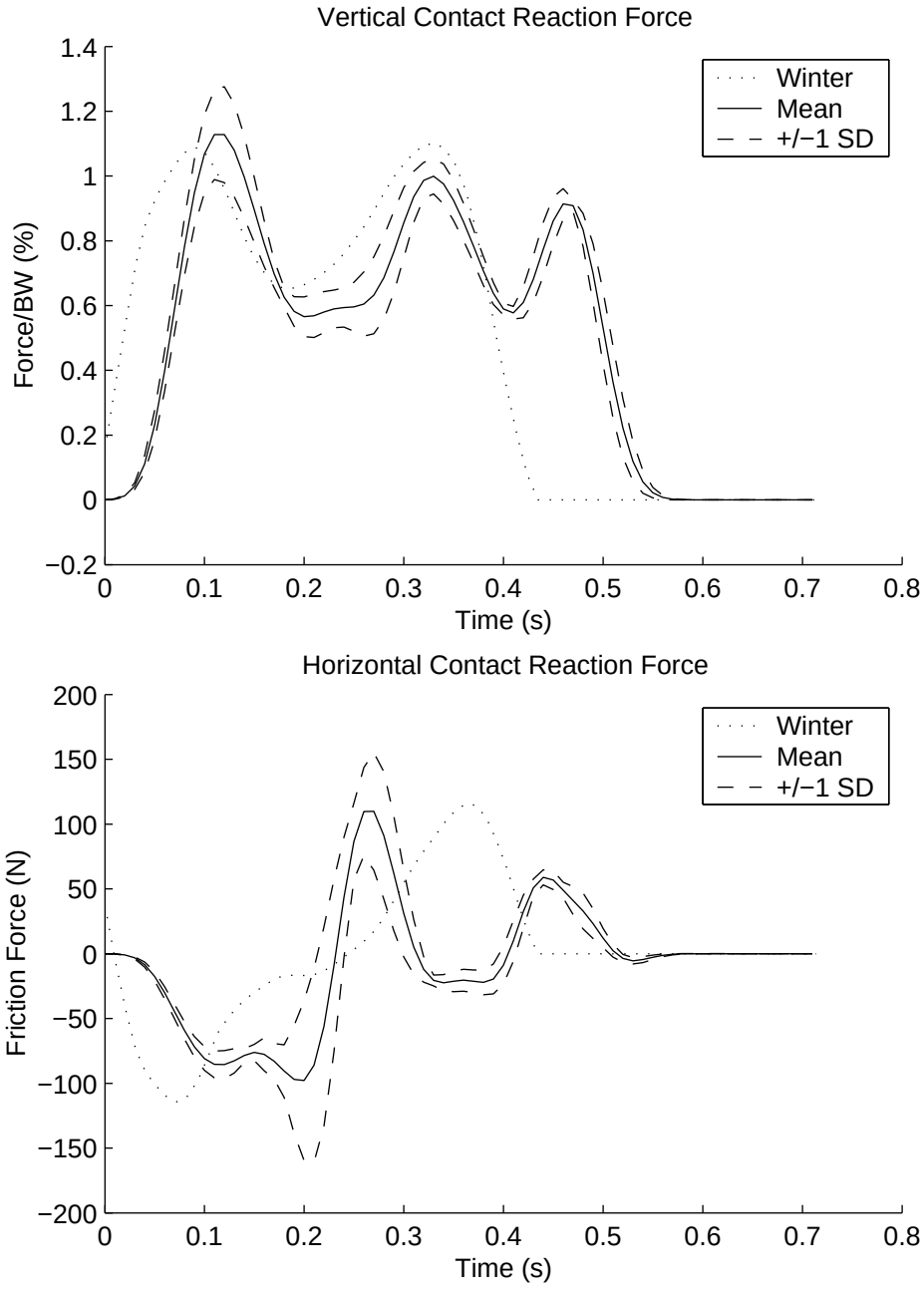

Figure 4.3: Computed Ground Reaction Contact Forces

Parameter	Symbol	Value
Spring Coefficient	k	$2.0^6 N/m$
Spring Exponent	e	2.2
Max Damping Coefficient	c_{max}	$1500 N/(m/s)$
Max Damping Penetration	d_{max}	$1mm$
Friction Coefficient	μ	0.4

Table 4.1: Contact Model Parameters

4.1.4 Degrees of Freedom and Torso Constraints

For a 2D model containing only revolute joints, the number of degrees of freedom (DOF) is given by the expression $DOF = 3nb - 2nj$, where nb is the number of rigid bodies in the system, and nj is the number of revolute joints. Each body has three DOF (two translational and one rotational), and each revolute joint removes two DOF.

For the model consisting of a HAT, three limb segments per leg, and three joints per leg (see Figure 4.1), $DOF = 3 \times 7 - 2 \times 6 = 9$. By specifying the trajectories of all six joints with kinematic drivers, six DOF are removed, leaving $DOF = 3$. These can be considered the vertical and horizontal position of the torso and its orientation, with the positions and orientations of the rest of the limb segments specified relative to the torso.

4.1.5 Prosthetic Modelling

To model the effect of a below-knee prosthetic limb, two different variations were made to the model. In the first, the kinematic driver controlling the ankle joint was replaced with a torsional spring-damper, representing a flexible ankle joint with energy storage capability. In the second variation, the ankle was replaced with a fixed joint allowing no rotation and no energy storage, representing a simple solid-ankle-cushioned-heel (SACH) prosthetic foot.

4.1.5.1 Spring-Damper Ankle Joint Model

The spring stiffness parameter was initially determined by dividing the maximum joint torque measured in the normal model by the maximum joint deflection angle. This resulted in the spring generating a torque and range of motion similar to the normal angle driver. The passive ankle parameters were then included as optimization variables in the optimization algorithm to allow the model to find the optimal values to minimize energy consumption.

4.1.5.2 SACH Ankle Joint Model

The fixed joint at the ankle was implemented with a motion driver with a fixed rotation. The use of a motion driver allowed the ankle torque to be measured while removing one degree of freedom from each leg.

4.2 Equations of Motion for a Multibody System

4.2.1 Kinematic and Dynamic Equations

Based on a multibody mechanical model of the human system, a set of equations can be derived that describe the motion of the system over time. The first set of equations are dynamic equations based on Newton's Second Law, $\vec{F} = m\vec{a}$ in vector form, and the corresponding equation for rotational motion $\vec{\tau} = I\vec{\alpha}$. In terms of the acceleration of the position vector ($\ddot{\vec{r}} = \vec{a}$) and orientation angle ($\ddot{\vec{\theta}} = \vec{\alpha}$), these give second-order vector differential equations of motion for each body.

Writing these vector equations in matrix form allows simpler manipulation of the equations for multiple bodies. Using bold symbols to represent column matrices where each element contains a component of the corresponding vector gives:

$$m\ddot{\mathbf{r}} = \mathbf{F} \tag{4.3}$$

$$I\ddot{\boldsymbol{\theta}} = \boldsymbol{\tau} \tag{4.4}$$

A second set of equations represents the kinematic constraints imposed by the joints in the model. The formulation of equations for a variety of kinematic constraints is given in [36]. For this model, equations for only revolute joints are required; these algebraic equations equate the position vectors of the connection points between pairs of connected bodies. Where $\mathbf{r}_i$ gives the position of the center of mass of body i and $\mathbf{s}_i^P$ is a vector from the center of mass to the joint position P on body i, the joint constraint between two bodies i and j is defined by requiring the position of the joint on both bodies to be equal:

$$(\mathbf{r}_i + \mathbf{s}_i^P) = (\mathbf{r}_j + \mathbf{s}_j^P) \tag{4.5}$$

A solution to the set of these equations for all the joints in the system gives the positions and orientations of each of the bodies in a feasible configuration.

4.2.2 Formulation of Kinematic Equations

More formally, the equations of motion for a constrained multibody system can be systematically assembled for solution by a computer algorithm as described in [36]. In such a formulation, the position and orientation of all bodies in the system are defined by a column matrix of *generalized coordinates* $\mathbf{q}$.

The kinematic constraint equations can then be written in terms of $\mathbf{q}$, and the set of all constraint equations are denoted by the column matrix of equations:

$$\mathbf{\Phi}(\mathbf{q}, t) = \mathbf{0} \tag{4.6}$$

Additionally, the velocity and acceleration of common joint points on bodies i and j must be equal. Differentiating the position constraint expression $\mathbf{\Phi}(\mathbf{q}, t) = \mathbf{0}$ with respect to time (using the chain rule) gives the velocity constraint equation:

$$\mathbf{\Phi_q}\dot{\mathbf{q}} + \mathbf{\Phi}_t = \mathbf{0} \tag{4.7}$$

where $\mathbf{\Phi_q}$ is the Jacobian matrix, obtained by taking the partial derivative of each of the equations in $\mathbf{\Phi}$ with respect to each of the generalized coordinates in $\mathbf{q}$, and $\mathbf{\Phi}_t$ is the partial derivative of $\mathbf{\Phi}$ with respect to time. Repeating the differentiation gives the acceleration constraint equations:

$$\mathbf{\Phi_q}\ddot{\mathbf{q}} + (\mathbf{\Phi_q}\dot{\mathbf{q}})_\mathbf{q}\dot{\mathbf{q}} + 2\mathbf{\Phi}_{\mathbf{q}t}\dot{\mathbf{q}} + \mathbf{\Phi}_{tt} = \mathbf{0} \tag{4.8}$$

The position, velocity, and acceleration constraint equations must all be satisfied at each instant in time during the model simulation.

4.2.3 Formulation of Dynamic Equations

In terms of the generalized coordinates and generalized forces, the dynamic equations of motion for an unconstrained system are given by:

$$\mathbf{M}\ddot{\mathbf{q}} = \mathbf{Q} \tag{4.9}$$

where $\mathbf{M}$ is a mass matrix containing the mass and moments of inertia of each of the rigid bodies, and $\mathbf{Q}$ includes the applied forces and torques acting on the system. The sets of dynamic and kinematic constraint equations, along with initial conditions $\mathbf{q}_0$ and $\dot{\mathbf{q}}_0$ at time $t = 0$, describe the behaviour of the system for any time $t > 0$.

4.2.4 Method of Lagrange Multipliers

The method of Lagrange multipliers is used to incorporate the constraint equations into the dynamic equations of motion, and is described in detail in texts on classical dynamics, such as [33]. The Lagrange Multiplier Theorem [36] guarantees that if the constraint equations $\mathbf{\Phi}_q \delta\mathbf{q} = 0$ hold for all $\delta\mathbf{q}$ (variations in $\mathbf{q}$) that satisfy the dynamic equations, then there must exist a vector $\boldsymbol{\lambda}$ such that, for any $\delta\mathbf{q}$,

$$(\mathbf{M}\ddot{\mathbf{q}} + \mathbf{\Phi}_\mathbf{q}^T\boldsymbol{\lambda} - \mathbf{Q})\delta\mathbf{q} = 0 \tag{4.10}$$

Since $\delta\mathbf{q}$ may take arbitrary values, the first term must be zero. Using this result gives the Lagrange multipliers form of the equations of motion:

$$\mathbf{M}\ddot{\mathbf{q}} + \mathbf{\Phi}_\mathbf{q}^T\boldsymbol{\lambda} = \mathbf{Q} \tag{4.11}$$

In this expression, the column of Lagrange multipliers $\boldsymbol{\lambda}$ represents the reaction forces of the constraints in the system. For pin joints, solving for the Lagrange multipliers gives the magnitude of the internal forces required to hold the two bodies together at that joint. Where a kinematic driving constraint is used to specify the motion of the system, a

corresponding Lagrange multiplier term represents the applied torque required to achieve the desired motion.

4.2.5 Solution of Dynamics Equations

Equations (4.9) and (4.11) together form a set of differential algebraic equations (DAEs) that define the response of the system to specified applied forces. Due to the complexity and nonlinearity of these equations of motion, it is generally not possible to find a closed-form solution. Instead, a numerical integration method is required to solve these equations of motion for the position $\mathbf{q}_{t+1}$ given $\mathbf{q}_t$.

A variety of numerical methods are available, with differing degrees of speed, accuracy, and robustness. The selection of an appropriate algorithm depends on the stiffness of the system being modelled, the nature of the applied forces (being continuous vs intermittent, as in the case of contact forces), and the relative importance of accuracy vs speed of convergence.

To determine an appropriate integration step size, and to ensure that the integrator numerical error was acceptably small, a convergence study was performed. In such a study, the simulation is repeated with progressively smaller integration step sizes. When the difference between results of consecutive simulations is sufficiently small, the step size is appropriate for the model and the selected integrator.

After experimentation with various integrator methods and formulations available, the Gear stiff (GSTIFF) integrator method and I3 formulation were found to give accurate results and reasonably fast simulations with a step size of 0.01 seconds.

The joint torques were computed for 15 consecutive steps of the walking model, and the average and standard deviation are plotted in Figure 4.4.

4.3 Implementation

4.3.1 Multibody Model

Rigid bodies are used to represent each lower limb segment, and the torso. The hip, knee and ankle are modelled as revolute joints connecting the lower limb segments and the

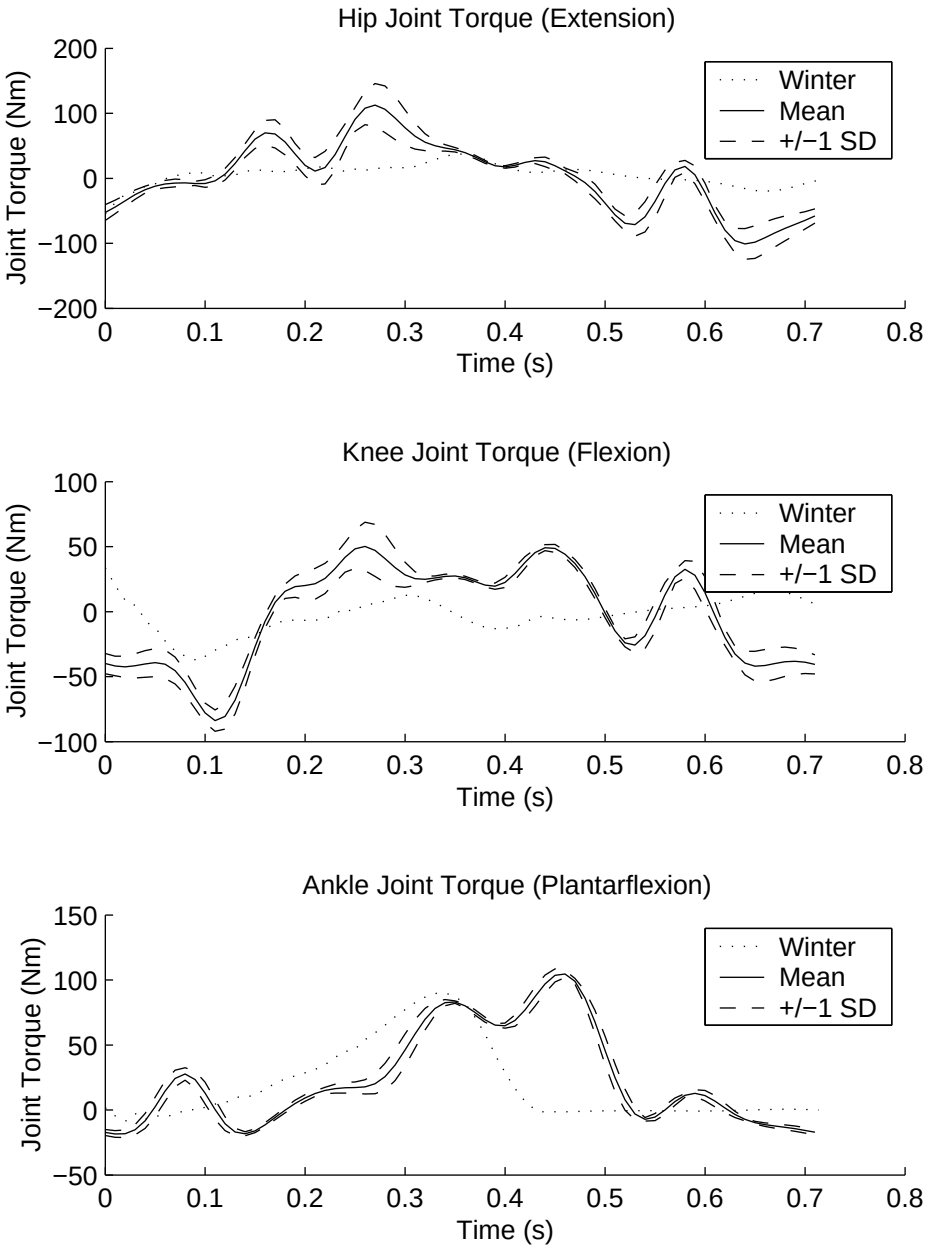

Figure 4.4: Computed Joint Torques

torso, completing the model components required for the simulation. Since the joints have parallel axes, the motion of the model is planar.

Additional rigid bodies for the pelvis, upper torso, neck and head are included to complete the visual representation and to correctly represent the mass distribution. However, all of the rigid bodies above the lower limbs are connected with rigid joints preventing any relative motion. For the purposes of the simulation, they can be considered a single rigid body.

The hip, knee and ankle joints are driven by feedback control torques. The expression for each joint torque drives the joint position through the desired kinematic pattern selected by the optimization algorithm, with an additional control component to maintain the balance of the model. The details of the control algorithm and joint torque calculations are described in Chapter 6.

The resulting model is shown in Figure 4.5. The applied joint torques are indicated at the hip, knee, and ankle joints, while the upper body components are rigidly connected.

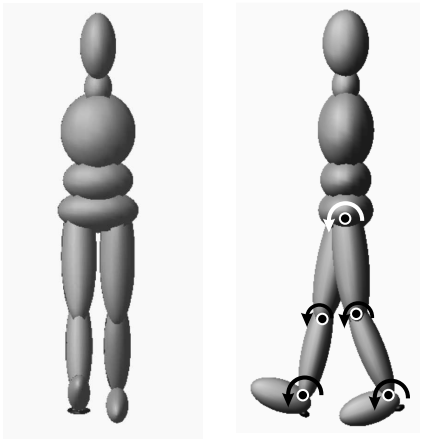

Figure 4.5: Mechanical model

The multibody model dimensions, moments of inertia, and joint positions were based on data from the LifeMOD Biomechanics Modeler, produced by Biomechanics Research Group Inc. The values are determined from the statistical average values for a 25 year old North American male subject. Table 4.2 summarizes the segment parameters used in the

model.

Segment	Mass (kg)	Izz ($kg \cdot m^2$)	Length (mm)
Head	5.03	2.70E-02	256
Neck	1.30	2.61E-03	145
Torso (including arms)	21.63	1.74E-01	348
Central Torso	7.47	4.94E-02	77
Lower Torso	8.63	6.77E-02	92
Upper Leg	7.88	1.49E-01	440
Lower Leg	3.54	3.96E-02	376
Foot	2.05	8.53E-03	220

Table 4.2: Limb Segment Parameters

Chapter 5

Muscle Model

5.1 The Muscle Force Distribution Problem

To obtain an estimate of the physiological energy cost of a given motion, a measure of the muscle forces involved is required. At each joint in the leg model, two or more muscle groups act in tension to produce a net joint moment on the two limb segments at that joint. The contribution of each muscle to the net moment is equal to the instantaneous muscle force times the moment arm between the muscle and the joint centre.

For a set of m muscles acting around n joints, the force to torque relationship may be summarized by the following equation:

$$\boldsymbol{\tau}_{(n\times 1)} = \mathbf{M}_{(n\times m)}\mathbf{F}_{(m\times 1)} \tag{5.1}$$

where $\boldsymbol{\tau}$ is the column matrix of joint torques required at an instant in time and $\mathbf{F}$ is the column of muscle forces. $\mathbf{M}$ is a matrix of moment arms, where the element $M(i,j)$ is the moment arm of muscle j about joint i.

The muscle force distribution problem is to solve Equation (5.1) for the muscle forces $\mathbf{F}$ given a set of joint torques $\boldsymbol{\tau}$. The problem is in general non-trivial because, as will be shown for the leg muscle model, the system contains more variables than equations ($m > n$).

In the human body, the moment arm of each muscle varies as a function of the angle of the joint it crosses, as does the joint centre. For the purposes of this model, the moment

arms are assumed to be constant, and the average moment arms are taken from the nominal values given by Raikova [51]. This assumption is common in models of human walking, since the range of joint motion is relatively small, resulting in a relatively small variation in the position of the joint centers and the muscle moment arms.

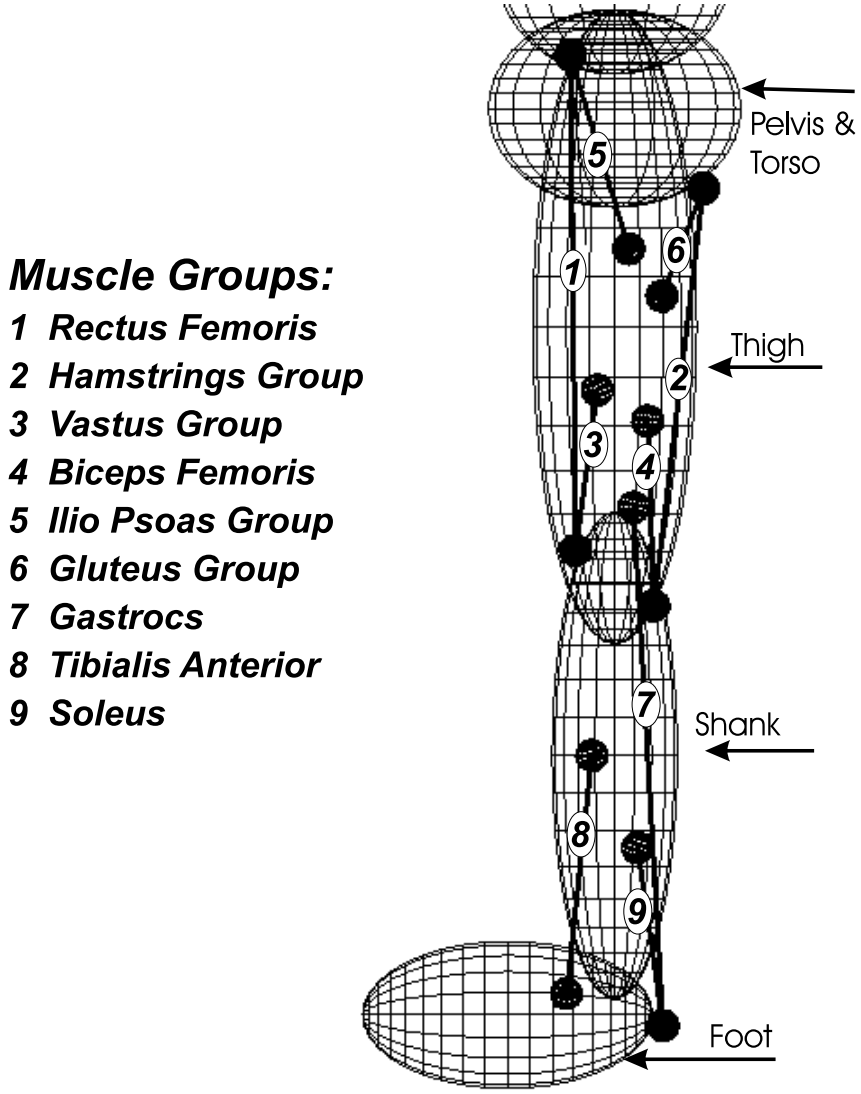

Figure 5.1: Lower Limb Muscle Model

Figure 5.1 shows the major muscle groups included in the model. The selected muscle groups are the primary actuators involved in the sagittal plane leg motion, and have been used in similar analyses, such as that by Spagele [60].

From the dynamic analysis of the mechanical model for a particular kinematic motion, the required joint moments are known for each instant in time of the simulation. The muscle force distribution problem is to determine the muscle forces that would be used to generate these joint torques. If a unique pair of muscles crossed each joint this would be a trivial problem; the active muscle would be selected based on the direction of the joint torque, and the force would be calculated by dividing the torque by the length of the moment arm.

As can be seen in Figure 5.1, the problem is complicated by the distribution of muscles in the leg. All of the joints are crossed by more than two muscles, which may all contribute to the net torque. In addition, some muscle groups (such as the hamstrings and rectus femoris) cross more than one joint; activation of the hamstrings will generate a torque around both the hip and knee joints. Table 5.1 lists the moment arms of the muscles about each joint, measured in cm [51]. A positive value indicates that a contractile force in the muscle will generate a positive torque about the joint; a negative value indicates a negative torque about the joint.

Muscle	Hip	Knee	Ankle
Rectus femoris	-4.0	-4.5	0.0
Biceps femoris long	9.0	4.5	0.0
Vasti	0.0	-4.5	0.0
Biceps femoris	0.0	4.5	0.0
Iliacus	-2.5	0.0	0.0
Gluteus	10.0	0.0	0.0
Gastroc	0.0	6.5	6.0
Tibialis anterior	0.0	0.0	-4.5
Soleus	0.0	0.0	6.0

Table 5.1: Muscle Moment Arms (cm)

With the additional complexities resulting from nine muscle groups available to generate only three joint torques, there are an infinite number of possible solutions to the muscle force distribution problem for each instant in time. The remainder of this chapter discusses the method used to find a unique solution while simultaneously evaluating the objective function of the outer optimization loop.

5.2 Solving the Force Distribution Problem

To find a unique set of muscle forces for a given set of joint torques, an additional assumption must be made about the body's selection of muscle groups. As in the motivation for the main optimization loop, the hypothesis is that biological systems tend to minimize energy consumption. The predicted muscle forces should reflect this objective, and should produce the required torques with the minimal metabolic energy cost.

The force distribution problem, sometimes referred to as 'the redundant problem in biomechanics,' may be described in terms of an optimization problem:

> Find the set of muscle forces (the optimization variables)
>
> that minimize some energy consumption estimate (the cost function)
>
> while generating the required joint torques (the constraint equations).

Given this description, the formulation of an optimization solution is relatively straightforward, with the exception of determining an appropriate cost function to estimate the energy consumption.

5.2.1 Physiological Cost Functions

The cost function must be an expression for the rate of metabolic energy consumption in terms of the specified muscle forces. Such an expression is not obvious, and depends on the efficiency of the muscles in converting metabolic energy into force at varying levels of activation.

Fortunately, this is not a new problem, and a significant amount of research has already been done to determine a relationship between force and metabolic energy cost. A recent

paper by Silva [57] gives an overview of the problem, and reviews a variety of different cost functions that have been proposed for solving for the force distribution at an instant in time, such as:

- summing the individual muscle forces;
- summing the cubes of the muscle stress;
- summing the squares of the normalized muscular forces.

After solving for the muscle forces in a simulation of walking gait with the latter two of these methods, Silva notes that the results for some subsets of the muscle model compared well with the results found by some authors, while other subsets of the model compared well with the results of other authors. In addition, Silva repeated the optimization with two locally convergent algorithms and found the results to be dependent on the optimization algorithm used; while different optimization packages found different solutions, they both satisfied the joint torque constraints and found a local minimum for the cost function.

This method, therefore, should not be expected to produce muscle force and activation patterns that exactly match those produced by direct EMG measurements in experimental studies. Some physiological factors, such as reducing repetitive stress of particular muscles, cannot be taken into account with an algorithm that only considers a single instant in time; such factors will always result in variations in experimental data that do not appear in the model. However, the optimization solution gives one reasonable muscle force solution that minimizes an estimate of energy consumption, and this can be used to estimate at least the relative difference in metabolic cost between two different sets of muscle forces.

Of the various cost functions considered, the summation of the cube of muscle stress model, first proposed by Crowninshield [19], was found to be effective and well supported by experimental data and physiological arguments. That measure, which Crowninshield termed ‘fatigue’, is discussed in more detail in the remainder of this chapter.

5.3 Fatigue Based Force Distribution

5.3.1 Physiological Basis for Force Distribution Method

Crowninshield [19] solved the force distribution problem by considering muscle fatigue as the objective to be minimized in muscle force distribution. He used the term *fatigue rate* to mean the inverse of the length of time a muscle could exert a constant force. The longer a muscle contraction could be maintained, the lower the fatigue rate of the muscle, and vice versa. By relating fatigue to muscle force exerted over time, Crowninshield developed a method to determine an optimal force distribution among the muscles acting at a joint.

Based on experimental measurements of endurance while maintaining a constant contractile force, a force-endurance relationship was found to be of the following form:

$$\log T = -n \log f + c_1 \tag{5.2}$$

where T is the maximum time (in seconds) that the muscle contraction could be held, f is the normalized muscle force (scaled by the maximum contractile force that can be generated by the muscle: $f = \frac{F}{F_{max}}$), and n and c_1 are constants that were determined by fitting the equation to the experimental data.

In addition, Crowninshield considered the maximum contractile force of a muscle as approximately proportional to muscle cross-sectional area. Dividing contractile force F by the physiological cross sectional area ($PCSA = volume/length$) of the muscle gives a measure of the stress σ in a muscle:

$$\sigma = \frac{F}{PCSA} \tag{5.3}$$

This scaling by $PCSA$ gives an intuitively reasonable result; smaller muscles will fatigue faster than larger ones exerting an equal force, and this is reflected in the higher muscle stress. A force distribution algorithm based on muscle stress measures will therefore allocate proportionally more force to the larger muscle groups.

Since the maximum muscle force was found to be proportional to the $PCSA$, the normalized force f in Equation (5.2) can be replaced with the muscle stress σ without changing the form of the endurance relationship. Substituting $f \propto \sigma$ into Equation (5.2)

and solving for T gives:

$$T = c_2 \frac{1}{\sigma^n} \tag{5.4}$$

where c_2 is a constant of proportionality that depends on the units of force and cross-sectional area. Note, however, that the exponential constant n is independent of the units and is the same constant as in Equation (5.2).

After fitting the experimental data from a variety of muscles across a range of forces, Crowninshield found the constant n to range from 2.54 to 3.14, with an average around 3. Using the substitution of $n = 3$ gives the proportional relationship from experimental data:

$$T \propto \frac{1}{\sigma^3} \tag{5.5}$$

To maximize the endurance T (or equivalently to minimize the fatigue rate) for a set of m muscles, the σ^3 terms for all muscles must be minimized. For the set of $m = 9$ muscles in the leg model, this can be formulated as a constrained optimization problem to minimize:

$$FatigueRate = \sqrt[3]{\sum_{i=1}^{9} \left(\frac{F_i}{PCSA_i} \right)^3} \tag{5.6}$$

subject to the constraints of generating the required joint torques:

$$\boldsymbol{\tau} = \mathbf{MF} \tag{5.7}$$

and the constraints that muscle forces always be non-negative:

$$\mathbf{F} \geq \mathbf{0} \tag{5.8}$$

The solution $\mathbf{F}$ to this optimization problem is the set of muscle forces that generate the required joint torques while minimizing the muscle fatigue rate at one instant in time during the simulation. The $FatigueRate$ corresponding to the optimal solution gives a measure of the physiological cost involved in generating the required muscle forces at an instant in time.

5.3.2 Calculation of Total Muscle Fatigue

To compute an estimate of the total muscle fatigue over the gait cycle, the fatigue rate is integrated over the time of the simulation:

$$Fatigue = \int FatigueRatedt \tag{5.9}$$

Numerically, using the results of the above optimization for each time instant, the total fatigue is calculated using a trapezoidal approximation:

$$Fatigue = \sum_{i=2}^{m} \frac{FatigueRate_{i-1} + FatigueRate_i}{2}(t_i - t_{i-1}) \tag{5.10}$$

where m is the number of time-steps in the simulation; for a typical simulation of 5 seconds of gait, each time-step is $(t_i - t_{i-1}) = 0.01s$ and $m = 500$.

To compute an objective value Φ for the outer loop optimization algorithm, the measure of fatigue is divided by the distance traveled in the simulation (d_{CM}). This gives an estimate of the physiological energy cost per unit distance traveled of the current kinematic trajectories.

$$\Phi = \frac{Fatigue}{d_{CM}} \tag{5.11}$$

5.4 Model Limitations and Alternatives

As with any model, the fatigue based muscle model is an approximation of the physical system it represents, and has limitations that should be investigated and understood before applying it to new problems. As already discussed, the results are dependent on the optimization algorithm used and the approximation of metabolic energy consumption and fatigue. In addition, the method presented has a number of other limitations.

5.4.1 Hill Model Relationships

One simplification of the model is that the force-length and force-velocity relationships of biological muscle are not taken into account. These relationships were modelled and

quantified in pioneering research by A. V. Hill [37]. His work has led to the creation of many variations of 'Hill' muscle models, which represent muscles as a combination of an active *contractile element* (CE) connected in parallel with a spring and damper *passive element* (PE) and in series with a *serial elastic element* (SEE). A Hill-type muscle model is shown in Figure 5.2,

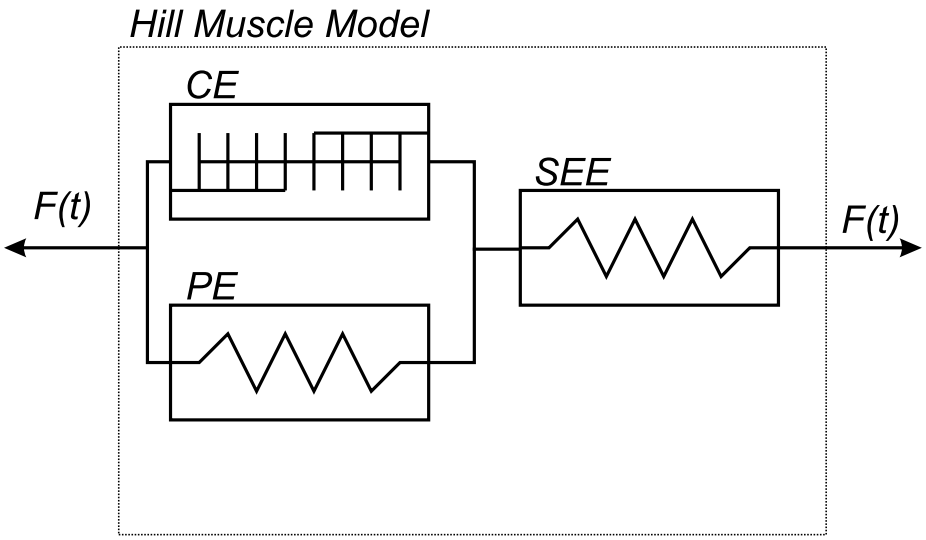

Figure 5.2: Hill-type Muscle Model

The force generated by the passive elements (PE and SEE) are functions of the instantaneous length ($l(t)$) and rate of change of length ($\dot{l}(t)$) of each element and the maximum isometric force the muscle can produce (F_0).

The force generated by the CE is a product of three terms, as shown in Equation (5.12) [57]. The first term is a function of the length of the CE, the second term a function of its rate of change, and the third term is the activation level $a(t)$, which varies between 0 and 1 and represents the level of neural stimulation of the muscle.

$$F_{CE}(t) = \frac{F_l(l(t))F_{\dot{l}}(\dot{l}(t))a(t)}{F_0} \tag{5.12}$$

Approximate analytic expressions for the passive element forces and the length and velocity dependent terms can be determined by fitting curves to experimental data. Examples

of these functions are given in [57].

The Hill muscle model requires a significantly different implementation than the fatigue calculation method. While the fatigue method operates only on the instantaneous muscle force, a Hill model is a dynamic system with state memory, and therefore requires an optimization over multiple simulation time-steps to find the optimal muscle force distribution over time.

To investigate the possibility of using a Hill based muscle model, the *Virtual Muscle* model presented by Brown et al [12] and Cheng et al [17] was considered.

5.4.2 The *Virtual Muscle* Simulation Package

The Virtual Muscle system is based on the Hill model, and includes detailed muscle parameters including mass, fascicle and tendon lengths, fibre types and recruitment patterns. An implementation of the model is available as a Matlab/Simulink package that computes the force output of the muscle over time given the activation level, length, and velocity.

While the detail included in the Virtual Muscle model may eliminate many assumptions and approximations that exist in the fatigue model, it did not prove to be practical for this application. Since the goal of this piece of the system is to find the optimal muscle force patterns for a set of muscles, the muscle simulation would have be executed many times in the course of the optimization process. Because of the detail included in the Simulink model, the model required several minutes of CPU time for a simulation of two steps of walking gait. Finding an optimal solution for one kinematic pattern (and the corresponding set of joint torques) may have been feasible; however, this process was required for every iteration of the outer optimization loop searching for the optimal kinematic patterns, and was therefore too detailed and too slow to be practical.

The fatigue method, though approximate, was much faster than a dynamic simulation, and was found to be a sufficiently accurate model for solving the muscle force distribution problem. The optimal muscle forces for 15 consecutive steps of the walking model were computed, and the average and standard deviation are plotted in 5.3.

The results compare reasonably to the simulation results produced by Silva [57] and Crowninshield [19].

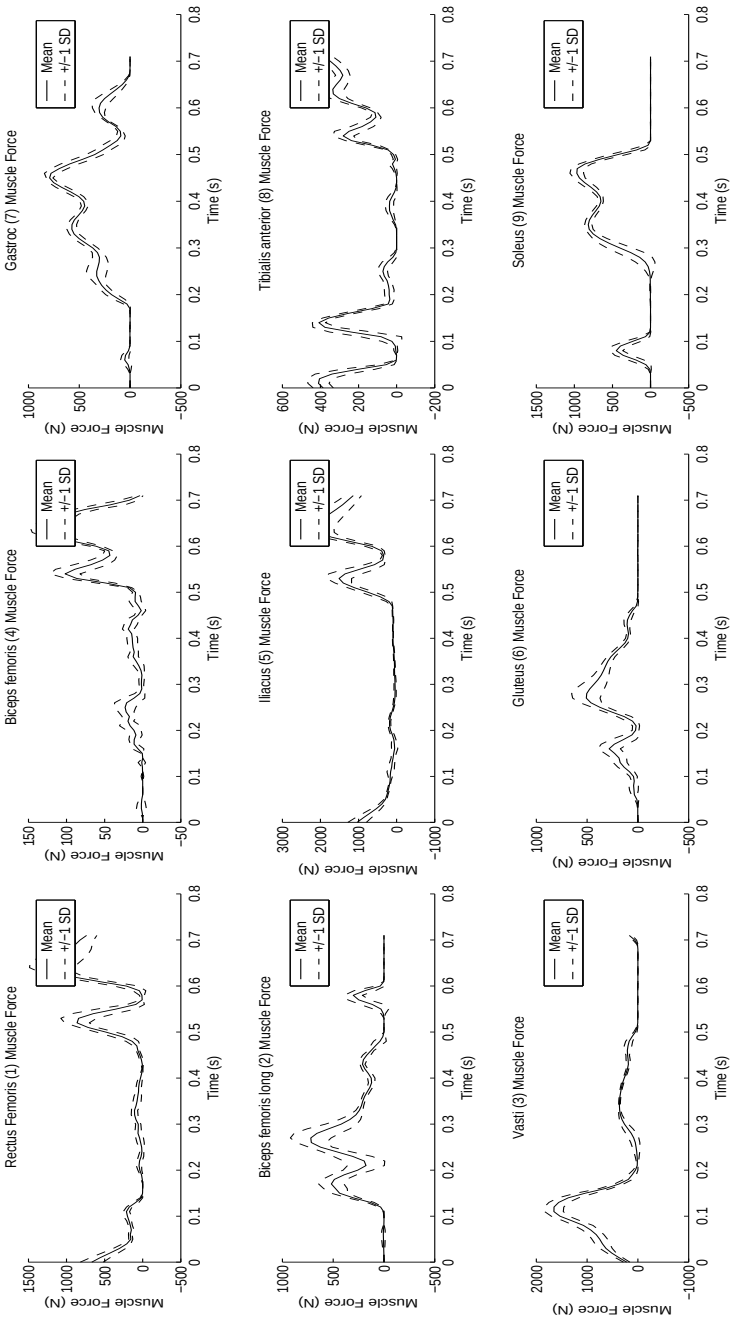

Figure 5.3: Computed Muscle Force Distribution

Chapter 6

Balance Controller Design

6.1 Balance Controller Overview and Requirements

Maintaining balance is a fundamental prerequisite for unaided human walking. While this ability is often taken for granted after it is learned early in life, balancing while walking involves a complex coordination of motion. In systems engineering terms, bipedal walking systems, whether biological or mechanical, are typically unstable dynamic systems; that is, a small bounded disturbance to the system (a push from behind) can lead to unbounded output (the system falling over) [30]. This is an inevitable side-effect of walking upright where, like an inverted pendulum, the centre of mass is relatively high and the base of support is relatively small, provided by a single foot during most of the gait cycle.

In human walking, the central nervous system dynamically maintains balance by continually moving the limbs in such a way as to keep the centre of gravity within a step-length of the base of support. One study has also found that the intrinsic properties of muscle can also contribute to the stability of human walking by absorbing dynamic perturbations [32].

When simulating human walking, the mechanical system model (as presented in Chapter 4) is also an unstable dynamic system, and does not have the benefit of a central nervous system or biological muscle to compensate for disturbances. The need for a mechanism to stabilize the mechanical model was evident from early experiments using forward dynamic simulations. Without a constraint to maintain the orientation of the torso, the

disturbance due to the kinematic motion of the lower limbs would eventually cause the model to fall over, as would be expected for an unstable dynamic system model. Since the motion is constrained to two dimensions, the instability led to either falling forward or falling backward, and was a function of the relative speed of the torso to the speed of the lower limbs. If the speed of the torso was too slow, the lower limb would walk out from under the centre of gravity, leaving the model to fall over backwards; if the speed of the torso was too high, the centre of mass would move ahead of the base of support during initial foot contact, and the model would stumble forwards.

This chapter discusses the development of a feedback control system required to maintain balance in the mechanical walking simulation.

6.1.1 Balance Control and Energy Consumption

The goal of this thesis is to investigate the change in metabolic energy consumption associated with changes to the model parameters and kinematics, particularly for amputee gait. One possible explanation for the observed increase in energy cost in amputee gait is that maintaining balance while walking is more difficult with a prosthetic limb and requires more metabolic energy from the remaining muscles.

To include this effect in the model, the simulation is executed for several periods of the gait cycle, and the model must maintain its balance throughout the simulation. If the metabolic cost of balancing the torso is greater for the prosthetic model, it should appear as an increased measure of total fatigue from the muscle force distribution model.

6.1.2 Existing Balance Control Algorithms

Control systems for balancing walking models have been the subject of numerous studies [31], [35], [39], [49]. This previous research has primarily investigated control algorithms applicable to physical bipedal walking systems, with the corresponding challenges of three-dimensional motion and unknown terrain. The balance controller required for the walking simulation in this thesis has somewhat different requirements than a physical model. The walking surface is known to be perfectly flat, and the motion is constrained to two dimensions, which simplifies the problem substantially.

However, the goal of the model is also different from most physical models, which adds some additional requirements to the balance controller. The purpose is not to simply walk with any possible stable gait, but to follow as closely as possible the pre-defined joint trajectories specified by the optimization algorithm. This requirement removes the freedom to arbitrarily control the joint positions to generate a stable gait pattern. Instead, a control system is required that closely follows the specified joint trajectories while maintaining the balance of the model. Because of these different requirements, the algorithms presented in most physical biped walking control papers are not directly applicable to the simulation control problem. However, some of the general design methods and philosophies can be adapted, particularly those proposed by Pratt [49], [50].

In studies of gait that use forward dynamic simulation, the balance problem has been largely ignored by only simulating and analysing a single step of the walking cycle [46], [2]. These simulations use an optimization of muscle activation patterns in order to drive the simulation of human walking. The objective of such studies is to find the optimal muscle activations that reproduce the joint kinematics observed by experimental measurements of human subjects. (As the goal is to track a pre-defined trajectory, this is referred to as a *tracking problem*). Since these simulations only operate for a single walking step, the long-term balance of the model is not a problem.

In a dynamic optimization by Anderson and Pandy [3], the goal was again to find the optimal muscle activation patterns to produce walking motion; however, the simulation was allowed to follow any kinematic trajectory produced by the muscle forces, rather than matching specified kinematics. Unlike the *tracking problem* investigations, this allowed for arbitrary motion during the simulation, and the only constraint imposed was that the initial and final states of the system be the same. This constraint would ensure that each step would start from the same initial conditions, and therefore produce a stable gait. However, the simulation was again only optimized over a single step, so no balance control was required to compensate for accumulated error over multiple steps. As a result, these prior walking simulation studies provided little insight into the balance control problem.

6.2 Initial Balance Control Designs

A number of different approaches were considered for solving the balance control problem. While the three methods reviewed in this section were not used in the final model, they are discussed briefly as they provide some background for the final controller design that follows in Section 6.3.

6.2.1 Perfect Initial Conditions

The balance of the walking model is associated with the relative speed of the torso and the lower limbs. In theory, if these are perfectly matched, the kinematic motion of the limbs driven at exactly the right speed would move the base of support (the feet) forward at precisely the same speed as the torso. In control terms, this would be an open-loop system. This would maintain the center of mass above the base of support, and keep the model balanced. The problem is then to find the speed of the torso that matches the speed of the lower limb kinematics, and set the torso to this speed as an initial condition.

To find the initial speed required, the optimization algorithm used for finding optimal joint kinematics was used, with some modifications. The optimization variable was the initial torso speed, and the objective function (to be maximized) was the distance travelled before losing balance.

Unfortunately, the dynamic system is extremely sensitive to the initial conditions after even a single period of the gait cycle. A change in the value of the initial speed of less than 0.1% will change the result of the simulation from falling backwards to stumbling forwards after only two steps. Solving for the required initial conditions after each modification of the joint trajectories would require an impractical amount of simulation time, and given the extreme sensitivity of the model to a single parameter, would be of questionable value.

6.2.2 Kinematically Driven Torso Orientation

Another solution considered was the addition of an external constraint on the torso, which would allow for translation in the horizontal and vertical directions, but fix the orientation of the torso relative to the ground. A rotational kinematic driver was applied to the torso

from the ground reference frame, and the orientation of the torso was driven to follow the pattern of torso sway measured from human walking in [69]. This approach is similar to one used by Skelly and Chizeck [59] where a "velocity controller" was used to apply an external force and torque on the torso relative to the reference frame.

The addition of the external constraint gave reasonable kinematic results, since it left the torso with only two degrees of freedom – vertical and horizontal translation. However, the joint torque results of the inverse dynamics simulation proved to be less useful after the addition of the new constraint.

The torso orientation constraint introduced an externally applied torque on the system that did not correspond to any forces in the body. The model was supported by the external constraint, and the energy optimization took advantage of the constraint by converging to walking patterns that used very little energy in the limb joints, but leaned back on the external constraint that was providing a support torque at no metabolic cost.

Since the energy introduced by the external constraint could not be measured in terms of metabolic energy cost, this approach was rejected. A balance controller was required that would give the model torso a rotational degree of freedom, and that could control the balance of the system using only the lower limb joint torques. The energy cost of maintaining balance would then be reflected in the metabolic energy cost of driving the joint torques.

6.2.3 Inverted Double Pendulum Controller

To actively control the balance of the model without external constraints, a design was considered that modelled the body as an inverted double pendulum. In this control model, the hip joint motion was modified from the original specified kinematic trajectories to control the orientation of the torso above the hips. The controller then computed torques used to drive the hip joints to the modified trajectories; the mechanical model was driven in a forward dynamics simulation with these computed torques. The ankle and knee joints were driven by kinematic drivers and were not included in the control loop.

6.2.3.1 Double Pendulum Representation

To design a balance controller based on a double pendulum representation, a simplified mathematical model of the system was required, in which the mechanical system was approximated as two links connected by a single joint. The torso represented the upper link, connected by a revolute joint at the hips to the lower limb assembly representing the other link. Controlling the common-mode motion of the two hips corresponded to controlling the centre joint in the double pendulum.

The multi-segment assembly of the lower limbs was approximated as a single rigid body since the knee and ankle joint positions were kinematically driven, and could not be influenced by the controller. Finally, the foot contact force was represented by a revolute joint between the lower link and the ground. This approximation was based on a single contact point for one foot, assuming a high friction coefficient and minimal slipping between the foot and the floor. The double-pendulum representation is shown in Figure 6.1.

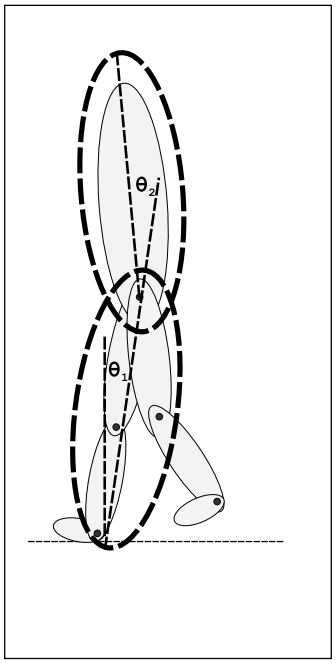

Figure 6.1: Double-Pendulum Representation of the Model

A controller for the system requires an expression for each of the system state variables; in this case, the angular position and velocity of the two links. The measurements of the upper link is readily available from the torso orientation computed in the mechanical simulation. The lower link, however, does not generally align with any elements in the mechanical model, so the measurement cannot be made directly. Instead, the effective orientation is measured by computing the average error of the absolute orientation of the thighs, relative to the desired hip joint angles.

The expression for this measure is given in Equation (6.1).

$$\theta_{1\_mea} = \left((\theta_{rthigh\_mea} - \theta_{rhip\_kin}) + (\theta_{lthigh\_mea} - \theta_{lhip\_kin}) \right) / 2 \tag{6.1}$$

where θ_{rthigh_mea} and θ_{lthigh_mea} are measured orientations of the right and left thigh angles in absolute coordinates, and θ_{rhip_kin} and θ_{lhip_kin} are the specified kinematic angles of the right and left hip joints.

6.2.3.2 Required Controller Behaviour

To gain some intuitive understanding of the behaviour of the inverted double pendulum model of the system and the required controller response, consider the control problem of compensating for the body falling backwards from the desired vertical orientation. This instability was observed in ADAMS simulations with no balance controller or torso orientation constraint, and occurs when there is insufficient momentum from push-off at the trailing foot to propel the torso over the stance leg. The condition is shown in the first box of Figure 6.2.

One intuitive response is to decrease the angle of both hip joints, essentially bending the torso forward from the hip joints. This will pull the torso and centre of gravity forward, which should stabilize the model.

However, since no part of the system is fixed to a ground reference frame, no segment of the model can be controlled in isolation. Modifying the joint trajectory at the hips will affect the orientation of both legs as well as the torso. The final orientation of the system depends on the ground contact forces at the feet and on the relative inertias of the segments on either side of the joint being controlled. As shown in the second diagram in Figure 6.2, the resulting effect may be the desired stabilizing control. Conversely, if the

foot contact forces do not resist the motion of the leg segments, the result may be an even less stable configuration, as shown in the third diagram. The orientation of the torso is moved closer to the vertical as desired, but at the same time the limb segments below are forced into a less stable configuration.

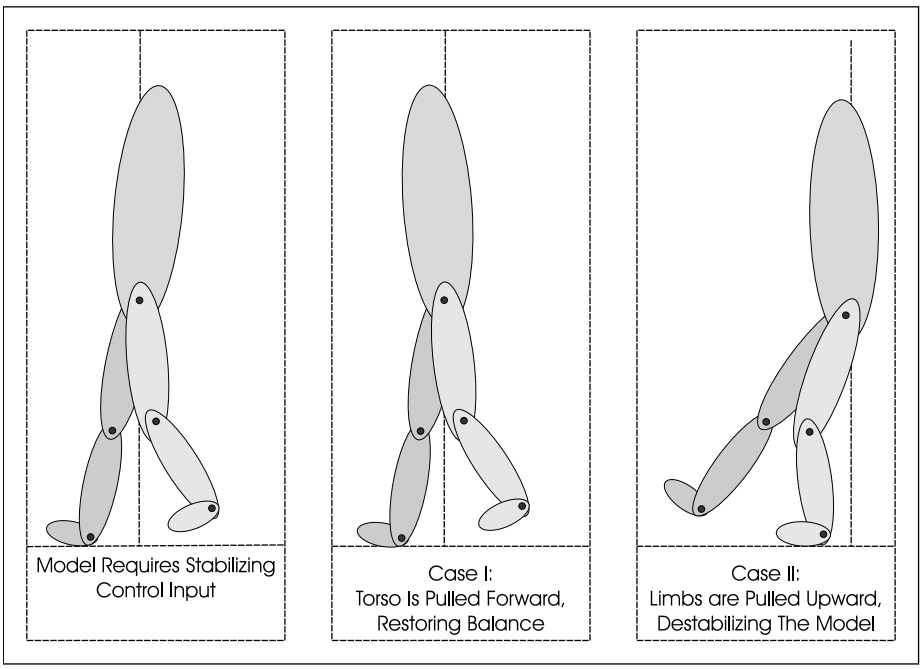

Figure 6.2: Two Results of Hip Joint Controller Compensation

From this simple example, it is clear that an intuitive algorithm of directly controlling the hip joint trajectories as a simple function of the torso angle will not result in an effective solution. A more complete model is required for the controller design, including measures of the full state of the system.

6.2.3.3 Controller Design

To construct a stabilizing controller based on the inverted double pendulum representation, the dynamic equations of motion were derived based on the mass and geometry of the two links (using the methods reviewed in Chapter 4).

The equations were linearized about the vertical position to allow for the use of linear control design methods, and a proportional-derivative (PD) controller was designed using a state-space model and linear quadratic regulator (LQR) techniques. The reference input for the controller is the orientation of the two links, which are both zero in the vertical configuration. The state variables included the absolute orientations of the two links, and the output of the controller is the desired joint angle at the hip joints.

For a full discussion of the derivation of the equations of motion, analysis of observability and controllability, and LQR controller design for an inverted double pendulum system, refer to the recent work by Demirci [24].

6.2.3.4 Controller Performance

In a numerical simulation of the controller driving an inverted double pendulum model, the controller was found to be effective in maintaining balance after injecting small disturbances, in agreement with the results in [24]. However, when applied to the walking simulation, the controller failed to maintain the stability of the system.

The failure of the controller was due to a number of problems. First, significant approximations were required to represent the walking model as a double pendulum, particularly the treatment of the lower limbs as a rigid segment. This approximation neglected the influence of the dynamics of the motion of the joints within the lower limbs. As well, the inertial properties of the lower link were treated as constant, while in the simulation they are functions of the configuration of the limb joints. The controller design proved to be quite sensitive to the inertial properties of each link; as the configuration of the lower limbs changed from the vertical stance assumed during the design, the inertial properties changed and the controller failed to stabilize the system.

The second reason for the controller failure is the representation of the foot contact as a pin joint. This approximation is only valid during the period of stance on one foot, as long as no slipping occurs. The transition from toe-off on one foot to heel contact on the other creates an instantaneous change in state that was not modelled in the controller design and destabilized the system.

6.2.3.5 Observations

The inverted double pendulum representation of the walking model was not suitable for the walking simulation balance controller. However, it was a useful exercise, as it led to the state variable representation of the net orientation of the lower limbs in Equation (6.1). This variable measures the difference between the desired hip joint position and the absolute orientation of the thigh. Assuming the torso is in the desired vertical position, this gives a measure of the error in absolute position of each leg; by averaging the values for both legs, the effective orientation of the lower body is computed. This representation proved to be useful in the final controller design that follows.

The failure of the double pendulum model led to a different approach to solving the balance control problem. Instead of viewing the problem as a generic non-linear unstable mechanical system, some features of the walking model can be used to advantage. Knowing the expected system behaviour from experience, the control problem can be broken down into smaller subproblems, each of which can be solved with a relatively simple linear controller and some intuitive design.

This approach is similar to that proposed by Pratt for controlling bipedal robots [49], [50], and led to the development of the velocity feedback balance controller that is discussed in the remainder of this chapter.

6.3 Velocity Feedback Balance Controller

Based on the results and observations discussed in Section 6.2, the control problem was broken into smaller blocks, and a feedback controller was designed as shown in Figure 6.3.

In Figure 6.3 and in the equations to follow in this chapter, unless otherwise noted, θ refers to the angle of an arbitrary joint (ankle, knee, or hip), and τ refers to the torque applied to one joint. The same symbols in bold ($\boldsymbol{\theta}$ or $\boldsymbol{\tau}$) refer to a column matrix containing the set of angles or torques applied to a set of joints.

For joint angle variables, the following subscripts are used to identify the purpose of the variable:

θ_{kin} identifies variables that are the kinematic joint trajectories specified prior to the be-

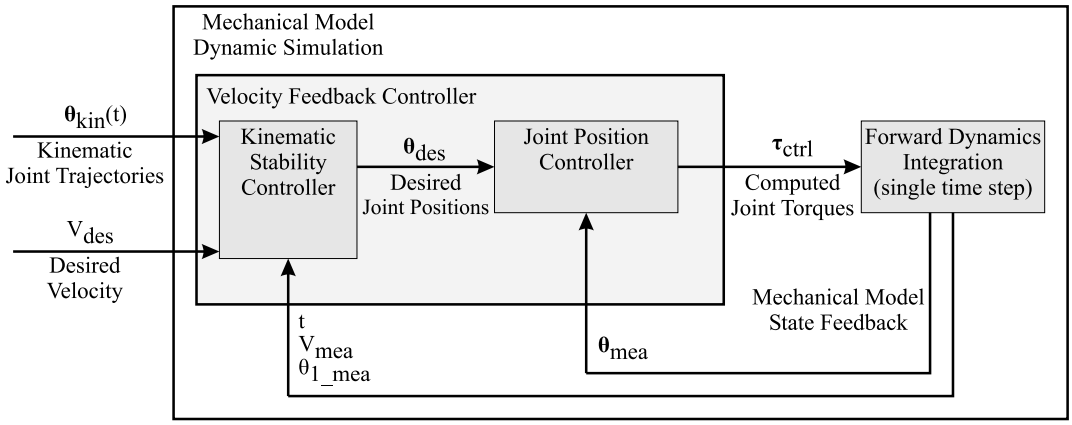

Figure 6.3: Velocity Feedback Control Structure

ginning of the simulation, and expressed as a Fourier series expansion.

θ_{des} identifies a desired joint position at an instant during the simulation. This desired value is computed based on the kinematic joint trajectories but modified according to the stability algorithm.

θ_{mea} identifies a variable at an instant in time that is measured from the model. These are used as state feedback variables for the control system.

θ_{err} identifies the error signal in the controller, which is computed as the difference between the desired and measured variables for a joint or body orientation.

θ_{nom} identifies a nominal value for a variable.

The remaining variables are defined for the controller equations:

V_{des} identifies the desired average forward speed of the centre of mass of the torso.

V_{mea} identifies the measured forward speed of the centre of mass of the torso.

θ_1 identifies the absolute orientation of all of the lower limb segments as computed in Equation (6.1).

In this control structure, all of the lower limb joints in the mechanical model are driven by torques computed by a feedback controller. The calculation of joint torques by the feedback controller is performed in two stages. The first stage in the feedback controller is the kinematic stability control block, which modifies the specified kinematic joint trajectories of the lower limb joints as required to maintain the balance of the model. This block uses feedback of the torso velocity and orientation from the mechanical model simulation; these two variables were observed to be the most significant factors in maintaining balance in the previous designs. The design of the kinematic stability controller is discussed in detail in Section 6.3.1.

The second stage in the feedback controller is the joint position control block. Since the desired joint positions are now dynamically computed by the stability controller, the joint motion cannot be driven by pre-determined kinematic functions of time. This restriction is imposed by the ADAMS simulation package; kinematic drivers may not be functions of measurements computed during the simulation. Instead, the joint position controller is used, which computes the control torques required to drive the joints to the desired trajectories determined by the kinematic stability controller. The torques are computed based on the desired joint positions and the feedback of the current joint positions and velocities of the simulation. Details of the joint position controller are discussed in Section 6.3.3.

The model is now driven in a forward-dynamics simulation with two nested feedback loops. The outer loop controls the orientation of the torso by modifying the original joint kinematics at each time step in response to changes in the orientation of the model. The inner loop drives the joints to the modified trajectories by computing a control torque to be applied at each joint. These computed joint torques are stored for each time step of the simulation, and are later used to estimate the muscle fatigue resulting from the actual simulation motion.

6.3.1 Kinematic Stability Controller Block Design

The goal of this control block is to modify the specified hip, knee, and ankle kinematic joint trajectories in such a way as to maintain the balance of the model. This loosely stated objective is indicative of the challenge in the design of the controller. The relationships

between the individual joint motions and the overall motion of the model (particularly the torso) is not intuitively obvious, and a number of different approaches were considered to implement the controller.

Analysis of the model as it lost balance indicated that the instability was closely coupled with a change in forward translational speed of the torso. As the model proceeded over several steps, it would either gain or lose speed, depending on the initial conditions. If it gained speed, eventually it would fall forward, since the motion of the feet did not keep up with the increasing speed of the torso; if it lost speed, it would topple backwards. Accordingly, it seemed reasonable that one factor in effectively maintaining balance is maintaining a relatively constant forward speed of the torso.

The torso velocity, however, cannot be directly controlled by the joint positions that the controller can vary. Instead, the torso velocity was found to be a function of the overall body orientation, as measured by the net lower limb orientation calculation developed in the inverted double pendulum model. To increase the torso velocity, the whole body must pitch forward more; to slow down, it must pitch forward less.

Again, the whole body motion cannot be simply controlled by modifying the joint positions to set a new orientation. The effect of changing any individual joint trajectory is dependent on the position of both legs, the phase of gait, and the current orientation of the torso. However, varying the speed of the lower limb motion effectively controls the pitch of the body by varying only a single parameter: the rate of the *time* variable used in evaluating the joint trajectories. By driving the legs through the walking gait faster, the lower body moves faster than the torso, decreasing the forward pitch of the body. By slowing the motion of the legs, the torso moves ahead of the feet, increasing the pitch of the body.

Figure 6.4 shows the subdivision of the stability controller block into simpler components, using the observed relationships between joint kinematics, torso pitch, and torso velocity.

6.3.1.1 Velocity Controller

The Velocity Controller is a proportional-integral (PI) controller block that attempts to maintain the forward velocity of the torso at the value specified. The block uses a reference

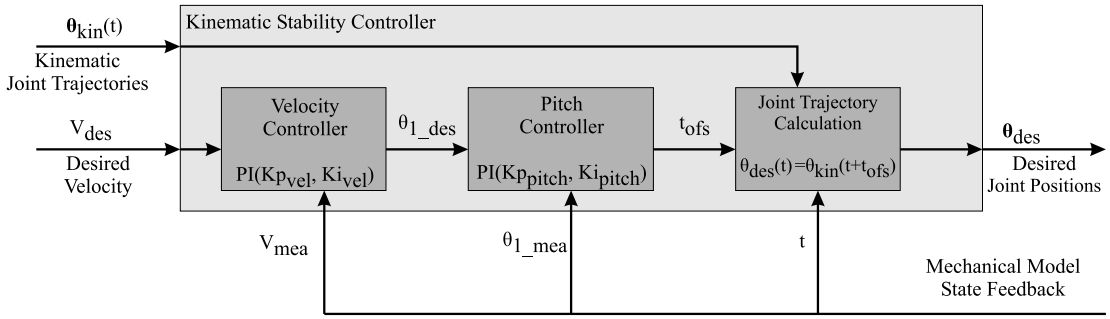

Figure 6.4: Kinematic Stability Controller Components

input of the desired torso velocity V_{des} and a state feedback input of the current torso velocity V_{mea} and generates an output that is the desired body pitch angle, θ_{1_des}. Since the block is operating on a velocity measure, the proportional term operates on the velocity error, and the integral term operates on the position error, correcting for the accumulation of the velocity error over time. A derivative term (in a full PID controller) would operate on the acceleration of the torso, and was found to be unnecessary. The block has two gain parameters, proportional Kp_{vel} and integral Ki_{vel}, used in the following control law:

$$\theta_{1\_des} = \theta_{1\_nom} - Kp_{vel}V_{err} - Ki_{vel}\int V_{err}dt \tag{6.2}$$

where $V_{err} = V_{mea} - V_{des}$ is the error in the forward velocity of the torso. θ_{1_nom} is a nominal offset representing the desired body pitch when the measured velocity reaches the desired velocity.

The effect of this control block is to increase the desired pitch angle of the body if the torso velocity decreases below the desired target velocity, and vice versa.

6.3.1.2 Pitch Controller

The Pitch Controller is a PI controller block with a reference input of the desired pitch, as computed by the torso Velocity Controller block. The state feedback for this block is the measure of θ_{1_mea}, as computed in Equation (6.1). The output of the Pitch Controller is an offset t_{ofs} that is added to the *time* variable when computing the desired joint trajectories.

The output is determined by two gains, proportional Kp_{pitch} and integral Ki_{pitch}, used in the following control law:

$$t_{ofs} = -1 \left(Kp_{pitch}\theta_{1\_err} + Ki_{pitch} \int \theta_{1\_err} dt \right) \tag{6.3}$$

where $\theta_{1\_err} = \theta_{1\_mea} - \theta_{1\_des}$ is the net error in the orientation of the lower limbs.

The effect of this block is to increase the time offset (and hence the speed of the legs as they move through the walking motion) if the pitch of the body is greater than the desired pitch, as determined in Equation (6.2), and vice versa.

6.3.1.3 Joint Trajectory Calculation

The final block within the stability controller is the joint trajectory calculation, which computes the desired joint positions at each time step of the simulation. Using the time offset computed in Equation (6.3), this block gives the updated joint angle at $time = t$:

$$\theta_{des}(t) = \theta_{kin}(t + t_{ofs}) \tag{6.4}$$

where $\theta_{kin}(t)$ is one of the six joint trajectories (hip, knee, or ankle for the left or right leg) specified as a Fourier series function of time before starting the simulation.

The output of this block is the set of joint angles that will maintain the stability of the model while approximating the specified kinematic joint trajectories. These joint angles will be used as the input to the position controller, as shown in Figure 6.3. For details of the implementation of the measures and control blocks, refer to Appendix A.

6.3.2 Controller Parameter Tuning

Determining appropriate values for all of the gains in the feedback control system is an interesting challenge. Although all of the controller blocks are linear systems, the behaviour of the walking model (or the *plant*, in control systems terms) is not readily described as a linear system. For example, an expression for the body pitch θ_{1_mea} in terms of the time offset t_{ofs} control is a non-linear and time-varying relationship since it depends on the current phase of the gait cycle. Linear control design theory is therefore not helpful in selecting appropriate gains for the control blocks.

Conveniently, however, the optimization algorithm that is used to vary the joint trajectories to find energy-optimal motions can be equally well applied to the variation of controller gains to optimize a controller quality objective. An optimization was designed that repeatedly ran the simulation with the same kinematic joint trajectories, while the controller gains of a particular control block were used as optimization variables and varied for each iteration. The objective function used was a measure of the error in the control variable for the block, as described for each block in the following sections.

6.3.2.1 Pitch Controller Block Tuning Results

The Pitch Controller block was tuned by varying the controller gains Kp_{pitch} and Ki_{pitch}, while attempting to minimize the error between the desired pitch (specified by the Velocity Controller) and the measured pitch θ_{1_mea}. The objective function is given in Equation (6.5).

$$\Phi_{pitch} = \int (\theta_{1mea} - \theta_{1des})^2 \, dt + 10000 P_{stab} \tag{6.5}$$

where P_{stab} is a penalty term that is added if the model loses balance (at time $t = t_{failure}$) before completing the simulation:

$$P_{stab} = (t_{sim\_length} - t_{failure}) \tag{6.6}$$

The large penalty coefficient of 10000 ensures that the penalty term is the most significant component in the objective if the model loses balance. The optimization first tunes the controller parameters to keep the model upright as long as possible, then fine-tunes the parameters to follow the desired pitch as accurately as possible.

Results of the optimization of the Pitch Controller are shown in Figure 6.5 (the results using an initial guess for the gain parameters) and Figure 6.6 (the results after optimization). In each figure, the plot on the left shows the desired pitch, measured pitch and error, and the plot on the right shows the controller output, the t_{ofs} variable.

Note that the controller performance was very poor using the initial guess for gain parameters. In Figure 6.5, the model lost balance falling forward at approximately $t = 2.5$ seconds, resulting in a large penalty term.

The results of the optimized controller demonstrate the controller maintaining balance for the duration of the simulation, and the orientation closely tracking the desired pitch.

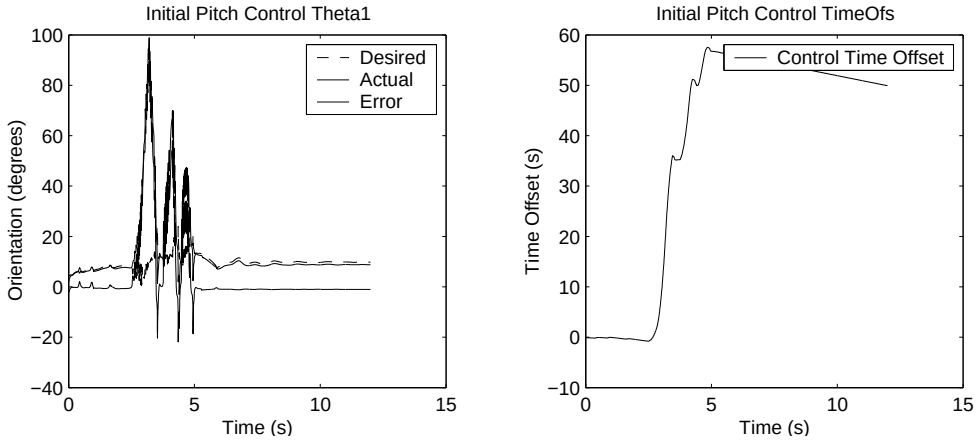

Figure 6.5: Pitch Controller Block Initial Performance

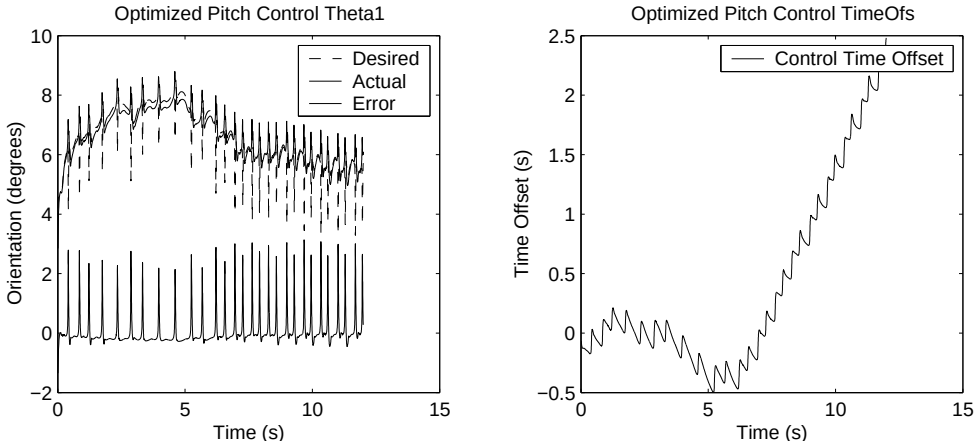

Figure 6.6: Pitch Controller Block Optimized Performance

The spikes in the pitch error signal are due to rapid changes in the desired orientation during changes in ground contact conditions. Heel contact and toe-off events result in changes in the torso velocity, which are passed through the Velocity Controller in the forms of rapid changes in desired pitch of approximately 3°. Since these spikes will also result in large joint torques (and therefore large muscle forces), they will increase the total fatigue calculation for the simulation. The optimization of joint kinematics to minimize fatigue will tend to minimize these spikes, as shown in the optimization results of Chapter 7.

6.3.2.2 Velocity Controller Block Tuning Results

The Velocity Controller block was tuned by varying the controller gains Kp_{vel} and Ki_{vel}, while attempting to minimize the error in between the desired velocity (specified as an input to the simulation) and the measured torso velocity.

The objective function is given in Equation (6.7).

$$\Phi_{vel} = \int (V_{mea} - V_{des})^2 \, dt + 10000 P_{stab} \tag{6.7}$$

where P_{stab} is the same penalty term used in Equation (6.7).

Results of the optimization of the Velocity Controller are shown in Figure 6.7 (the results using an initial guess for the gain parameters) and Figure 6.8 (the results after optimization). In each figure, the plot on the left shows the desired velocity, measured velocity and error, and the plot on the right shows the controller output, the desired pitch.

After the first 7 seconds of the simulation, the torso velocity approaches a steady-state value. Using the initial gain values, the steady-state velocity is approximately $0.2\frac{m}{s}$ below the specified $V_{des} = 1.2\frac{m}{s}$ After optimization of the Velocity Controller gains, the objective value is reduced by half, and the average steady-state velocity is approximately the desired $V_{des} = 1.2\frac{m}{s}$

The optimal gains found by the controller optimizations were used in the stabilizing controller for the metabolic energy optimizations, and are listed in Table 6.1.

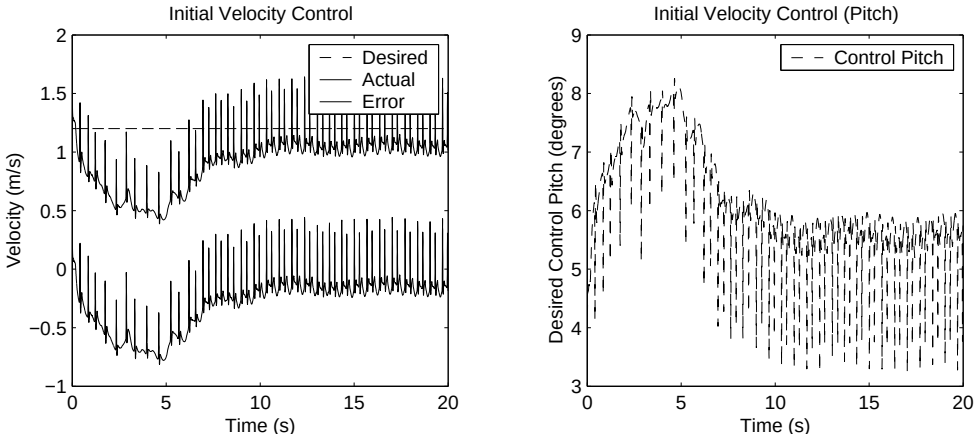

Figure 6.7: Velocity Controller Block Initial Performance

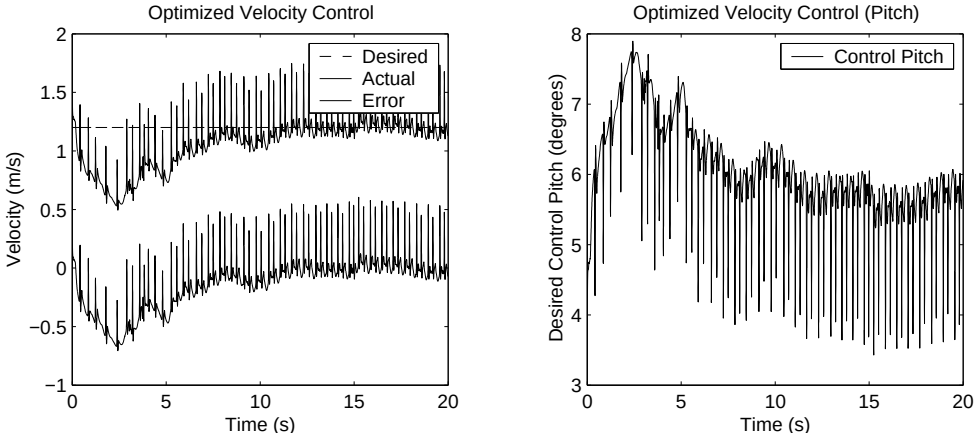

Figure 6.8: Velocity Controller Block Optimized Performance

Gain Parameter	Optimized Value
$Kp_{pitch}\left(\frac{s}{degree}\right)$	0.01
$Ki_{pitch}\left(\frac{s}{s \cdot degree}\right)$	2.65
$Kp_{vel}\left(\frac{degree \cdot s}{(m)}\right)$	3.75
$Ki_{vel}\left(\frac{degree}{m}\right)$	0.27

Table 6.1: Feedback Controller Gains

6.3.3 Joint Position Controller

The joint position controller, the second block in Figure 6.3, is required to compute torques that will drive the joint angles in the model to the desired positions, as determined by the stability control block. This is a position tracking problem, which can be modelled at each joint as a single torque driving a rigid link to a desired reference position, which varies as a function of time. Unlike the kinematic stability controller, this problem can be solved using a proportional-derivative (PD) controller and linear control design methods, with some simplifying assumptions.

The joint controller consists of one controller for each joint, as shown in Figure 6.9.

The controller uses two gains, Kp and Kd, to compute the applied torque τ_{ctrl}:

$$\tau_{ctrl} = Kp(\theta_{des} - \theta_{mea}) + Kd(\dot{\theta}_{des} - \dot{\theta}_{mea}) \tag{6.8}$$

τ_{ctrl} is the computed torque required to track the desired joint angle, θ_{des}, based on the error between the actual and desired position and velocity of the joint.

To find reasonable values for the controller gains, a model of the dynamics of the plant is required. In the walking simulation, the dynamics of the system at each joint change depending on the phase of gait. For example, during the swing phase the ankle joint needs a relatively small gain since it only has to overcome the inertia of the foot to track a desired trajectory. During the stance phase, however, a much larger gain is required, since the ankle joint torque must be large enough to control the inertia of the entire body that is balanced above it.

To simplify the design problem, the worst case (highest gain) scenario is used for de-

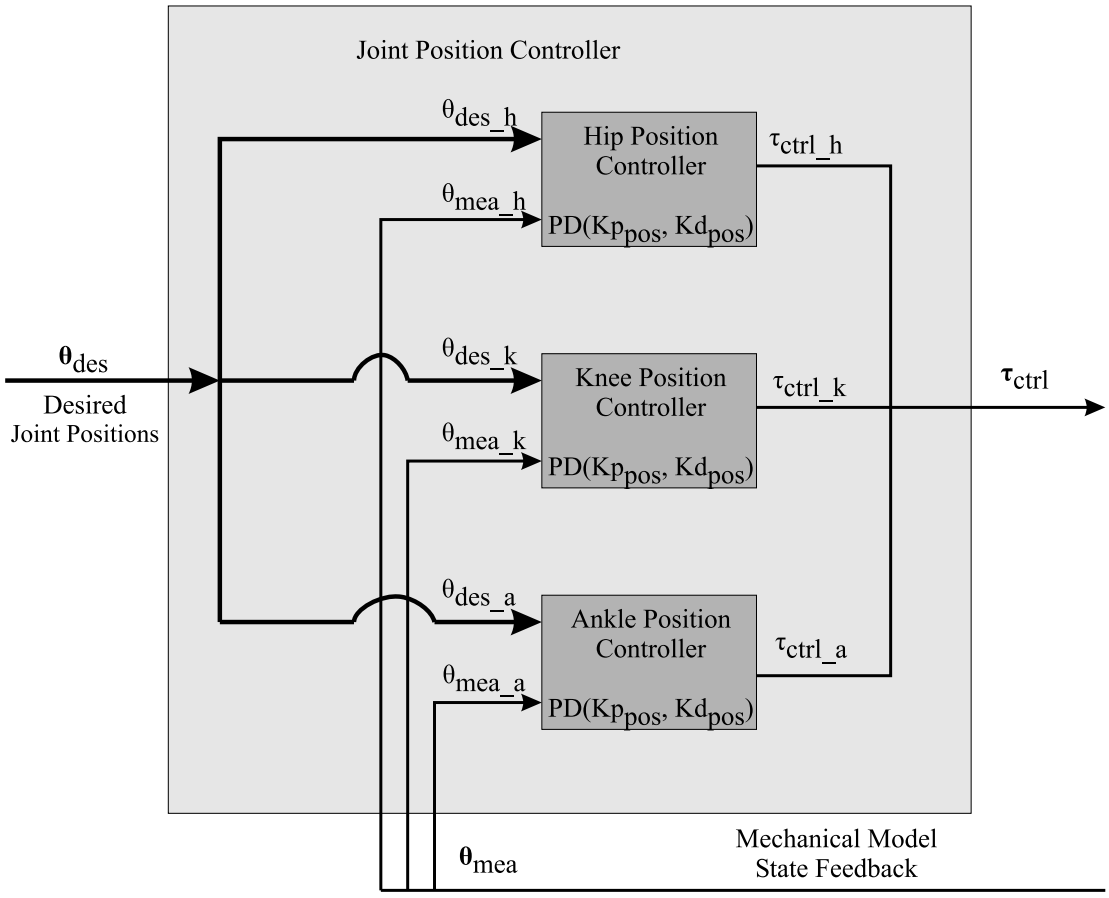

Figure 6.9: Joint Controller Model

termining appropriate gains, and the same gains are used at all joints throughout the simulation. The side effect of using gains that are higher than actually required is that the tracking error will be even less than the maximum tolerance used in the controller design, and higher joint torques may be generated. However, since the goal of the final optimization is to find trajectories that minimize energy (which will generally minimize joint torques), the optimization algorithm should avoid any trajectories that lead to unreasonably high joint torques despite larger than required controller gains.

For the worst case control problem, the plant model is straightforward. The torque at the ankle joint is controlling the position of the entire mass of the body, which is balanced

above it, as shown in Figure 6.10.

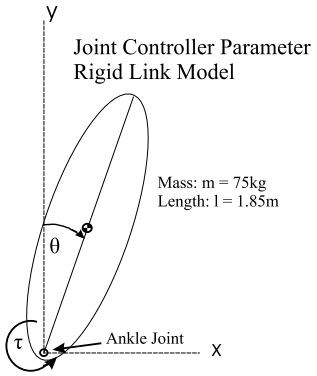

Figure 6.10: Rigid Body Model For Joint Controller Parameter Estimation

Neglecting the external torque due to gravity, (since the gravity vector acts primarily through the ankle joint and therefore has a negligible moment arm), the dynamic equation is simply:

$$\tau_{ctrl} = I\ddot{\theta} \tag{6.9}$$

where I is the moment of inertia about the ankle joint, and can be approximated by $I = \frac{1}{2}ml^2$. For a body mass of $m = 75kg$ and height $l = 1.85m$, this gives $I = 128kg \cdot m^2$.

To determine reasonable gains for the controller, the dynamic equation can be converted to a state-space representation, with the state vector $\mathbf{x}$ containing the state variables θ and $\dot{\theta}$:

$$\dot{\mathbf{x}} = \mathbf{A}\mathbf{x} + \mathbf{B}u \tag{6.10}$$

$$\mathbf{x}(0) = \mathbf{0} \tag{6.11}$$

where u is the control torque τ, $\mathbf{x}(0)$ is the initial condition, and the constant matrices $\mathbf{A}$ and $\mathbf{B}$ are given by:

$$\mathbf{A} = \begin{bmatrix} 0 & 1 \\ 0 & 0 \end{bmatrix} \tag{6.12}$$

$$\mathbf{B} = \begin{bmatrix} 0 \\ \frac{1}{I} \end{bmatrix} \tag{6.13}$$

In this form, the linear quadratic regulator (LQR) method can be applied to find the optimal controller feedback matrix $\mathbf{F}$ required to supply the control torque $u(t) = \mathbf{F}\mathbf{x}(t)$. The optimal control input is defined as that which minimizes the performance integral:

$$\Phi = \int_0^\infty (\mathbf{x}^T\mathbf{Q}\mathbf{x} + \mathbf{u}^T\mathbf{R}\mathbf{u})dt \tag{6.14}$$

The elements $\mathbf{Q}$ and $\mathbf{R}$ in the performance equation allow a weighting between minimization of tracking error ($\mathbf{x}^T\mathbf{Q}\mathbf{x}$) and minimization of control effort ($\mathbf{u}^T\mathbf{R}\mathbf{u}$). For this control problem, the goal is optimal tracking of the specified joint kinematics; the $\mathbf{Q}$ element is therefore weighted more heavily.

Given the state-space description of the system and the values of $\mathbf{Q}$ and $\mathbf{R}$ in the performance equation, the LQR algorithm finds an optimal feedback matrix $\mathbf{F}$ by solving the algebraic Riccati equation:

$$\mathbf{A}^T P_c + P_c\mathbf{A} - P_c\mathbf{B}\mathbf{R}^{-1}\mathbf{B}^T P_c + \mathbf{Q} = 0 \tag{6.15}$$

Refer to [5] for details regarding the solution of the Riccati equation.

The LQR method was used to solve for the controller feedback gains with an initial set of performance weights:

$$\mathbf{Q} = \begin{bmatrix} 100 & 0 \\ 0 & 10^6 \end{bmatrix} \tag{6.16}$$

and

$$\mathbf{R} = \begin{bmatrix} 1 \end{bmatrix} \tag{6.17}$$

The value of 100 in the $\mathbf{Q}$ matrix represents the weight applied to the velocity tracking error of $\dot{\theta}$, while the value of 10^6 represents the weight applied to the position tracking error. As discussed, the values in $\mathbf{Q}$ are given a much greater weight than the control cost term ($R = 1$) because the control effort should not be minimized at this controller. The energy cost of a large control torque will be reflected in the fatigue calculations of the energy optimization loop, which should lead to a more efficient kinematic pattern in the following iterations.

The LQR algorithm gives an optimal gain matrix of $\mathbf{F} = [\ 10 \quad 1000\ ]$, which corresponds to proportional and derivative gains of $Kp = 1000$ and $Kd = 10$ respectively.

The results of the LQR method give optimal gains for the linearized system including significant assumptions. To find the optimal gain parameters for the actual model, the optimization method applied to the Velocity and Pitch control blocks was applied to the joint position controller. Using the LQR design values as an initial guess for all of the joints, the optimal values were found as listed in Table 6.2.

Gain Parameter	Optimized Value
Kp_{hip}	$2625(N \cdot m)/(degree)$
Kp_{knee}	$1984(N \cdot m)/(degree)$
Kp_{ankle}	$1996(N \cdot m)/(degree)$
Kd_{hip}	$19.4(N \cdot m)/(degree \cdot s)$
Kd_{knee}	$12.5(N \cdot m)/(degree \cdot s)$
Kd_{ankle}	$27.5(N \cdot m)/(degree \cdot s)$

Table 6.2: Joint Position Controller Gains

6.4 Summary

The balance control of a bipedal walking model is a challenging project in itself. The attempts to design a controller while treating the walking model as a generic mechanical system resulted in a complex and unsuccessful control algorithm. However, breaking the control problem down into a sequence of subproblems (velocity, pitch, joint trajectory speed, and joint position), each of which could be solved with a simple linear controller, resulted in an effective control system, as shown in the results in Chapter 7.

The velocity feedback controller allows the model to walk without external support constraints, and enables the metabolic cost of maintaining balance to be included in the fatigue calculations that follow.

Chapter 7

Results and Discussion

7.1 Introduction

The data presented in this chapter are the final results of the fatigue-minimization optimization process. This optimization varied the joint kinematic trajectories to find an optimal walking gait for the model, minimizing the cost function

$$\Phi = \frac{Fatigue}{d_{CM}} \tag{7.1}$$

where $Fatigue$ is the total fatigue for the duration of the simulation, summed across all muscles in the model, and d_{CM} is the horizontal distance travelled by the centre of mass of the torso. This expression of the cost of locomotion leads the optimization routine to a solution that minimizes the estimate of metabolic energy consumption while maximizing distance travelled.

Detailed results are presented for the normal walking model, including comparisons to data gathered from experimental studies [69]. The results demonstrate the effectiveness of the optimization approach for finding a minimal-fatigue walking gait for the model.

Following the normal walking model data, results are presented for two variations, modelling a bi-lateral below knee amputee, as shown in Figure 7.1. In the first variation, the ankle joints torque drivers are replaced with passive rotational spring-dampers, representing energy-storing prosthetic joints. In the second variation, the ankle joint torque

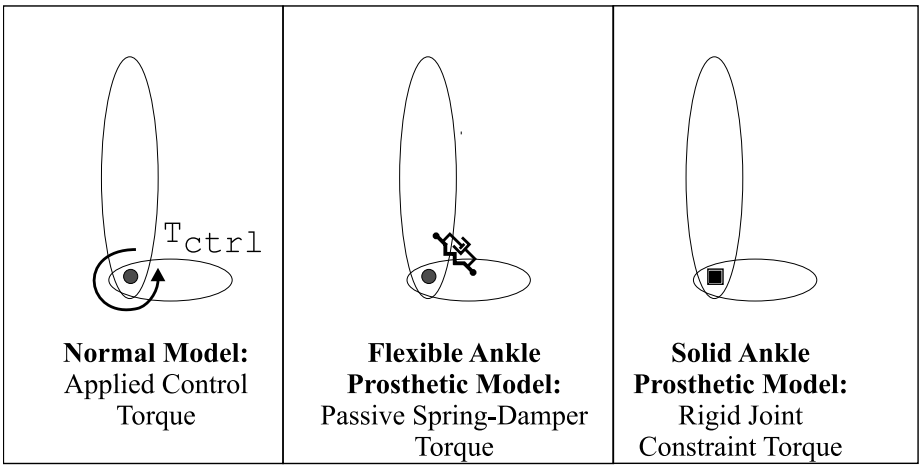

Figure 7.1: Normal and Prosthetic Ankle Joint Models

drivers are replaced with fixed joints, modelling solid-ankle cushioned-heel (SACH) prosthetics. The results of the prosthetic model simulations are discussed with comparison to experimental measurements of below-knee amputee gait made by Winter and Sienko [71].

7.1.1 Processing and Plotting of Results

The results presented in this chapter were determined by averaging the data for several consecutive steps of simulated walking, taken after the balance controller reached a steady state walking speed. Where applicable, the average and standard deviations are shown.

Typical experimental kinematic data must be filtered to remove noise from analog sensors. The experimental results included in this chapter for comparison to simulation results are taken from Winter [69], and have been appropriately low-pass filtered as described in [69]. The simulation results, however, have no sensor error, negating the need for filtering. The plots of simulation results are therefore based on the raw, un-filtered data. Some plots contain higher frequency components than would be found in actual human motion, due primarily to the behaviour of the balance controller. Rather than low-pass filter these results, the higher frequency components are included to illustrate the actual behaviour of the model.

In all figures showing the horizontal time scale as a percentage of the gait cycle, the plot begins at $t = 0$, corresponding to the instant of expected heel contact based on the original (experimental) kinematic data. For the experimental data (labelled *Winter* in the figures), this is exactly the moment of right heel contact. For the simulation results, heel contact may occur earlier or later in the plots, as will be seen in the floor reaction force figures. This allows for comparison of the timing of heel contact and toe-off events, relative to the joint kinematics that define the time scale of the plots.

7.2 Normal Model Results

7.2.1 Motion Snapshots

The motion of the walking model is captured in Figure 7.2, containing 15 snapshots of the model spaced at 0.1 second intervals. While individual images cannot capture the dynamics of the motion, they provide some reference points for comparison to human motion captured on film.

7.2.2 Joint Kinematics

Figure 7.3 shows the optimized joint kinematics found by the optimization process for the normal model. The dotted lines show the joint trajectories measured in normal walking gait, taken from [69]. The solid lines plot the optimally computed solution that minimizes muscle fatigue for the model, averaged over 10 seconds of the walking simulation. The dashed lines show ± 1 standard deviation from the average.

The optimized hip joint kinematics are relatively close to the original experimental data. The knee motion shows some significant variation at the end of the gait cycle, where the extension of the knee is delayed by approximately 15% of the gait cycle. This additional flexion may be caused by the lack of pelvis rotation and torso sway in the 2-D model. Lacking the rotation at the pelvis to raise the entire leg during the swing phase, additional knee flexion is required for the foot to clear the ground.

The ankle joint kinematics produced by the optimization are also significantly different than the original data. During part of the stance phase (15% - 40% of the gait cycle) there is

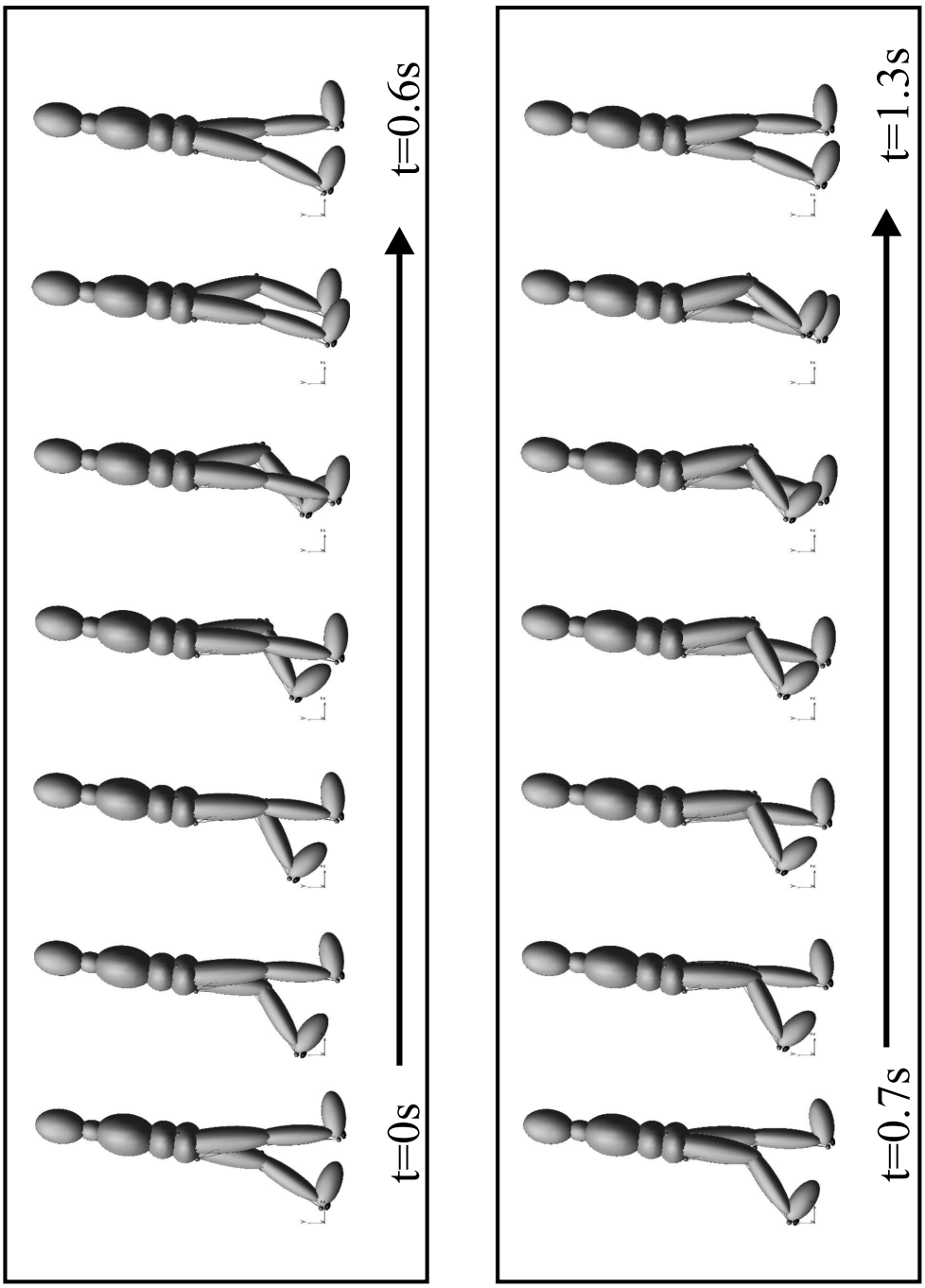

Figure 7.2: Optimized Model Walking Motion

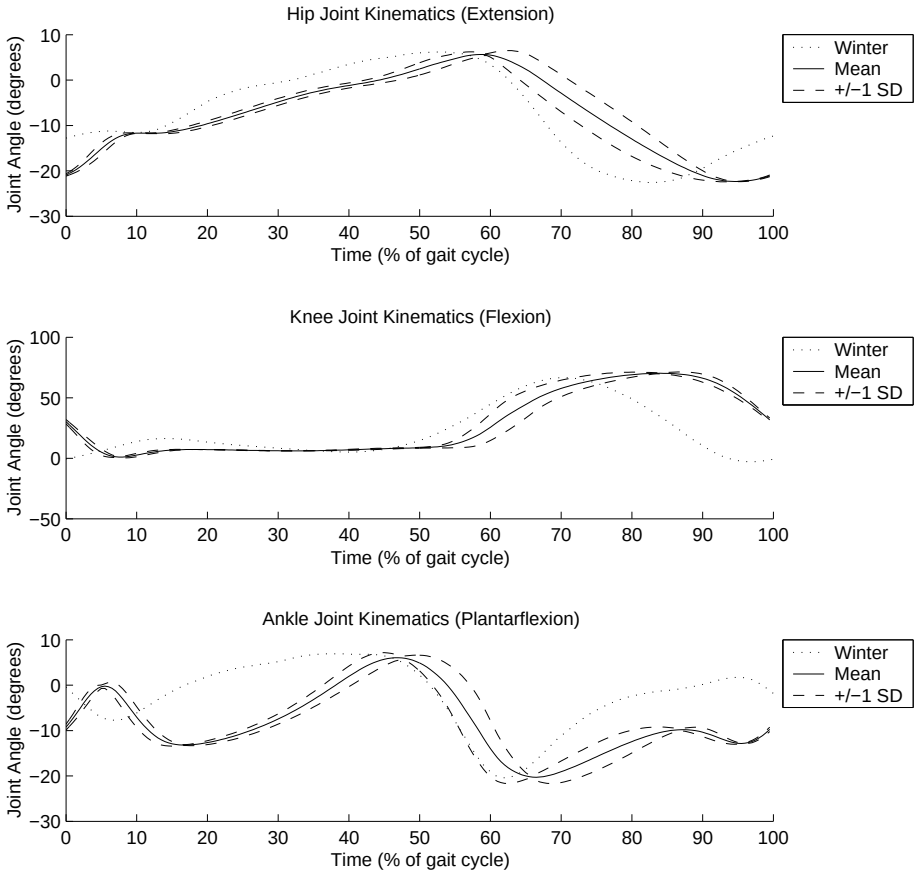

Figure 7.3: Normal Model Joint Kinematics

much greater dorsiflexion in the simulation results, which may be due to the approximation of the foot contact model using only two contact points. This simple model was required for speed of simulation execution, and did not represent the continuous contact surface of the foot, which may have affected the rolling motion of the ankle over the foot during stance. During push-off, the optimally computed ankle motion matches the experimental data very closely. In the swing phase, more dorsiflexion is again observed compared to the experimental results, which would tend to increase toe clearance for the model simulation. The additional clearance would be required for the model for the same reasons as the increased knee flexion discussed above.

7.2.3 Computed Ground Reaction Forces

Figure 7.4 shows the computed ground reaction forces of the optimized solution for the normal model. The dotted lines show the reaction forces measured in normal walking gait, taken from [69]. The solid lines plot results of the optimized simulation, averaged over 10 seconds of the walking simulation. The dashed lines show ± 1 standard deviation from the average.

The magnitude of the vertical contact reaction forces match the experimental data reasonably closely, with peaks at about 1.1% of the body weight. The standard deviation range indicates a significant variability in the contact force just following heel contact, which is partially due to the step-to-step variation in timing of the heel contact event. The horizontal reaction forces have greater variation from the experimental data, showing a more abrupt braking effect following heel contact, followed by a forward propulsion early in the stance phase.

The behaviour of the horizontal friction force is strongly influenced by the balance controller, which attempts to maintain a constant speed and orientation of the torso. To maintain the orientation of the torso, the controller accelerates or decelerates the motion of the lower limbs, and this in turn generates friction forces at the ground contact points to maintain balance. When the controller attempts to maintain a constant speed, rather than anticipating the typical acceleration of the pelvis during push-off and deceleration during weight acceptance, it produces some additional frictional forces that are not seen in experimental data. These variations might be reduced by a feed-forward term in the

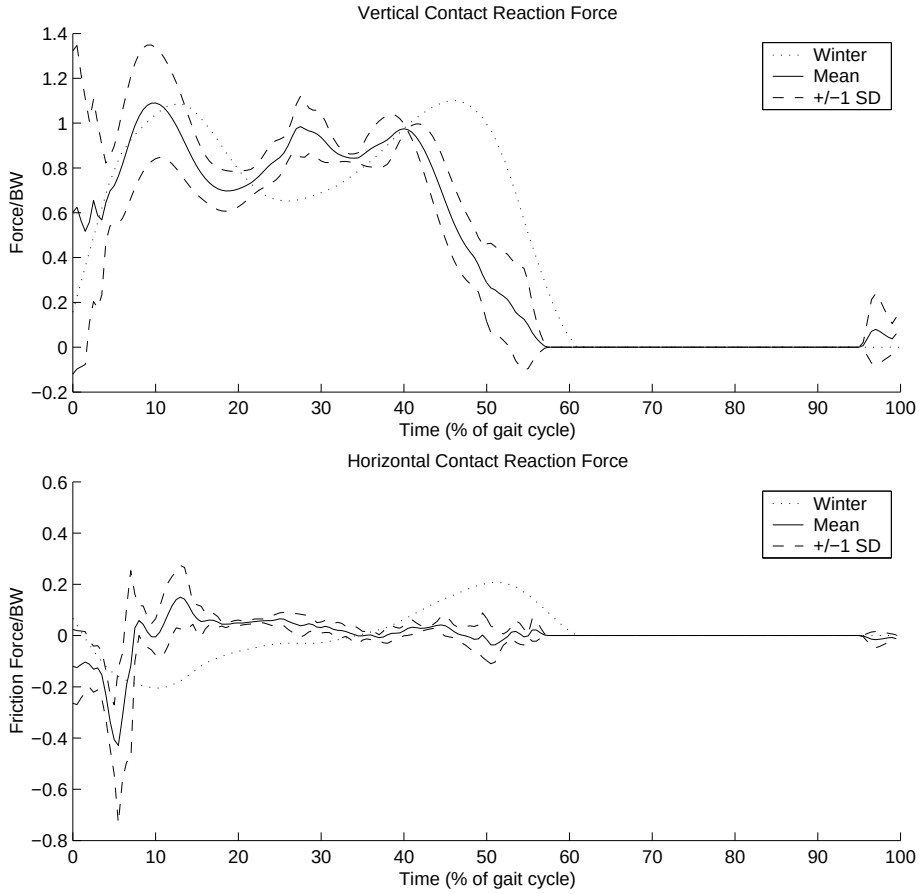

Figure 7.4: Normal Model Ground Reaction Forces

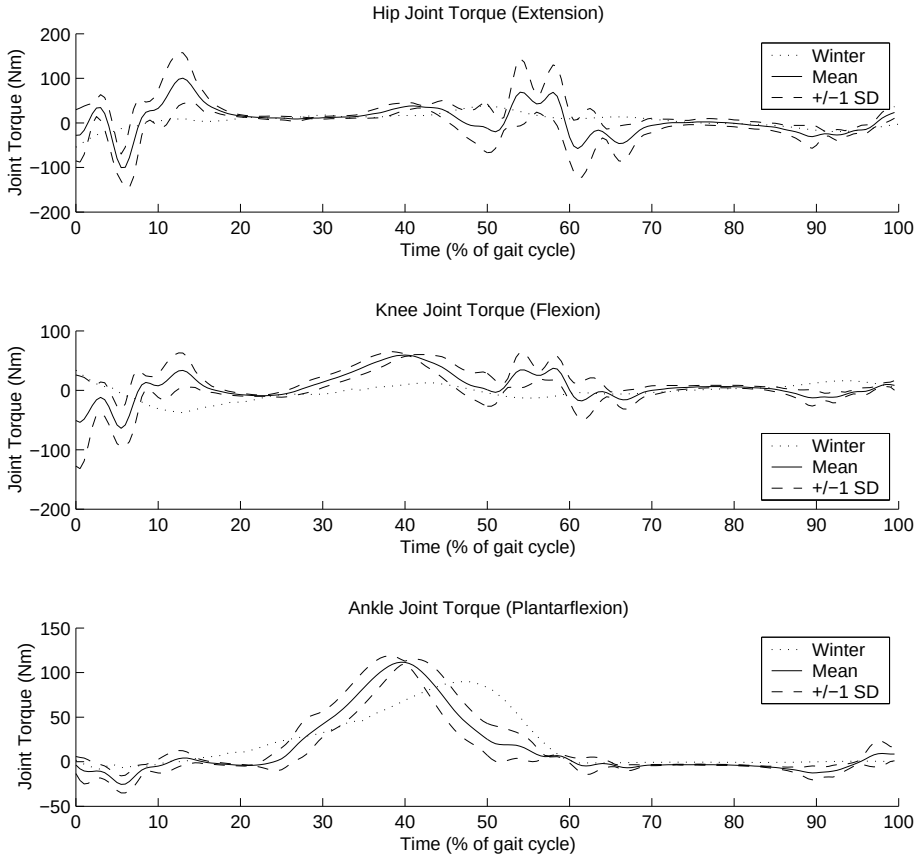

Figure 7.5: Normal Model Joint Torques

controller to anticipate the variation in torso speed at particular phases of the gait cycle.

7.2.4 Joint Torques

Figure 7.5 shows the joint torques computed by the optimized normal model simulation. The dotted lines show the joint torques computed by Winter [69] from experimentally measured gait kinematics and an inverse dynamics solution. The solid lines plot the optimized solution that minimizes muscle fatigue for the model, averaged over 10 seconds of the walking simulation. The dashed lines show ± 1 standard deviation from the average.

The joint torques at the hip and knee show some oscillatory behaviour at the heel

contact events (of both left and right limbs). This appears to be coupled to the horizontal friction forces that are generated at those instances by the balance controller, as discussed in subsection 7.2.3. Note that the friction contact force has a moment arm about the knee joint equal to the length of the shank, and about the hip joint equal to the length of the shank and thigh. The joint position controller generates the additional torques to compensate for the effect of the ground contact forces.

Outside of the heel contact events, the knee and hip joint data matches the experimental data reasonably well. The knee joint requires some additional flexion torque at push off, likely to increase clearance during the swing phase.

The ankle joint torques are not significantly affected by the balance controller and the horizontal ground reaction forces because of the small moment arm about the ankle joint. The ankle torques match the experimental data in magnitude, with a more rapid generation of power at the push-off phase.

7.2.5 Muscle Forces

Figure 7.6 shows the computed muscle forces for the optimized solution of the normal walking model. The numbers in the title of each sub-plot correspond to the numbering of muscle groups used in Figure 5.1.

The muscle forces computed are those that produce the required joint torques (shown in subsection 7.2.4) while minimizing the total muscle fatigue rate at each instant in time, using the method proposed by Crowninshield [19] described in Chapter 5.

The timing of most of the muscle activations, discussed below, is reasonably well correlated with results of experimental EMG measurements of human walking and other walking simulations [3] [19].

At the ankle joint, the soleus and gastrocs show the typical power generation at late stance to toe-off (30% - 50% of the gait cycle), providing the plantarflexor torque required for propulsion. Following toe-off (60%-70%) the tibialis anterior shows activation, lifting the toe to clear the floor during the swing phase.

At the knee joint, the continued force of the gastrocs and activation of the biceps femoris following toe-off serve to flex the knee in preparation for the swing phase. The rectus femoris and vasti groups provide an extensor torque at the end of the gait cycle as

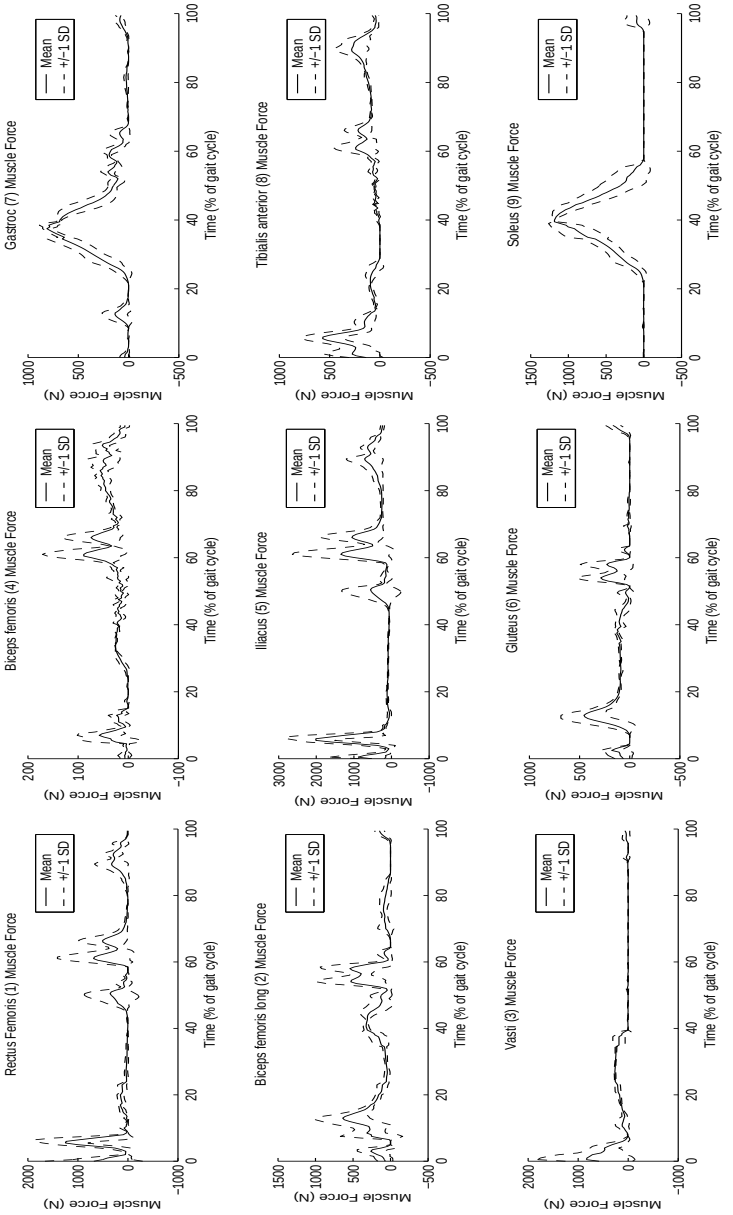

Figure 7.6: Normal Model Computed Muscle Forces

the knee is extended for heel contact.

At the hip joint, the rectus femoris and illiacus groups are active at the beginning of the swing phase (60%-70%), providing acceleration of the entire leg through the swing motion. The gluteous muscles are active through the stance phase, providing a propulsive extensor torque at the hip.

In comparison to the results found in simulation by Anderson and Pandy [3], the rectus femoris, biceps femoris, iliacus and gluteus display some larger than expected forces at the heel contact events. These forces correspond to the large torques about the knee and hip due to the frictional forces on the ground, and are a result of the balance controller's reaction to the change in torso speed at heel contact. Although the behaviour of the balance controller injects some additional high-frequency torques (and corresponding muscle forces) into the solution, the results outside of the heel contact periods indicate that the optimization methods reasonably model the muscle force distribution in human walking.

As discussed in [19], the correlation of predicted muscle forces with experimental EMG measurements does not in itself prove that the force distribution algorithm based on muscle fatigue minimization is the same as that used by the human body when walking. However, the plots of muscle forces presented here demonstrate the effectiveness of the optimization method in finding a suitable set of muscle forces that is a solution to the redundant force problem in Equation 5.1.

Based on these muscle forces, the muscle stress and muscle fatigue rates are computed as defined in Equations 5.3 and 5.6. Integrating the fatigue rates over the period of the simulation gives the total muscle fatigues, summarized at the end of the chapter in Table 7.1.

7.3 Prosthetic Ankle Model Results

The data presented in this section are the results of the same optimization used in the normal model, with the exception that the ankle joint torque drivers were replaced with passive joints, and the muscle groups crossing the ankles (the gastrocs, soleus, and tibialis anterior) were removed from the muscle model. The limb segment dimensions and mass properties were not changed from the normal model. Results are presented for two pros-

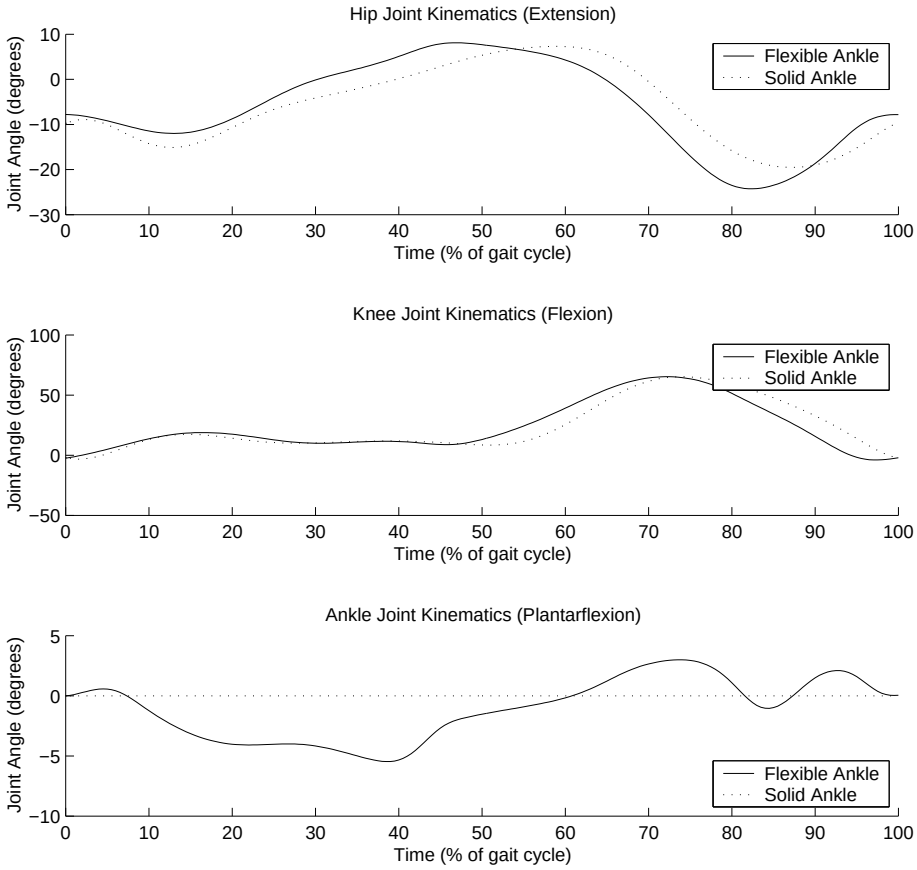

Figure 7.7: Prosthetic Ankle Model Joint Kinematics

thetic models: the flexible ankle model, where the ankle joint is modelled by a rotational spring-damper joint; and the solid-ankle-cushion-heel (SACH) model, where the ankle is modelled as a fixed joint.

7.3.1 Joint Kinematics

Figure 7.7 shows the optimized joint kinematics found by the optimization process for the two prosthetic ankle models. The hip and knee joint kinematics were varied relatively little from the experimental data used to initialize the optimization for both the flexible

and solid ankle models. The ankle joint in the flexible ankle model, however, follows a different kinematic pattern than the normal walking model, since it is not actively driven. There is no plantarflexion motion driving the push-off phase, and no dorsiflexion to lift the foot during the swing phase. In the solid ankle model, there is of course no kinematic motion of the ankle.

7.3.2 Computed Ground Reaction Forces

Figure 7.8 shows the computed ground reaction forces of the optimized solution for the prosthetic models. The time scale of plots is derived from the expected heel contact times based on the original kinematic trajectories, rather than the actual heel contact times during the simulation. This allows for comparison of the heel contact event time in relation to the joint kinematics.

The magnitudes of the ground reaction forces are similar to those for the normal walking model. However, the timing of the reaction force data displays a prominent difference between the normal and prosthetic model simulations. For the flexible ankle model, heel contact occurs about 75% into the gait cycle, as the foot hits the ground before the knee is extended, and the stance phase lasts for approximately 70% of the gait cycle, rather than the 60% expected in normal walking gait. This extension of the stance period is in agreement with observations of amputee gait by Winter [71], who reported stance periods of 64% and 68% for amputee subjects.

The increased contact period results in a longer period of double-support, where the model has both feet on the ground. The optimization may have converged to this solution to improve balance control. During the double-support phase, the model has a longer base of support; this would lead to a more stable configuration, which would require less active work by the balance controller to keep the model upright. That is, without active control of the ankle joints, the most efficient method of maintaining balance for the model may be to increase the statically stable period of double-support.

7.3.3 Joint Torques

Figure 7.9 shows the joint torques computed by the prosthetic model simulations. The

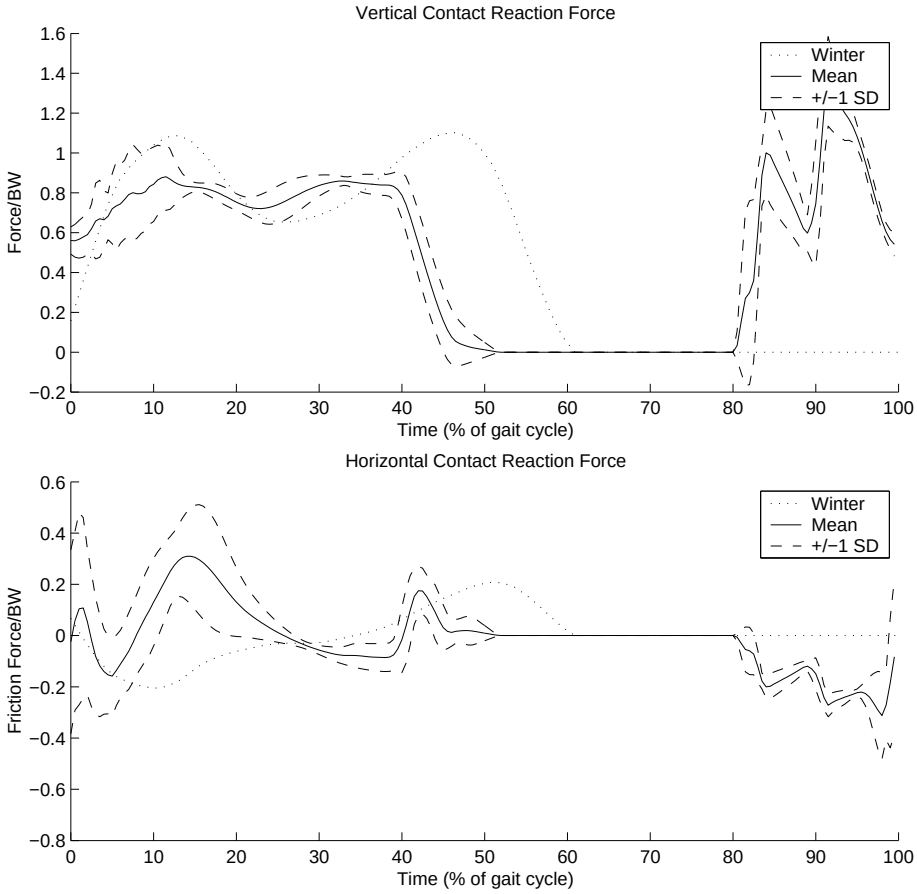

Figure 7.8: Prosthetic Model Ground Reaction Forces

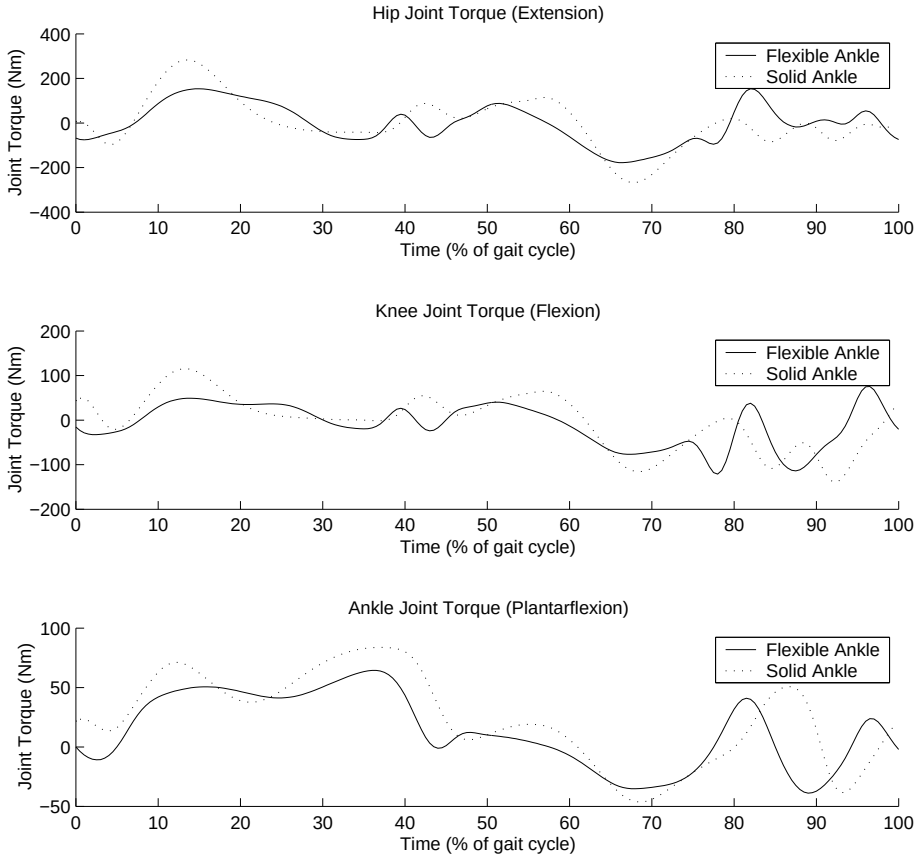

Figure 7.9: Prosthetic Model Joint Torques

pattern of passive ankle joint torques are surprisingly similar for the flexible and solid ankle models. Despite the rigid joint, the SACH model creates a typical plantarflexion torque during the push-off phase, which behaves similarly to the flexible and normal ankle models in torque response. The peak magnitudes of the flexible and SACH ankle model torques ($70 - 90Nm$) are less than those for the normal model ($125Nm$). This is in agreement with the observations of Winter [71] that found amputee gait producing only about 2/3 of the plantarflexion torque seen in normal gait.

The knee and hip joint torques are greater for the prosthetic models than for the normal model, making up for the lack of power generation at the ankle. In addition, part of the increase in hip torque is likely due to greater control forces generated by the balance controller operating with passive ankle joints. This additional torque is reflected in the corresponding muscle forces and total muscle fatigue for the prosthetic models.

7.3.4 Muscle Forces

Figure 7.10 shows the computed muscle forces for the optimized solution for the prosthetic walking models. The muscle forces computed are those that produce the required joint torques while minimizing the total muscle fatigue rate at each instant in time.

The computed forces for the six remaining muscles in the prosthetic models are generally more active than those in the normal model, as required to generate the increased propulsion and control torques, particularly at the hip. This general trend is in agreement with the experimental results in [71], which found greater EMG activity in most leg muscle groups throughout the gait cycle for the amputee subjects. The EMG measurements, however, show a great deal of hyperactivity and co-contraction that is not present in the simulation results. For example, the EMG results indicate significant activation of both the gluteus maximus (hip extensor) and rectus femoris (hip flexor) groups throughout the stance period. This behaviour is not seen in the model simulation results, where the hip extensors are generally passive when the flexors are active, and vice versa. Similar co-contraction behaviour is seen for the knee joint in the experimental EMG results of [71], and is absent in the simulated results.

Muscle co-contraction serves to increase the stiffness of a joint [69], which leads to increased control of the joint. This is likely a significant factor in amputee gait, where

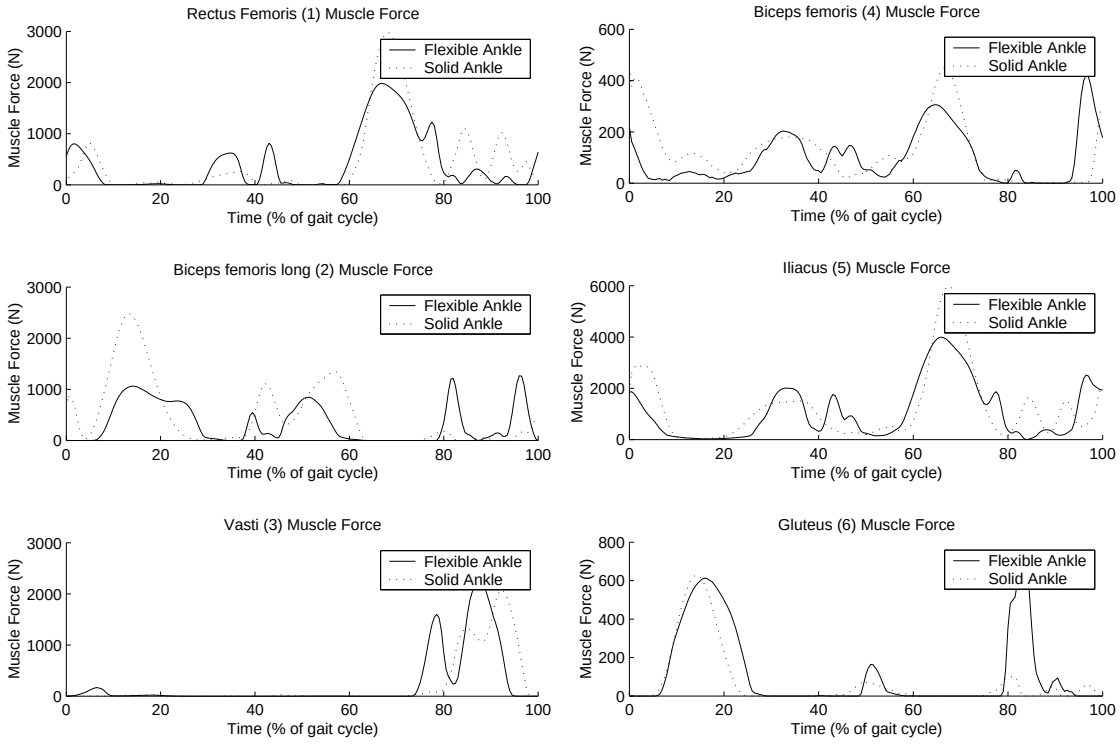

Figure 7.10: Prosthetic Model Computed Muscle Forces

additional joint stiffness is desired for safety and control. This factor is not considered in the simulated muscle fatigue distribution model. Instead, the objective of the model is to minimize total muscle fatigue, which minimizes muscle co-contraction except where required to generate the specified joint torques. While the model does not include the additional cost of control in terms of joint stiffness and muscle co-contraction, the additional work required to maintain the balance of the model is represented by the higher muscle forces in the prosthetic model.

Comparing the flexible and solid ankle models, with the exception of the vasti and gluteus groups, the peak muscle forces are noticeably greater in the solid ankle model. This suggests that greater control torques (and hence faster muscle fatigue) are required than for the flexible ankle model.

As for the normal walking model, the muscle stress and muscle fatigue rates are computed from these force curves, and the total muscle fatigues are summarized in Table 7.1.

7.4 Total Fatigue Comparison

Table 7.1 summarizes the results of the total computed muscle fatigue for the optimized simulation of each model. The fatigue measure is computed for each muscle by integrating the individual muscle fatigue rate, as described in Chapter 5, over the duration of the walking simulation (approximately 10 seconds). The values in Table 7.1 have been normalized by dividing by the total muscle fatigue for the normal model and multiplying by 100. This normalization shows the percentage of the total fatigue for each muscle in the normal model, and shows the relative increase in total fatigue for the two prosthetic models.

These results show the redistribution of muscle fatigue in the prosthetic models. Where the muscles crossing the ankle joint have been removed, the fatigue in the remaining muscles is increased for the flexible ankle model, and increased further for the solid ankle model.

To compute a physiological cost of walking, the total fatigue is divided by the horizontal distance travelled by the center of mass. This normalizes the results for simulations that generated a faster or slower walking speed, and is the objective function used in the optimization of joint kinematics. The normalized results are listed in Table 7.2.

Muscle	Normal	Flexible Ankle	Solid Ankle
Rectus femoris	22.28	47.52	67.82
Biceps femoris long	6.93	15.35	28.71
Vasti	3.47	9.41	8.42
Biceps femoris	7.43	29.70	39.60
Iliacus	24.26	64.36	89.60
Gluteus	4.46	7.43	6.44
Gastroc	7.92	N/A	N/A
Tibialis anterior	17.33	N/A	N/A
Soleus	5.94	N/A	N/A
Total muscle fatigue	100.0	173.76	240.59

Table 7.1: Muscle Fatigue Distribution

	Normal	Flexible Ankle	Solid Ankle
Total muscle fatigue	2.02	3.51	4.86
Distance Travelled (m)	15.4	15.2	9.74
Fatigue / Distance	0.13	0.23	0.50

Table 7.2: Muscle Fatigue per Unit Distance Travelled

The optimized results indicate that the model correctly predicts a higher cost of walking per unit distance travelled for the prosthetic models than the normal model. This result agrees with the observations of metabolic energy consumption in experimental studies [38], and suggests that the model takes into account factors that have been ignored in simpler analyses [34].

The results also show that the flexible prosthetic ankle model, which allows for energy storage in the ankle joints during the stance phase, involves a lower level of fatigue than the simple SACH ankle prosthetic model. While the total muscle fatigue for the SACH model was greater, the distance travelled was less. This was due to the balance controller slowing the walking motion for the SACH model; without flexibility in the ankle joint, the controller required a more vertical stance and slower gait to maintain stability. The lower fatigue requirements for the flexible ankle model agree with the results of experimental studies comparing the metabolic energy consumption of amputees using an energy-storing ankle joint [43].

Chapter 8

Conclusions and Future Development

The development of this research required the use of several methods of gait analysis in addition to the common multi-body mechanical tools. These methods included optimization of kinematics to minimize energy consumption; a method of muscle force distribution to solve the redundant force problem; a stabilizing controller design to maintain balance; and a prosthetic model that could be used to explore the difference in muscle forces and energy flow from the normal walking model.

In this chapter, the effectiveness of each of these methods is discussed, and conclusions from the results in Chapter 7 are presented. The chapter concludes with a discussion of some features that may improve the model and some directions for future research.

8.1 Optimization Methods in Gait Analysis

The use of an optimization method in the model was motivated by the hypothesis that the pattern of normal human walking is selected to minimize metabolic energy requirements. Three different applications were found for optimization to be used to find an optimal gait pattern, which are discussed below.

8.1.1 Kinematic Trajectory Selection

To find an optimal gait pattern for the model, the joint trajectories were modified by the optimization algorithm to minimize the total fatigue per unit distance travelled. The effect of this optimization was significant. Optimization of kinematics for the normal model reduced the computed total fatigue measure by approximately a factor of two from the fatigue computed for the initial joint kinematic trajectories. While the actual variation in the kinematics selected by the optimization was relatively small, the effect on the estimated metabolic cost of walking was substantial.

The pattern search algorithm worked well for this problem. It is suitable for nonlinear problems in which there is no analytical expression for the objective function, as is the case in these simulations. The pattern search is not a global optimization method; unlike a genetic-algorithm search for example, it does not attempt to find a global minimum solution. Instead, it finds a local minimum within a configurable search range, starting from a suitable initial guess. This feature is appropriate for the walking simulation problem, since an appropriate initial guess is available from the kinematic measurements in experimental studies. The purpose of the kinematic optimization was to tune the gait pattern to compensate for the variation in the model from the original walking subject, and it accomplished this effectively.

8.1.2 Muscle Force Distribution

The determination of the set of muscle forces used to generate the necessary joint torques at each instant of the simulation also required an optimization method. This optimization selected one of an infinite number of possible muscle force solutions, by finding the solution that minimizes the total instantaneous fatigue rate.

For this problem, the MATLAB *fmincon* function was used, which uses an SQP (sequential quadratic programming) search algorithm to find an optimal solution $\mathbf{X}$ to the matrix equation $\mathbf{A} = \mathbf{BX}$ while minimizing an objective function (the total instantaneous fatigue rate) and satisfying a set of constraint equations (the generation of required joint torques from muscle forces).

The difficulty in this optimization is in the selection of an appropriate objective function

that reasonably represents the muscle recruitment patterns observed in animals. The fatigue model, based on the work of Crowninshield [19], uses a static optimization at each time step, and was found to be satisfactory despite its limitations, such as a lack of dynamic state memory as discussed in Chapter 5. The success of the static optimization results are in agreement with those of Anderson and Pandy [4], who found that optimization of gait based on muscle activity using both static and more computationally intensive dynamic optimization methods gave very similar results.

With additional computational resources, the fatigue model could easily be replaced with a more sophisticated model that includes the force versus length and force versus velocity relationships of muscle. A Hill-based muscle model, as reviewed in Chapter 5, would more accurately represent the behaviour of muscle in the system, and could be used to compute a more accurate measure of metabolic energy cost. Incorporating such a model into the system would be a straightforward replacement of the metabolic cost calculation in the objective function for the optimization loop. For practical purposes on a single CPU machine, however, the simulation of a Hill-based dynamic muscle model required an unacceptable amount of computation time compared to the static optimization approach.

8.1.3 Balance Controller Optimization

The tuning of the balance controller also relied on an optimization approach to select appropriate values for the gain parameters.

The control problem was broken down into three stages that could be designed with a physically intuitive approach, similar to the methods proposed by Pratt for controlling bipedal robots [50]. After an initial attempt at solving the stability problem with a monolithic nonlinear controller, the intuitive strategy proved to be straightforward to understand and more effective in controlling the model.

Because of the very nonlinear nature of the problem, traditional control design methods could not be used to determine the controller gains. Instead, the same method used to optimize the joint kinematics was used to find optimal values for the gains by minimizing the variation in stride period between each step.

The resulting controller was very effective in maintaining the balance of the model for a simulation of arbitrary user-specified length. With the controller maintaining balance

during the simulation, many consecutive steps could be analyzed, in contrast to the typical analysis of only a single-step [3]. Since the controller drove the joint torques, and did not rely on any external support for the model, the total muscle fatigue calculations include the energy cost of maintaining balance.

8.2 Increased Energy Cost in Prosthetic Models

The results of the three models, normal, flexible ankle prosthesis, and solid ankle prosthesis, show variations in total muscle fatigue that are in agreement with those observed in physiological studies [38]. The normal model with an actuated ankle produced the least muscle fatigue; the passive flexible ankle model involved greater fatigue; and the solid ankle model produced the greatest total muscle fatigue.

The higher levels of fatigue for the prosthetic models correlate with the higher energy cost of amputee gait observed by Hoffman [38] and Waters [65]. The reduced levels of fatigue for the flexible ankle over the solid ankle prosthetic model correlate with the observations of Macfarlane [43] when comparing the energy cost of amputees using flexible and solid prosthetic ankle joints.

These results contrast favourably with those of Gitter [34], which found that center-of-mass dynamic analysis models predicted that prosthetic gait should require less energy than normal gait.

However, a comparison of the computed muscle force patterns for the prosthetic model to the EMG muscle activation patterns observed in amputee gait by Winter and Seinko [71] show a distinct contrast. The experimentally measured activation patterns indicate a significant amount of muscle co-contraction at the hip and knee joints, which is not present in the simulated model results. The net results of the simulation are correct, predicting a higher metabolic cost for amputees. This additional cost is computed as a result of higher individual muscle forces creating control torques at the knee and hip, whereas in the physiological system a higher level of muscle co-contraction is used to increase joint stiffness and control. An enhancement to the simulation may model this physiological behaviour by including a factor in the joint position controller that increases the control gains or joint damping as a function of the co-contraction around the joint.

8.3 Contributions

This thesis represents two contributions to research into the modelling and simulation of human locomotion. First, a method of stabilizing a forward dynamics simulation of human walking has been described. This method uses feedback control to modulate the speed of the lower limbs in such a way as to maintain the balance of the walking model. The use of such a balance controller allows for steady-state analysis of many steps of the walking gait, and enables investigation into the changes in stability and cost of locomotion for different models.

The second contribution is the development of a mechanical and metabolic energy cost estimation model, which was applied to the comparison of normal and amputee gait. This model successfully generated results indicating a higher cost of locomotion for amputees, in agreement with experimental studies.

8.4 Future Development

The model presented can be enhanced in a number of areas, and may be applied to numerous investigations into energy cost of walking gait.

8.4.1 More Efficient Dynamic Model

The ADAMS mechanical simulation package was selected for the development of this model for ease of design and visualization of the model behaviour. However, now that the model has been developed, a more efficient dynamic simulation package would be appropriate to reduce the computational cost of the simulation and optimization processes. For example, a system such as DynaFlex [55] can be used to symbolically generate a smaller set of dynamic equations based on a linear graph representation of the mechanical system. Optimized C code can then be generated to compute the numerical solutions for the system simulation. A more efficient simulation system will enable more detailed modeling in future research, such as incorporation of dynamic muscle models into the mechanical system.

In addition to improved computational efficiency, an improved implementation of the model will allow for the use of a more distributed simulation architecture on a networked

cluster of computers. This will enable the parallel execution of many simulations, greatly speeding the optimization process.

8.4.2 Improved Muscle Model

The muscle stress based estimation of energy cost was selected for the initial implementation of the walking model because it showed reasonable correlation with physiological data [19] and was computationally efficient, as required for the optimization methods. To improve the fidelity of the model, this calculation block could be replaced with a more realistic expression of metabolic energy cost as a function of muscle force, length, and velocity, using one of the many models based on the work of Hill [37].

The muscle model could also be improved with the addition of a spring component to account for energy storage in dynamic muscle motion. The work of Brown and Cheng [12] may provide some insights into a more comprehensive muscle model, though their implementation is too detailed and CPU-intensive to be practical in this application.

8.4.3 Improved Objective Function

A number of alternative objective functions have been suggested for solving the muscle force distribution problem, and would also be suitable for computing the objective value of the kinematic optimization loop. Some of these are reviewed by Silva [57], as discussed in Chapter 5, and could be incorporated easily into the model for comparison with the current results.

Additional components may be added to the objective function to model other physiological goals of human walking. For example, there may be a tendency to minimize internal joint forces between limb segments; this could lead to a gait with less shock at the instant of heel contact. There may also be a physiological goal of minimizing vertical displacement or velocity of the head. Including these factors with appropriate weights in the objective function could lead the optimization to a more natural and smoother simulation of walking gait.

8.4.4 Improved Controller Design

The balance controller effectively stabilizes the model, but could be improved to produce a more natural behaviour. One feature of the controller is an extremely fast response. This is generally desirable in a feedback controller design, since it minimizes the feedback delay that can lead to an unstable system. However, the speed of the controller and simulated actuator is much faster than a physiological muscle system; this leads to the high-frequency signals in the muscle force and joint torque results that could not be generated by a physiological system. To better model the human control system, the output of the controller could be low-pass filtered and delayed to approximate the force generation and twitch response time of muscle. This would produce smoother force and torque results that resemble more closely those measured in experimental studies.

However, this change alone will degrade the controller performance, and likely make it difficult to find controller gains that can balance the model. To compensate, one or more feed-forward terms could be added to the controller. The current design uses only feedback control; that is, the controller can only respond to errors in the current state of the system. By adding feed-forward control components, the controller would be able to reduce tracking errors by predicting the future required controller output based on the current state.

Feed-forward controller terms would reasonably model a biological control system, which produces muscle activations in anticipation of required forces, particularly in cyclic motion such as walking. In combination with a bandwidth-limited response, the controller would more accurately model human walking behaviour.

8.4.5 Prosthetic Limb Design Applications

One of the goals of this thesis was to develop a model that could be used to improve the design of prosthetic limbs. While the current model has been developed as a research platform, the methods presented here could be used in the development of a prosthetic design tool that allows prosthetic designers to evaluate the effect of parameter changes on the efficiency of gait.

An initial investigation could examine the effect of varying the mass and mass dis-

tribution of the limb segments in the prosthetic model. By making the mass of one leg an optimization variable, the ideal mass to minimize muscle fatigue can be found by the optimization algorithm. The results of such a study would provide insights into the value of lighter and more costly materials for prosthetic limb design.

By replacing the knee joint with a passive model, the relative metabolic energy cost of a wide variety of existing prosthetic knee designs can be investigated. To effectively evaluate these more complex designs, the model will likely need to consider additional optimization goals, such as joint stiffness and static stability, which become more significant in above-knee amputees.

8.4.6 Summary

The model presented has demonstrated an effective estimation of the relative energy cost for amputee gait from a mechanical model simulation. The application of the methods developed in this thesis will hopefully lead to improved prosthetic design and greater mobility for lower-limb amputees.

Appendix A

Implementation Details

A.1 Modelling and simulation software packages

Two software packages were used for the implementation of the methods developed in this thesis. ADAMS was used to develop and simulate the mechanical model, and MATLAB was used to run the optimization algorithm, including computation of the muscle forces and fatigue.

A.2 ADAMS modelling and simulation package

ADAMS is a mechanical system modelling and simulation package available from MSC Software. For the implementation of this project, MSC.ADAMS Version 12 was used. It provides a graphical interface for developing 3D mechanical models (ADAMS/View), and a simulation engine for both kinematic and dynamic analysis (ADAMS/Solver).

A.2.1 Simulation configuration and execution

To enable scripted automation and repeatability of the simulation, the model was built using ADAMS command files that describe each component of the model, the constraints, and the simulation parameters in text. For each run of the simulation, the parameters of the model can be varied by generating a text command file that sets the appropriate

parameters. The model was generated using rigid bodies connected by revolute joints, based on the parameters listed in Chapter 4.

By default, ADAMS creates 3D models. To restrict the analysis to motion in the sagittal plane, the torso was connected to the ground via a constraint allowing only vertical and horizontal translation, and rotation in the sagittal plane.

A.2.2 Simulation parameters

The following parameters were used for the ADAMS solver for the dynamics equations.

Parameter	Value
Formulation	I3
Integrator	GSTIFF
Integrator Tolerance	1.0E-5
Time Step	0.01s

Table A.1: ADAMS simulation parameters

A.3 MATLAB

MATLAB Version 6.5 was used to implement the energy optimization algorithm and muscle force distribution calculation described in Chapter 3.

A.3.1 Initial trajectory coefficients

The optimization of joint trajectories requires an initial guess for the values of the optimization variables, in this case, coefficients of the Fourier series expressions for the joint motions. The MATLAB function $lsqcurvefit$ was used to compute the initial values for the coefficients. The $lsqcurvefit$ function fits functions to data points by solving an optimization problem where the optimization variables are the function parameters and the objective function is the sum of the mean squared error between each data point and the corresponding value of the curve function.

The equation for each joint has the form of Equation A.1.

$$\theta_j(t) = C_0 + \sum_{k=1}^{5} \left[A_k \sin\left(\frac{2\pi kt}{period}\right) + B_k \cos\left(\frac{2\pi kt}{period}\right) \right] \tag{A.1}$$

For each joint, $lsqcurvefit$ was used to solve for C_0, A_k and B_k, for $k = 1...5$, while fitting the equation to the data given in [69]. The resulting computed coefficients are given in Table A.2.

Coefficient	Hip Joint	Knee Joint	Ankle Joint
C_0	-0.1256	0.4177	-0.0400
A_1	0.1175	-0.3847	0.1095
B_1	-0.1851	-0.1410	0.0093
A_2	0.0035	0.1891	-0.1320
B_2	0.0679	-0.2619	0.0025
A_3	-0.0356	0.0729	0.0164
B_3	0.0153	0.0056	-0.0360
A_4	0.0017	0.0134	-0.0252
B_4	0.0027	-0.0174	0.0387
A_5	0.0045	0.0079	-0.0173
B_5	0.0114	-0.0039	-0.0070

Table A.2: Initial values of Fourier series coefficients

A.4 ADAMS/MATLAB Interface

ADAMS supports a number of interfaces for implementing control systems, including a MATLAB interface and an internal control systems interface. For this design, however, the simplest mechanism was to implement control blocks using ADAMS measures and differential equation expressions. The required state variables are either available as ADAMS measures or computed from available measures, and the output of each block is implemented as a function measure, which is computed at each time step. The control gains are all created as design variables, so they may be easily set and modified.

ADAMS operates in either an interactive mode with a graphical user interface, or in a non-interactive 'batch' mode where it executes a sequence of instructions from a command file. The second mode was used to implement the simulation interface between ADAMS and MATLAB Version 6.5. A command file was created that loaded the mechanical model, then read a parameter command file specifying model parameters and joint trajectories, executed the simulation over several steps of the gait cycle, and finally wrote the kinematic and kinetic results to text files.

For every iteration of the optimization algorithm running in MATLAB, the ADAMS simulation had to be executed with a particular set of parameters and joint trajectories. The parameters and trajectories were written to the ADAMS parameter command file. The MATLAB dos() function was then used to execute ADAMS with the simulation command file that generated the kinematic and kinetic results corresponding to the optimization variables of the current iteration.

The MATLAB dlmread() function read the results from the text files into MATLAB arrays, where they were available for further calculations. Based on the joint torque data, the required muscle forces are calculated (as described in Chapter 5). The total fatigue computed from the muscle forces over the gait cycle was then used to evaluate the objective function for one iteration of the optimization algorithm.

References

[1] R. Alexander. Optimization of gaits in the locomotion of vertebrates. *Physiological Reviews*, 69:1199–1227, 1989.

[2] F. C Anderson and M. G. Pandy. Three-dimensional computer simulation of gait. In *1999 Bioengineering Conference*, Big Sky, Montana, June 1999. The American Society of Mechanical Engineers.

[3] F. C. Anderson and M. G. Pandy. Dynamic optimization of human walking. *Journal of Biomechanical Engineering*, 123:381–390, October 2001.

[4] F. C. Anderson and M. G. Pandy. Static and dynamic optimization solutions for gait are practically equivalent. *Journal of Biomechanics*, 34:153–161, 2001.

[5] P. J. Antsaklis and A. N. Michel. *Linear Systems*. McGraw-Hill, 1997.

[6] Aristotle. *On the Gait of Animals / by Aristotle; translated by A. S. L. Farquharson*. The University of Adelaide Library Ebooks, http://etext.library.adelaide.edu.au/a/a8/gait.html, 2000.

[7] E. Ayyappa. Normal human locomotion, part 1: Basic concepts and terminology. *Journal of Prosthetics and Orthotics*, 9(1):10–17, 1997.

[8] E. Ayyappa. Normal human locomotion, part 2: Motion, ground reaction force and muscle activity. *Journal of Prosthetics and Orthotics*, 9(2):42–57, 1997.

[9] L. Bianchi, D. Angelini, G. P. Orani, and F. Lacquaniti. Kinematic coordination in human gait: relation to mechanical energy cost. *Journal of Neurophysiology*, 79:2155–2170, 1998.

[10] J. Booyens and W. R. Keatinge. The expenditure of energy by men and women walking. *Journal of Physiology*, 138:165–171, 1957.

[11] N. A. Borghese, L. Bianchi, and F. Lacquaniti. Kinematic determinants of human locomotion. *Journal of Physiology*, 494(3):863–879, 1996.

[12] I. E. Brown, E. Cheng, N. Lan, R. Davoodi, and G. E. Loeb. A comprehensive model of muscle force generation under dynamic physiological conditions. pages 169–172. IFESS, 1999.

[13] R. G. Burdett, G. S. Skrinar, and S. R. Simon. Comparison of mechanical work and metabolic energy consumption during normal gait. *Journal of Orthopaedic Research*, 1:63–72, 1983.

[14] G. E. Caldwell and L. W. Forrester. Estimates of mechanical work and energy transfers: demonstration of a rigid body power model of the recovery leg in gait. *Medicine and Science in Sports and Exercise*, 24:1396–1412, 1992.

[15] G. A. Cavagna. Force platforms as ergometers. *Journal of Applied Physiology*, 39:174–179, 1975.

[16] G. A. Cavagna, H. Thys, and A. Zamboni. The sources of external work in level walking and running. *Journal of Physiology*, 262:639–657, 1976.

[17] E. J. Cheng, I. E. Brown, and G. E. Loeb. Virtual muscle: A computational approach to understanding the effects of muscle properties on motor control. *Journal of Neuroscience Methods*, 101:117–130, 2000.

[18] P. J. Corcoran and G. L. Brengelmann. Oxygen uptake in normal and handicapped subjects, in relation to speed of walking beside velocity-controlled cart. *Archives of Physical Medicine*, 51:78–87, 1970.

[19] R. D. Crowninshield and R. A. Brand. A physiologically based criterion of muscle force prediction in locomotion. *Journal of Biomechanics*, 14(11):793–801, 1981.

[20] J. M. Czerniecki. Rehabilitation in limb deficiency. 1. gait and motion analysis. *Archives of Physical Medicine and Rehabilitation*, 77:S–3 – S–8, 1996.

[21] J. M. Czerniecki, A. Gitter, and K. Weaver. Effect of alterations in prosthetic shank mass on the metabolic costs of ambulation in above-knee amputees. *American Journal of Physical Medicine and Rehabilitation*, 73:348–352, 1994.

[22] M. Damsgaard, S. T. Christensen, and J. Rasmussen. An efficient numerical algorithm for solving the muscle recruitment problem in inverse dynamics simulations. Zurich, Switzerland, July 2001. Society of Biomechanics, XVIIIth Congress.

[23] D. T. Davy and M. L. Audu. A dynamic optimization technique for predicting muscle forces in the swing phase of gait. *Journal of Biomechanics*, 20(2):187–201, 1987.

[24] M. Demirci. Design of feedback controllers for linear system with applications to control of a double-inverted pendulum. *International Journal of Computational Cognition (http://www.YangSky.com/yangijcc.htm)*, 2(4):65–84, 2004.

[25] J. E. Jr. Dennis and R. B. Schnabel. *Numerical Methods for Unconstrained Optimization and Nonlinear Equations*. Prentice-Hall Series in Computational Mathematics. Prentice Hall, NJ, 1983.

[26] J. M. Donelan, R Kram, and Kuo A.D. Mechanical and metabolic determinants of the preferred step width in human walking. *Proceedings of the Royal Society of London, B*, 268:1985–1992, 2001.

[27] J. M. Donelan, R. Kram, and A. D. Kuo. Simultaneous positive and negative work in human walking. *Journal of Biomechanics*, 35:117–124, 2002.

[28] H. Elftman. Forces and energy changes in the leg during walking. *American Journal of Physiology*, 125:339–356, 1939.

[29] O. Fischer. *Einfuhrung in die Mechank lebender Mechanismen*. Leipzig, 1906.

[30] G. F. Franklin, D. J. Powell, and A. Emami-Naeini. *Feedback Control of Dynamic Systems*. Addison-Wesley, 3rd edition, 1994.

[31] J. Furusho and M. Masubuchi. A theoretically motivated reduced order model for the control of dynamic biped locomotion. *ASME Journal of Dynamic Systems, Measurement, and Control*, DSMC-109:155–163, 1987.

[32] K. G. M. Gerritsen, Bogert AJ, van den, M Hulliger, and R. F. Zernicke. Intrinsic muscle properties facilitate locomotor control – a computer simulation study. *Motor Control*, 2:206–220, 1998.

[33] J. H. Ginsberg. *Advanced engineering dynamics*. Cambridge University Press, Cambridge, 2nd edition, 1995.

[34] A. J. Gitter, J. M. Czerniecki, and K Weaver. A reassessment of center of mass dynamics as a determinant of the metabolic inefficiency of above knee amputee ambulation. *American Journal of Physical Medicine and Rehabilitation*, 74:332–338, 1995.

[35] C.L. Golliday and H. Hemami. An approach to analyzing biped locomotion dynamics and designing robot locomotion controls. *IEEE Transactions on Automatic Control*, AC-22-6:963–972, 1977.

[36] E. J. Haug. *Computer aided kinematics and dynamics of mechanical systems*. Allyn and Bacon, Massachusetts, USA, 1989.

[37] A. V. Hill. The heat of shortening and the dynamic constants of muscle. *Proceeds of the Royal Society of London: Series B*, 126:136–195., 1938.

[38] M. D. Hoffman, L. M. Sheldahl, K. J. Buley, and Sandford P. R. Physiological comparison of walking among bilateral above-knee amputee and able-bodied subjects, and a model to account for the differences in metabolic cost. *Archives of Physical Medicine and Rehabilitation*, 78:385–392, 1997.

[39] S. Kajita and K. Tani. Study of dynamic biped locomotion on rugged terrain. In *Proc. of the 1991 IEEE International Conference on R and A.*, pages 1405–1411. IEEE, 1991.

[40] A. D. Kuo. Stabilization of lateral motion in passive dynamic walking. *International Journal of Robotics Reserach*, 18:917–930, 1999.

[41] A. D. Kuo. A simple model of bipedal walking predicts the preferred speed-step length relationship. *Journal of Biomedical Engineering*, 123(3):264–269, 2001.

[42] R. M. Lewis and V. Torczon. Pattern search algorithms for bound constrained minimization. *SIAM Journal on Optimization*, 9(4):1082–1099, 1999.

[43] P. A. Macfarlane, D. H. Nielson, and D. G. Shurr. Mechanical gait analysis of transfemoral amputees: Sach foot versus the flex-foot. *Journal of Prosthetics and Orthotics*, 9(4):144–151, 1997.

[44] P. E. Martin, G. E. Heise, and D. W. Morgan. Interrelationships between mechanical power, energy transfers, and walking and running economy. *Medicine and Science in Sports and Excercise*, 25(4):508–515, 1993.

[45] A. E. Minetti and F. Saibene. Mechanical work rate minimization and freelly chosen stride frequency of human walking: a mathematical model. *Journal of Experimental Biology*, 170:19–34, 1992.

[46] R. R. Neptune. Computer modeling and dynamic stimulation of normal and pathological human locomotion. In *Seventh International Symposium on the 3-D Analysis of Human Movement*, Newcastle upon Tyne, England, July 2002. Centre for Life.

[47] R. W. Norman, M. T. Sharratt, J. C. Pezzack, and E. G. Noble. Reexamination of the mechanical efficiency of horizontal treadmill running. *Biomechanics VI B*, Reference in Shorten 1981, 1976.

[48] M. G. Pandy and N. Berme. A numerical method for simulating the dynamics of human walking. *Journal of Biomechanics*, 21:1043–1051, 1998.

[49] J. E. Pratt. Virtual model control of a biped walking robot. Master's thesis, Massachusetts Institute of Technology, August 1995.

[50] J. E. Pratt. *Exploiting Inherent Robustness and Natural Dynamics in the Control of Bipedal Walking Robots*. PhD thesis, Massachusetts Institute of Technology, June 2000.

[51] R. T. Raikova and B. I. Prilutsky. Sensitivity of predicted muscle forces to parameters of the optimization-based human leg model revealed by analytical and numerical analyses. *Journal of Biomechanics*, 32:1243–1255, 2001.

[52] P. J. Rasch and R. K. Burke. *Kinesiology and Applied Anatomy*, chapter 1. Lea and Febiger, Philadelphia, seventh edition, 1989.

[53] Knowledge Revolution. *Working Model 2D Users Guide*. San Mateo, CA, 1996.

[54] D. G. E. Robertson and D. A. Winter. Mechanical energy generation, absorption and transfer amongst segments during walking. *Journal of Biomechanics*, 13:845–154, 1980.

[55] P. Shi and J. McPhee. *DynaFlex Users Guide*. Systems Design Engineering, University of Waterloo, Canada, August 2002.

[56] M. R. Shorten, S. A. Wooton, and C. Williams. Mechanical energy changes and the oxygen cost of running. *Engineering Medicine*, 10:213–217, 1981.

[57] M. P. T. Silva and Jorge A. C. Ambrosio. The effect of different physiological cost functions on the solution of the redunant problem in biomechanics. Lisbon, Portugal, July 2003. IDME/IST.

[58] M. P. T. Silva and Jorge A. C. Ambrósio. Solution of redundant muscle forces in human locomotion with multibody dynamics and optimization tools. *Mechanics Based Design of Structures and Machines*, 31:381 – 411, 2003.

[59] M. Skelly and H.J. Chizeck. Simulation of bipedal walking. In *IASTED International Conference on Applied Modeling and Simulation (AMS 2002)*, Cambridge, Mass., Nov 2002.

[60] T. Spagele, A. Kistner, and A. Gollhofer. Modelling, simulation and optimisation of a human vertical jump. *Journal of Biomechanics*, 32:521–530, 1999.

[61] R. L. Waters. *Gait Analysis (Perry, J)*, chapter 21: Energy Expenditure, pages 444–488. SLACK Incorporated, 1992.

[62] R. L. Waters, J. Campbell, and J. Perry. Energy cost of three-point crutch ambulation in fracture patients. *Journal of Orthopaedic Trauma*, 1:170–173, 1987.

[63] R. L. Waters and B. R. Lunsford. Energy cost of paraplegic ambulation. *Journal of Bone and Joint Surgery*, 67(A):1245–1250, 1985.

[64] R. L. Waters, B. R. Lunsford, J. Perry, and R. Byrd. Energy-speed relationship of walking: standard tables. *Journal of Orthopaedic Research*, 6:215–222, 1998.

[65] R. L. Waters, J. Perry, D. Antonelli, and H. Hislop. The energy cost of walking of amputees - influence of level of amputation. *Journal of Bone and Joint Surgery*, 58(A):42–46, 1976.

[66] R. L. Waters and J. S. Yakura. The energy expenditure of normal and pathological gait. *Critical reviews in Physical and Rehabilitation Medicine*, 1:187–209, 1989.

[67] K. R. Williams and P. R. Cavanagh. A model of the calculation of mechanical power during distance running. *Journal of Biomechanics*, 16:115128, 1983.

[68] D. A. Winter. A new definition of mechanical work done in human movement. *Journal of Applied Physiology*, 46:79–83, 1979.

[69] D. A. Winter. *Biomechanics and Motor Control of Human Movement*. John Wiley & Sons, Inc., New York, 1990.

[70] D. A. Winter, A. O. Quanbury, and G. D. Reimer. Analysis of instantaneous energy of normal gait. *Journal of Biomechanics*, 9:253–257, 1976.

[71] D. A. Winter and S. E. Sienko. Biomechanics of below-knee amputee gait. *Journal of Biomechanics*, 21:361–367, 1988.

[72] J. M. Workman and B. W. Armstrong. Oxygen cost of treadmill walking. *Journal of Applied Physiology*, 18(4):798–803, 1963.

[73] G. T. Yamaguchi. *Performing Whole-Body Simulations of Gait with 3-D Dynamic Musculoskeletal Models*, chapter 43, pages 663–679. Springer-Verlag, NY, 1990.

[74] M. Y. Zarrugh and C. W. Radcliffe. Predicting metabolic cost of level walking. *European Journal of Applied Physiology*, 38:215–223, 1978.

[75] M. Y. Zarrugh, F. N. Todd, and H. J. Ralston. Optimization of energy expenditure during level walking. *European Journal of Applied Physiology*, 33:293–306, 1974.